Practical Stabilization of Systems With Countable Set of Actions

Almuzakki, Muhammad Zaki

DOI:
10.33612/diss.915192889

Practical Stabilization of Systems With Countable Set of Actions:

A Nearest Action Selection Approach

Muhammad Zaki Almuzakki

Practical Stabilization of Systems With Countable Set of Actions:

A Nearest Action Selection Approach

Muhammad Zaki Almuzakki

This work has been carried out at Engineering and Technology institute Groningen (ENTEG), Faculty of Science and Engineering, University of Groningen, The Netherlands.

The work presented in this dissertation is supported by Lembaga Pengelola Dana Pendidikan Republik Indonesia (LPDP-RI).

This work has been completed in partial fulfilment of the requirements of the Dutch Institute of Systems and Control (DISC) for graduate study.

Part of this work was carried out in the Ocean Grazer project (interested reader may access https://www.rug.nl/research/cmme/ocean-grazer-project for more information about the project). Most of the main findings in this thesis are motivated by the original design of the Ocean Grazer wave energy converter and their Ocean Battery.

Practical Stabilization of Systems With Countable Set of Actions: A Nearest Action Selection Approach
Muhammad Zaki Almuzakki

Printed by Ipskamp Printing

ISBN/EAN: 978-94-6473-411-9

university of groningen

Practical Stabilization of Systems With Countable Set of Actions

A Nearest Action Selection Approach

PhD Thesis

to obtain the degree of PhD at the
University of Groningen
on the authority of the
Rector Magnificus Prof. J.M.A. Scherpen
and in accordance with
the decision by the College of Deans.

This thesis will be defended in public on
Monday 11 March 2024 at 09:00 hours

by

Muhammad Zaki Almuzakki

born on 1 June 1991
in Bangkalan, Indonesia

Supervisors:
Prof. B. Jayawardhana
Prof. A.I. Vakis

Assessment committee:
Prof. S. Trenn
Prof. T.A.E. Oomen
Prof. K. Fujimoto

To my beloved family
my parents,
my wife, Nadia, and
my sons, Kafa and Kaif...

Acknowledgments

As I reflect on the culmination of this significant chapter, I am filled with gratitude for the support and guidance that have shaped my Ph.D. journey. Completing this research marks the end of a transformative and intellectually enriching period, and I extend my deepest appreciation to those who have been instrumental in this endeavor.

First of all, i would like to express my deepest gratitude to my primary advisor and mentor, Prof. Bayu Jayawardhana, whose unwavering guidance, insightful feedback, and continual support have been instrumental in the successful completion of this PhD journey. His expertise and encouragement have shaped my academic and research endeavors, and I am truly fortunate to have had the opportunity to work under his supervision.

Special appreciation goes to Prof. Bambang Hari Wibisono, the Indonesian Education and Culture Attaché to the Netherlands (2013–2018), for his instrumental assistance in securing the LPDP scholarship that has made this academic pursuit possible. His support has been a crucial factor in enabling me to focus on my studies and research.

I am sincerely thankful to my second promotor, Prof. Antonis I. Vakis, for his scholarly input, encouragement, and collaborative spirit in helping this research towards successful completion.

I extend my heartfelt thanks to Prof. Stephan Trenn, Prof. Tom Oomen, and Prof. Kenji Fujimoto for graciously taking the time to assess and provide constructive feedback on my thesis. Their expertise and thorough evaluation have significantly enriched the quality of this work. I express my appreciation also to Dr. Aneel Tanwani for engaging discussions and hosting me during a 2-week research visit in Toulouse. A significant portion of this thesis would not have been possible without your invaluable contributions and guidance.

I would like to acknowledge and appreciate my colleagues from DTPA, SMS, ODS, the Ocean Grazer project, and the Mechatronics and Control of Nonlinear Systems group: Qingkai, Nelson, Carlo, Weijia, Jiajia, Xiaodong, Tony, Rodolfo, Marco, Yuzhen, Alain, Mark, Henk, Tabitha, Leonardo, Yu Kawano, Pablo, Lorenzo, Emin, Rafael, Jesus, Yanji, Alva, Matteo, Anja, San-

tiago, Michele, Miao, Luke, Junjie, Amir, Monica, Mehran, Sebastian, Haiwen, Liangming, Hadi, Mauricio, Marijn, Matthijs, Tinghua, Bo, Sepide, Juan, Hao, and many others, whose names i cannot possibly mention in one breath, for their camaraderie, intellectual exchange, and collaborative efforts, which have contributed to a stimulating research environment. Special thanks to all of DTPA's supporting staff, with a heartfelt appreciation for individuals such as Frederika, whose assistance has been invaluable throughout my PhD journey. Additionally, I express deep gratitude to Arijit, Zhiyu, Lihua, Bangguo, Linda, Luis, Emmanuel, Jin, Vaibhav, Bahadir, Pelin, Saeed, and others for creating cherished memories during my 2-month visit to Groningen. Their warmth and camaraderie significantly enriched this experience, and I am thankful for the joyous moments shared with this wonderful group. Also thanks to Krishna and his family for not only being friends but also wonderful neighbors. Our shared experiences, knowledge, and the joy of living were truly special. The moments of learning and the delightful shared meals enriched our connection, and my family and I genuinely appreciated having you as neighbors. I also want to say thank you to Jurrien for generously agreeing to assist in translating the summary of my thesis into Dutch, despite our not having met before. Your willingness to lend a helping hand is sincerely appreciated.

I would also like to express my heartfelt gratitude to all Indonesian communities in Groningen: PPIG, deGromiest, and Indonesian Diaspora, for all their support. My first special thanks go to Mas Yudi, Mba Sofa, and Arham for their exceptional kindness. Their warm welcome marked our first introduction to the Groningen community, making a lasting impression. I vividly recall Mas Yudi's thoughtful gesture of picking me up at the Groningen station amidst a cold, gloomy, and rainy afternoon, followed by Mba Sofa's heartwarming hospitality with a delicious meal prepared at K94. Their generosity and warmth during our initial days in Groningen left a lasting and cherished memory. I also express my gratitude to Mas Rully, Mba Intan, and Kinan for graciously hosting me during my initial days in Groningen. Their welcoming hospitality and engaging discussions made for a wonderful start to my time in the city. The next list of my special thanks goes to Mas Fajar, Mba Monik, Runa, and Senja for being exceptional friends, neighbors, and family. Mas Fajar, you are truly one of our heroes, and I am profoundly thankful for your unwavering support, especially during emergencies. Your readiness to drive us to the hospital, whether during the day or midnight, has been invaluable, particularly during Kafa's illness and Nadia's delivery of our first child. To Mba Monik, your friendship with Nadia has been a source of great comfort, and we appreciate your presence in her life in Groningen. To Runa and Senja, your time spent playing and adventuring with Kafa is treasured, even if Kafa may not recall those moments in the years

to come. Your warmth and companionship have made a significant impact on our family, and we are truly grateful.

I offer my sincere thanks to Mas Zainal, Mba Ayu, Aira, and Biya for the countless beautiful memories we've shared. Our journey to Morocco, among many others, remains a truly unforgettable moment. Mas Zainal and Mba Ayu, your roles as our dearest brother and sister, as well as Kafa's second parents during our time in Groningen, have been truly appreciated. Aira and Biya, your nurturing presence has made you Kafa's most caring big sisters, and for that, we are grateful. I also would like to thank Mas Ega, Mba Irma, Mimi, Lili, Zizi, and Qiqi for being enduring neighbors, no matter where we are. Your enduring friendship has not only made our neighborhoods feel like home but has also been our family's go-to destination whenever we seek companionship during moments of boredom. Next on our list, I express gratitude to Mas Ali, Mba Liany, and Cici, the cheerful and inspiring members of our extended family. I should not forget the family of Didin, Anis, and Aqmar for bringing joy into our lives during our time in Groningen. My sincere gratitude also goes to Mas Wandy, Mba Cici, Mikail, and Mikhayla, particularly for our spontaneous travels without plans, which turned out to be truly wonderful experiences. I extend heartfelt gratitude also to Budhe Arie, Om Herman, Tante Indah, Om Yon, Budhe Nunung, Om Archi, and other members of the Indonesian Diaspora for creating cherished memories. Your roles as our parents, best friends, and grandparents to our dearest Kafa are truly appreciated.

I want to express my gratitude to the incredible team of friends, or "team bapak-bapak" and "team ibu-ibu," including Mas Adhyat, Mas Krisna, Kang Hegar, Mas Amak, Fika, Mas Panji, Mas Latif, Yusron, Azka, Mas Azzam, Mas Ade, Mas Didik, Mas Rifqi, Mas Sutrisno, Kang Deni, Kang Angga, Mas Khairul, Mas Aziz, Mas Lana, Mas Surya, Pak Asmoro, Mas Romi, Mas Joko, Mas Habibi, Mas Akbar, Mas Chalis, Mas Ristiono, Mas Ivan, Mas Budi, Mas Rangga Kresna, Mas Kuswanto, Afif, Mas Donny, Pak Yopi, Mas Ali, Mas Iging; and Mba Nuri, Mba Icha, Teh Ica, Mba Putri, Nisa, Mba Septi, Aidina, Mba Ghina, Jecika, Mba Rosel, Mba Indri, Mba Retno, Mba Amalina, Mba Arum, Yassaroh, Bu Rini, Mba Arlina, Mba Uci, Mba Ma'wa, Mba Andis, Mba Jean, Mba Afifah, Mba Dita, Mba Noni, Mba Lia, Mba Fitri, Mba Wiwik, Mba Dewi, Mba Yossy, Mba Desti; former housemates; and everyone who played a role in making Groningen feel like our second home. Living thousands of kilometers away from Indonesia was undoubtedly a roller coaster for our new family, but your presence in our lives has consistently been the best support.

Let's not overlook Affan and my Indonesian peers under Pak Bayu's direct guidance: Mas Agung (also Mba Inna, Dhia, and Delisha), Mas Ridho, and Mas Yulyan. To Affan, my high-school schoolmate and dorm-mate, you were

the first person to welcome me upon my arrival in the Netherlands. Your willingness to travel from Delft to Schiphol airport in the early morning just to guide me on using public trains properly is truly priceless. Mas Agung, being my first Indonesian office-mate, we found common ground, especially as both of us hail from eastern Java. Our discussions about various topics significantly eased the tensions of PhD research. Without you, my office life would certainly have been different. To Mas Ridho and Mas Yulyan, even though our first meeting lasted less than two months, it felt like we had been friends forever. We delved into discussions about family life, education in Indonesia, daily life in Groningen, and many other interesting topics. Our frequent weekend travels, from long-range biking (which i rarely did) to extended trips to the south of the Netherlands with discounted tickets, were truly unforgettable. As a fun fact, we discovered that we are all connected through one person - the brilliant Affan.

Last but certainly not least, to my beloved family...

To my parents (Abi Jamaluddin, Ibu Afri Asiatin, Abah Achmad Ubaedillah, and Mama Siti Rif'ah), siblings (Ain, Hana, Lathief, Faiqoh, Zaim, Fiana, Nuha, Fikra, and Zaka), and my little nephews (Uwais, Afza, and Naura), your unwavering encouragement and belief in my capabilities have been my pillars of strength. Your support has been the driving force behind my academic achievements.

To my wife, Nadia, and my sons, Kafa and Kaif, your love, understanding, and patience have been my anchor during the challenging moments of this academic pursuit. Your unwavering support and sacrifices are the driving force behind my accomplishments.

This thesis stands as a testament to the collective efforts and unwavering support of these extraordinary individuals. As I write this section, reminiscing about my small family's experience during our time in Groningen, I find myself moved to tears. The privilege of learning and growing with such an exceptional group of mentors, colleagues, and loved ones is something for which I am profoundly grateful.

Muhammad Zaki Almuzakki
Jakarta
February 12, 2024

List of Publications

Journal Papers

1. **MZ Almuzakki**, B Jayawardhana, and A Tanwani, “Nearest neighbor control for practical stabilization of passive nonlinear systems," *Automatica*, vol. 141, p. 110278, 2022.

2. **MZ Almuzakki** and B Jayawardhana, “Cooperative Nearest-Neighbor Control of Multi-Agent Systems: Consensus and Formation Control Problems," *IEEE Control Systems Letters*, vol. 7, pp. 1873-1878, 2023.

3. **MZ Almuzakki**, B Jayawardhana, A Tanwani, and AI Vakis, “Exponential Stability of LTI Systems with Infinitely Countable Input Set via Nearest-Action Control," *Submitted*.

Conference Proceedings

4. **MZ Almuzakki**, JJ Barradas-Berglind, Y Wei, M Muñoz-Arias, AI Vakis, and B Jayawardhana, “A port-Hamiltonian Approach to Cummins' Equation for Floater Arrays with Linear Power-Take Off Systems," *6th IFAC Workshop on Lagrangian and Hamiltonian Methods for Nonlinear Control (LHMNC)*, 2018.

5. B Jayawardhana, **MZ Almuzakki**, and A Tanwani, “Practical Stabilization of Passive Nonlinear Systems with Limited Control," *11th IFAC Symposium on Nonlinear Control Systems (NOLCOS)*, 2019.

6. Y Wei, JJ Barradas-Berglind, **MZ Almuzakki**, M van Rooij, R Wang, B Jayawardhana, and AI Vakis, “A Fourier Approximation Method for the Multi-Pump Multi-Piston Power Take-Off System," *International Conference on Offshore Mechanics and Arctic Engineering (OMAE)*, 2018.

7. Arvind Ragghav V, **MZ Almuzakki**, B Jayawardhana, and AD Mahindrakar, “Asymptotic Stabilization of Passive Nonlinear Systems with Finite Countable Control Actions: mixed switching – nearest action control approach," *Submitted*.

Contents

List of Notations

$\mathbb{N}$	$0, 1, 2, \ldots$ the set of natural numbers
$\mathbb{R}$	the set of real numbers
$\mathbb{R}^n$	n-dimensional real vector space
$\mathbb{R}^{m\times n}$	the space of $m \times n$ real matrices
$\mathbb{C}$	the set of complex numbers
$\mathbb{C}^n$	n-dimensional complex vector space
$\mathbb{C}^{m\times n}$	the space of $m \times n$ complex matrices
$\|\cdot\|$	Euclidean norm of a vector in $\mathbb{R}^n$ or induced norm of a matrix in $\mathbb{R}^{m\times n}$ or 2-norm of a vector in $\mathbb{C}^n$ or matrix norm in $\mathbb{C}^{n\times n}$ induced by 2-norm on $\mathbb{C}^n$
$\|z\|_I$	the essential supremum norm of a signal $z : \mathbb{R}_{\geq 0} \to \mathbb{R}^n$ over an interval $I \subset \mathbb{R}_{\geq 0}$
$\mathbb{B}_\epsilon(c)$	a closed ball of radius ϵ centered at $c \in \mathbb{R}^n$ defined by $\mathbb{B}_\epsilon(c) := \{\xi \in \mathbb{R}^n \mid \|\xi - c\| \leq \epsilon\}$
$\mathbb{B}_\epsilon$	$\mathbb{B}_\epsilon(0)$
$\langle \mu, \nu \rangle$	the inner product of two vectors $\mu, \nu \in \mathbb{R}^m$
$\langle \mu, \mathscr{S} \rangle$	the set of all inner products between a vector $\mu \in \mathbb{R}^m$ and all vectors in the set $\mathscr{S} \subset \mathbb{R}^m$ given by $\langle \mu, \mathscr{S} \rangle := \{\langle \mu, \nu \rangle \mid \nu \in \mathscr{S}\}$
$\mathrm{card}(\mathscr{U})$	the cardinality of a finite countable set $\mathscr{U}$
$\mathrm{conv}(\mathscr{U})$	the convex hull of a set $\mathscr{U}$
$\mathrm{int}(S)$	the interior of a set $S \subset \mathbb{R}^n$
e_i	a unit vector whose i-th element is 1 and the other elements are 0
$\mathbb{1}$	a vector whose entries are 1
$\mathrm{Im}(M)$	image of matrix M
$\mathrm{Ker}(M)$	kernel of matrix M
$\cap$	intersection
$\oplus$	direct sum of two vector spaces
$\otimes$	the Kronecker product of two matrices

$\succ$	$M \succ 0$ is used to indicate that the matrix M is positive definite
$\succcurlyeq$	$M \succcurlyeq 0$ is used to indicate that the matrix M is positive semi-definite

List of Abbreviations

DOF	Degree of Freedom
GAS	Globally Asymptotically Stable
GEPS	Globally Exponentially Practically Stable
GES	Globally Exponentially Stable
GPS	Globally Practically Stable
IRF	Impulse Response Function
ISpS	Input-to-State Practical Stable/Input-to-State Practical Stablility
ISS	Input-to-State Stable/Input-to-State Stability
LTI	Linear Time Invariant
MAS	Multi Agent System
MIMO	Multi-Input Multi-Output
MPP	Multi Piston-Pump
NAC	Nearest Action Control
OG	Ocean Grazer
pH	port-Hamiltonian
PTO	Power Take-Off
WEC	Wave Energy Converter

List of Figures

This page intentionally left blank.

Chapter 1 | Introduction

"Sometimes limitation requires simple solution"

-Author-

Contents

The main contributions of this thesis are on the energy-based modeling, analysis and control methods with applications in renewable energy systems that are written in two parts. In the first part of the thesis, we present the design and analysis of feedback control systems with countable set of actions. Nearest-action selection based control laws are presented for a class of linear systems and of nonlinear systems, and the analysis is presented based on the passivity-based control theories. The main results are applied to the control of energy storage systems and of multi-agent systems. In the second part of the thesis, we present the energy-based hydrodynamic modeling of the Ocean Grazer wave energy converters.

1.1 Stabilization with Countable Sets of Actions

In several applications ranging from control of physical systems to networked control, exact implementation of a feedback control law is not possible due to the constraints at the level of sensors/actuators, or the constraints at the level of communication channels. An example for such problem is the design of

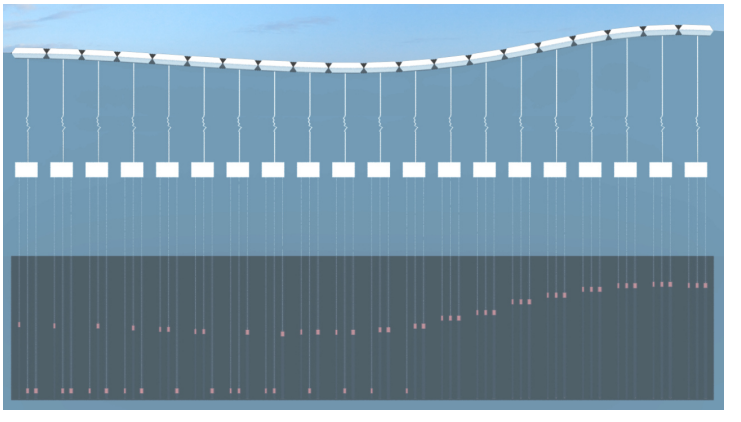

Figure 1.1: The schematic of the Ocean Grazer wave energy converter's multi piston-pump power take-off (MPP-PTO) system. Each MPP-PTO unit has a set of three different pistons that can be activated/deactivated individually. This results in seven possible active combination of pistons to be activated according to the available excitation force provided by the incoming waves [1].

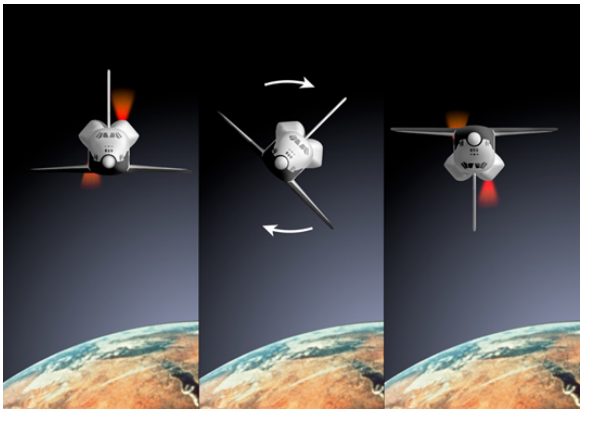

Figure 1.2: An example of how a space shuttle is steered by actuating a fixed set of thrusters. The image is taken from howthingsfly.si.edu.

mechatronics systems with limited actuation, such as, a fixed set of constant actuator systems in the Ocean Grazer wave energy converter as in Figure 1.1 [1, 2] or a fixed configuration of constant thruster systems in the space rockets/ space shuttles. By constant actuator or thruster systems, we mean that these systems can only provide piecewise constant actuation with limited discrete values. Another example is when we want to automate a (possibly old) multi-gear bike using a single motor with fixed velocity. Each gear can be considered as a fixed set of constant actuator system which corresponds to certain fixed velocity.

Problems related to the analysis or design of control laws in the presence of such constraints have received considerable attention in the literature [3, 4, 5, 6, 7, 8]. Analysis and control design methods for systems with binary input or minimal information have been discussed, among many others, in [6, 9] for linear systems, and in [3, 4, 8, 10] for the networked control systems setting. As these papers consider the use of binary input values per input dimension, the stabilization of an m-dimensional input-output system implies that there should be at least 2^m admissible input values and the stabilizing control law must dynamically assign one of these values as control input at every time instance. In general, these admissible input values can be written in the form of a finite countable input set $\mathscr{U} := \{u_0, u_1, u_2, \ldots, u_p\}$ with $u_i \in \mathbb{R}^m$ for each $i = 0, \ldots, p$.

In most of the existing works, the input set $\mathscr{U}$ is chosen such that the resulting partition has some structure. For instance, when

$$\mathscr{U} := \{-N, -N+1, \ldots, N-1, N\}^m,$$

a partition in the form of a regular grid facilitates the control design and analysis as studied in [3, 4, 5, 8, 11, 12, 13]. Other examples include the use of logarithmic quantizers [6, 14]. When we restrict ourselves to the case of static finite-level quantized feedback, it has been established that the state converges to a ball around the origin, where the radius of this convergence ball decreases with the increase of quantization levels. However, if we fix the cardinality of the discrete set $\mathscr{U}$ then an interesting question is to find the quantization mapping $\phi : \mathbb{R} \to \mathscr{U}$, or the partition, which minimizes the size of ball around the origin where the trajectories converge asymptotically. The paper [15] casts such question as an optimization problem (without taking system dynamics into consideration), which results in the so-called Voronoi tessellations.

Another interesting question about finding the minimal set $\mathscr{U}$ for feedback stabilization has also received considerable attention. One question regarding this matter is on the minimal cardinality of the set $\mathscr{U}$. For example, in [16], it is shown that for a class of discrete-time linear systems, they are stabilizable

if the number of bits per sample (rate of communication) is greater than the intrinsic entropy of the system. Similar results are available for continuous-time systems setting in [17, 18]. Thus far, a dedicated study on computing the entropy of generic class of systems is still lacking. Therefore, the question of how many symbols are necessary or sufficient for the stabilization of generic (nonlinear) systems is not well-studied in literature. In [8, 10], for a class of nonlinear passive systems Σ, they are shown to be practically stabilizable by using binary control for each input dimension. In this particular case, the input set $\mathscr{U}$ contains $2^m + 1$ elements, e.g., $\mathscr{U} = \{0\} \cup \{-1, 1\}^m$.

As a relaxation of the aforementioned results for a generic class of multi-input multi-output systems, we show in this thesis that such practical stabilization can be achieved by simply using $m + 1$ elements in $\mathscr{U}$, in addition to $\{0\}$ or the required constant input u^* when the system is required to track a desired constant reference y^*. We propose the nearest-action based control laws, namely the nearest action control (NAC), and analyze the stability of the closed-loop systems when the input u can only be taken from the finite discrete set $\mathscr{U}$. Moreover, we provide algorithmic procedure to construct minimal discrete sets that are able to practically stabilize the systems by means of NAC. Our design methodology is such that the overall closed-loop system is an interconnection of a passive or positive real system with an optimization-based selection rule for the input. Dynamical systems where the inputs are computed from solving an optimization problem, and are discontinuous appear in different applications [19]. Passivity or positive realness of the open-loop system is an important structural property that facilitates the analysis. When quantization effect is of a particular concern, the interconnection of passive or positive real systems and quantizers has been studied for the past decade in various different contexts. For instance, the practical stability analysis of passive systems in a feedback loop with a quantizer using an adapted circle criterion for nonsmooth systems is presented in [20].

On one hand, the ability of practically stabilizing a generic class of passive nonlinear systems using only $m+1$ numbers of nonzero actions can be thought of as a significant reduction in terms of the necessary number of actions in the action set $\mathscr{U}$. On the other hand, such result may not be applicable when distributed control problems such as the cooperative control of multi agent systems is in consideration. For this purpose, the usual quantization procedures such as the binary/ternary quantizers [21] are readily implementable since the quantization procedures are in general implemented element-wise, see also [3]. However, when each agent can only realize actions from a (possibly finite) countable set of actions, which cannot be quantized element-wise, an interesting question is whether the proposed nearest action control can be

implemented in distributed fashion and what is the maximum possible error that will arise from implementing distributed NAC.

Further discussion that is often asked in this line of research is regarding the performance, in particular the convergence rate, of the closed-loop system when our NAC is implemented. For this particular problem, the usual approach is to add countably many, possibly infinite, control actions in the direction of the original input set. For example, in [22], a logarithmic quantizer per input dimension is used to stabilize multi-input multi-output linear system with quadratic performance. In [23], a uniform quantizer is used to render single-input single-output linear systems practically stable with exponential rate. In both examples, it is observed that when the quantization error is bounded, the state trajectories are shown to converge towards the desired equilibrium either quadratically or exponentially fast.

The problem of stabilizing linear time invariant (LTI) systems with sector bounded nonlinear feedback law is known as the Lur'e problem (also known as the absolute stability problem) [20, 23, 24]. Typically, the associated LTI systems are considered to be controllable and observable; and the nonlinear feedback law satisfies a sector condition. The main goal on this type of problem involves finding the conditions on the transfer function of the linear systems and on the sector condition such that the closed-loop interconnection is globally asymptotically stable. The papers [20, 23] address the Lur'e problem for practical stabilization using the notion of input-to-state practical stability.

1.2 Energy-based Modeling of the Ocean Grazer Wave Energy Converter

Wave Energy Converters (WECs) are devices designed to harvest ocean wave energy and converting the harvested energy to other form of consumable energies such as electricity. A lot of concepts has been proposed to extract the ocean wave energy, ranging from oscillating water columns (OWCs), Attenuators, terminators, and point absorbers-type of device. Some examples are the Spar-buoy Oscillating Water Column [25], the Pelamis WEC [26], the Wave Dragon WEC [27], and the Ocean Grazer WEC [28, 29].

Different approaches to harvest available ocean wave energy have been proposed. The main objective of the various designs is to extract and produce as much energy as possible from the ocean while minimizing the overall production costs. For this purpose, many recent research on WECs are moving towards narrow-spaced array concept which has the potential to increase the energy extraction. An example of such devices is the Wave Star WEC where many point absorber type of WECs are put next to each other to simultaneously absorb

as much energy as possible from the incoming waves [30]. The latest problem can be seen from [1] where it shows that applying different configurations may increase the performance of a device with multiple floating element. However, these kind of concepts increase the complexity of the (numerical) modeling of the respective design and thus the control design for the whole device.

In this thesis, we are dealing with WEC modeling with at least one floating element exists in the system. This design is widely used in the modern WECs technology. The modeling of floating bodies are commonly addressed by the well-known Cummins' equation [31]. However, the time-domain numerical simulation using the Cummins' equation maybe very expensive in terms of computation time due to its mixed differential and integral in the structure of the equation, especially when dealing with the simulation of multiple floating bodies. By the Cummins' equation, we can describe the modeling of a complete WEC system as an interconnection between different subsystems, namely, the floating element, the body-to-body radiation system, the power take-off (PTO) unit, and the mooring system.

The hydrodynamics of floating bodies described by the Cummins' equation are inherently passive. For the purpose of the second part of this thesis, a passivity-based time-domain modeling, that is the port-Hamiltonian (pH) framework, is used in this work since it generally uses energy terms as its common languange between communicating systems [32]. This is in line with the research on WECs where the transfer of energy plays the central role in the system. An attempt of WECs modeling using pH framework was done by Barradas-Berglind, *et. al.*, in [33]. However, the hydrodynamics properties that are mainly appearing in the radiation system were not addressed. In this case, the radiation system is the main sources of the increase in the computational complexity of the model.

In order to tackle the computational complexity problems in the Cummins' equation, Yu and Falnes in [34] proposed a state-space approximation for the integral part that describes the radiation system specifically to reduce the computational complexity, but it did not guarantee the dissipativity of the radiation system. Further method was proposed in [35] where passivity property of the radiation force is addressed. In addition, an explicit approximation to the radiation kernel is recently proposed in [36] where the formula is designed to approximate sinusoidal function with dissipating amplitude. The latter will be explained further as a part of this thesis.

The Ocean Grazer (OG) WEC is a novel hybrid multiple point absorber type WEC that is designed to absorb most of the energy provided by wide spectrum of ocean waves. The adaptability in OG-WEC is enabled by the multi piston-pump power take off (MPP-PTO) system [1, 29]. For each floating element

in OG-WEC, it is connected to an MPP-PTO unit which is a set of three individual hydraulic type pumping systems with different dimensions which can be activated either individually, in pairs, or all together at any time instances. The key idea of the MPP-PTO concept is that we can activate all three pumps when the available potential energy is high enough, or only activate them partly when the incoming waves do not carry enough force to push the total weight of all three pumps. This allows for optimized energy extraction and adaptation to changing situations in the ocean.

Although the key idea behind the concept of OG-WEC's MPP-PTO is clear, the set of switching algorithms to determine which pump to be activated for which wave conditions needs to be established. To achieve this, several attempts to model the behavior of the OG-WEC has been developed [1, 28, 29, 33]. In particular, [1] showed that proper switching mechanism of the MPP-PTO concept allows the OG-WEC to optimally extract potential energy from the incoming waves. However, the developed models were not addressing either the problem of passivity of the whole structure or the hydrodynamics components of the floating subsystems. In order to cover the missing parts of the previous models, we propose a port-Hamiltonian approach to model the OG-WEC in this thesis.

1.3 Outline and Contributions

1.3.1 Outline and Contributions Part I

In the first part of this thesis, we study the development of NAC for practical stabilization of multi-input multi-output dynamical systems. To be more precise, we consider single and/or multi agent described by multi-input multi-output continuous time systems Σ where the state is given by $x(t) \in \mathbb{R}^n$, the output signal is represented by $y(t) \in \mathbb{R}^m$, and the input is given by $u(t) \in \mathscr{U} \subseteq \mathbb{R}^m$. Furthermore, the system Σ has an asymptotically stabilizing static output-feedback law $y \mapsto F(y) \in \mathbb{R}^m$. For a given ball $\mathbb{B}_\epsilon \subset \mathbb{R}^n$, with $\epsilon > 0$, determine the finite countable set $\mathscr{U} := \{u_0, u_1, \ldots, u_p\} \subset \mathbb{R}^m$ with minimal cardinality, and describe the mapping $\phi : \mathbb{R}^m \to \mathscr{U}$ such that the closed-loop system of Σ with $u = \phi(F(y))$ satisfies $x(t) \to \mathbb{B}_\epsilon$ as $t \to \infty$ for all initial conditions $x(0) \in \mathbb{R}^n$.

The results for the first part are found in Chapter 3 to Chapter 5. Our first contribution is on the control design and practical stability analysis of passive systems with limited actions by means of what we call later as nearest action control (NAC). We then implement our proposed NAC to the case of distributed control of multi agent systems. Lastly, we improve our result on

NAC by extending the set of limited actions according to specific geometric distributions to guarantee exponential practical stability.

In Chapter 3, we study the problem of practical stabilization of a generic class of passive nonlinear system when its input can only be chosen from a finite countable set $\mathscr{U} := \{u_0, u_1, \ldots, u_p\}$. In this chapter, we propose a nearest action input selection approach where at least one action in $\mathscr{U}$ can be chosen in each time instance. By abusing the passivity and norm-observability properties of the system, we show that practical stability up to a desired margin can be achieved by selecting the nearest possible action in $\mathscr{U}$ to the usual continuous control input when the set $\mathscr{U}$ satisfies some geometric assumptions. Moreover, we show in this chapter that practical stabilization is possible with significantly lower number of actions compared to existing results on stabilization by limited actions such as the stabilization by binary/ternary quantizers. In addition, we present a constructive algorithm to design some minimal input $\mathscr{U}$ that satisfy the conditions for practical stability using our proposed nearest-action control.

In Chapter 4, we apply our result on practical stabilization with NAC to the case of cooperative control of multi agent systems. In this chapter, we implement an agent-wise NAC algorithm to the well-known consensus and distance-based formation control law in order to practically achieve consensus or some desired formations. For this purpose, we consider that each agent can only realize actions that are available in a finite countable set $\mathscr{U}$. Our results show that consensus or a desired formation can be achieved with margin up to the total natural maximum absolute error of all agents. The results are then verified using Monte-Carlo simulation approach.

In our final contribution for the first part of this thesis, as studied in Chapter 5, we are interested in improving the convergence rate of our proposed NAC. For this purpose, inspired by many studies about exponential convergence of systems with limited actions, we propose a *directional* extension of the set $\mathscr{U}$ studied in Chapter 3 according to uniform/logarithmic distribution. Furthermore, we propose the accompanying nearest-action based control laws that are decomposable for simpler implementation and analysis. The closed-loop system with our NAC is then analyzed using absolute stability analysis approach to establish global exponential (practical) stability. In addition, we propose the use of weak sector condition for multi-input multi-output system in the analysis as opposed to the strong sector condition used in [23, 37].

1.3.2 Outline and Contributions Part II

The second part of this thesis studies primarily the development of energy-based hydrodynamic model for understanding the behavior of one-column floaters array connected to MPP-PTO units as part of the Ocean Grazer's project. The

main consideration for the model is to accurately describe the behavior of the OG-WEC along with its MPP-PTO systems. In addition, energical properties of each subsystem in OG-WEC are to be understood.

The results of the second part of this thesis are found in Chapter 6 and Chapter 7. In Chapter 6, we propose a port-Hamiltonian (pH) approach to the well-known Cummins' equation. One of the main contribution of this chapter is the development of the radiation subsystem's model in pH framework. In particular, an approximation of the radiation kernel via enforced positive realness is proposed. The resulting model is validated against existing hydrodynamic modeling toolbox by considering simplified linear power take-off system in the model.

Finally, we extend our work with simplified linear PTO in Chapter 6 by considering instead the interconnection with MPP-PTO units that represents the OG-WEC. The resulting model is delivered and validated in Chapter 7. In addition, a simplified version of the model in Chapter 7 is used as an academic example in Chapter 5.

Chapter 2 | Preliminaries

"To solve math problems, you need to know the basic mathematics before you can start applying it"
-Catherine Asaro-

Contents

In this chapter we review some relevant existing results on practical stabilization of systems with countable set of information/actuation as well as some relevant notations. The information provided in this chapter are mainly for Part I of this thesis.

2.1 Class $\mathcal{K}$, $\mathcal{K}_\infty$, and $\mathcal{KL}$ function

A continuous function $\gamma : \mathbb{R}_{\geq 0} \to \mathbb{R}_{\geq 0}$ is of class $\mathcal{K}$ if it is continuous, strictly increasing, and $\gamma(0) = 0$. We say that $\gamma : \mathbb{R}_{\geq 0} \to \mathbb{R}_{\geq 0}$ is of class $\mathcal{K}_\infty$ if γ is of

class $\mathcal{K}$ and $\lim_{s\to\infty}\gamma(s)=\infty$. A continuous function $\omega:\mathbb{R}_{\geq 0}\times\mathbb{R}_{\geq 0}\to\mathbb{R}_{\geq 0}$ is of class $\mathcal{KL}$ if for each fixed s, $\omega(r,s)$ belongs to class $\mathcal{K}$, and for each fixed r, $\omega(r,s)$ is decreasing with respect to s and is such that $\omega(r,s)\to 0$ as $s\to\infty$.

2

2.2 Passive systems and observability notions

2.2.1 Passivity nonlinear systems and norm observability

We consider nonlinear systems described by

$$\Sigma\ :\begin{cases}\dot{x}=f(x)+g(x)u\\ y=h(x)\end{cases} \tag{2.1}$$

where the state $x(t)\in\mathbb{R}^n$ and the input and output signals $u(t),y(t)\in\mathbb{R}^m$. The functions f, g, and h are assumed to be continuously differentiable, $f(0)=0$, $g(x)$ is full-rank for all x, and $h(0)=0$.

The fundamental property that we associate with Σ is that, it is *passive*, i.e., for all pairs of input and output signals u,y, we have $\int_0^T\langle y(t),u(t)\rangle\mathrm{d}t>-\infty$ for all $T>0$; see [38, 39, 40] for some primary references on passive systems. By the well-known Hill-Moylan conditions, the passivity of Σ implies that there exists a positive definite storage function $H:\mathbb{R}^n\to\mathbb{R}_{\geq 0}$ such that $\langle\nabla H(x),f(x)\rangle\leq 0$ and $\langle\nabla H(x),g(x)\rangle=h^\top(x)$. Without loss of generality, we assume that the storage function H is *proper*, i.e. all level sets of H are compact.

Using the passivity assumption on Σ, it is immediate to see that $u\equiv 0$ implies that all level sets of H are positively invariant. More precisely, for any $c>0$, if $H(x(0))\leq c$ then $H(x(t))\leq c$ for all $t\geq 0$. In other words, if we initialize the state of Σ such that $x(0)\in\Omega_c:=\{\xi|H(\xi)\leq c\}$ with $u\equiv 0$ then $x(t)\in\Omega_c$ for all $t\geq 0$. We will use this property later to establish the practical stability of our closed-loop systems in conjunction with the following observability notion from [41].

Definition 2.1. The system (2.1) is large-time initial-state norm observable if there exist $\tau>0$, and $\gamma,\chi\in\mathcal{K}_\infty$ such that the solution x of (2.1) satisfies

$$\|x(t)\|\leq\gamma(\|y\|_{[t,t+\tau]})+\chi(\|u\|_{[t,t+\tau]})$$

for all $t\geq 0$, $x(0)\in\mathbb{R}^n$, and locally essentially bounded and measurable inputs $u:\mathbb{R}_{\geq 0}\to\mathbb{R}^m$. ⋄

In this thesis, we will use the large-time initial-state norm observability property for the autonomous system (with $u=0$):

$$\dot{x}=f(x),\qquad y=h(x). \tag{2.2}$$

In this case, large-time initial-state norm observability of (2.2) implies

$$\exists\, \tau > 0, \gamma \in \mathcal{K}_\infty \text{ such that, for each } x(0) \in \mathbb{R}^n,$$
$$\|x(t)\| \leq \gamma(\|y\|_{[t,t+\tau]}), \quad \forall t \geq 0. \quad (2.3)$$

We note that in the standard passivity-based control literature, the notion of zero-state observability or zero-state detectability is typically assumed for establishing the convergence of the state to zero in the Ω-limit set. However, these notions cannot be used to conclude the boundedness of the state trajectories given the bound on the output trajectories. Therefore, instead of using these notions, we will use the above large-time initial-state norm observability for deducing the practical stability based on the information on y in the Ω-limit set.

Remark 2.2. If the dynamics in system (2.2) are linear, that is, $\dot{x} = Ax$, $y = Cx$, and the pair (A, C) is observable, then one can quantify γ in (2.3) using the observability Gramian. In particular, if for $\tau > 0$

$$W_\tau(t) = \int_t^{t+\tau} e^{A^\top(s-t)} C^\top C e^{A(s-t)}\, \mathrm{d}s$$

then $x(t) = (W_\tau(t))^{-1} \int_t^{t+\tau} e^{A^\top(s-t)} C^\top y(s)\, ds$, for each $t \geq 0$, and $\tau > 0$, which in particular yields

$$\|x(t)\| \leq \|(W_\tau(t))^{-1}\| \int_t^{t+\tau} \|e^{A^\top(s-t)} C^\top\|\, \mathrm{d}s \sup_{s\in[t,t+\tau)} |y(s)|$$

for each $t \geq 0$, and any $\tau > 0$. ◇

2.2.2 Constant-incremental passivity of nonlinear systems

In many cases, the desired equilibrium point of the passive nonlinear system Σ as in (2.1) is not equal to the minimum of the associated storage function H. Instead, it may correspond to an arbitrary constant input. For these cases, a constant input $u^* \in \mathbb{R}^m$ with its corresponding steady-state solution $x^* \in \mathbb{R}^n$ defines the steady-state relation given by the set

$$\mathcal{E} := \left\{ (x^*, u^*) \in \mathbb{R}^n \times \mathbb{R}^m \,\middle|\, 0 = f(x^*) + g(x^*)u^* \right\}. \quad (2.4)$$

The problem of practically stabilizing the system Σ around $x^* \in \mathbb{R}^n$ is equivalent to practically stabilizing $\overline{x} = x - x^*$ around the origin, with $\overline{(\cdot)} = (\cdot) - (\cdot)^*$ denoting the incremental variable. Thus, the incremental system is given by

$$\overline{\Sigma} : \begin{cases} \dot{\overline{x}} &= \overline{f}(\overline{x}) + g(\overline{x} + x^*)\overline{u}, \\ \overline{y} &= h(\overline{x} + x^*) - h(x^*), \end{cases} \quad (2.5)$$

with $\overline{f}(\overline{x}) = f(\overline{x}+x^*) - f(x^*) + (g(\overline{x}+x^*) - g(x^*))u^*$. For this matter, the passivity of the mapping $\overline{u} \mapsto \overline{y}$ is, in the original system Σ, referred to as incremental passivity with respect to constant input; and is defined as follows [42].

Definition 2.3 (Constant Incremental Passivity). Consider the nonlinear system Σ as in (2.1). The system Σ is said to be incrementally passive with respect to constant input if, for every $(x^*, u^*) \in \mathscr{E}$, the corresponding incremental system $\overline{\Sigma}$ in (2.5) with input $\overline{u}$ and output $\overline{y}$, is passive; that is, there exists a storage function $H_0 : \mathbb{R}^n \to \mathbb{R}_{\geq 0}$ such that

$$\dot{H}_0 = \langle \nabla H_0, \dot{\overline{x}} \rangle \leq \langle \overline{u}, \overline{y} \rangle. \tag{2.6}$$

$\diamond$

Note that the incremental passivity is a stronger requirement than the passivity notion considered in the preceding subsections. In particular, one can find examples of systems which are passive but not incrementally passive. Also, constant incremental passivity defined above is equivalent to shifted passivity as in [39, 43] and equilibrium-independent passivity as in [44]. Nevertheless, the term constant incremental passivity is preferred in this paper because the pair (x^*, u^*) can be arbitrary and most importantly, the incremental function is used in the definition.

2.3 Set-valued analysis: Basic notions

2.3.1 Regularized differential inclusions

It turns out that a mapping which maps output from a continuum to a discrete set of control actions is essentially discontinuous (with respect to usual topology on $\mathbb{R}^m$). Differential equations with such state-dependent discontinuities need regularization so that the solutions are properly defined. For a discontinuous map $F : \mathbb{R}^n \to \mathbb{R}^n$, we can define a set-valued map $\mathscr{K}(F)$ by convexifying F as follows

$$\mathscr{K}(F(x)) := \bigcap_{\delta > 0} \overline{\text{co}}(F(x + \mathbb{B}_\delta))$$

where $\overline{\text{co}}(S)$ is the convex closure of S. The set-valued mapping $\mathscr{K}(F)$ is the Krasovskii regularization of F, and under certain regularity assumptions on F, $\mathscr{K}(F)$ is compact and convex-valued, and moreover it is upper semicontinuous [45, Chap. 1, Def. 1].

For an upper semicontinuous mapping $\Phi : \mathbb{R}^n \rightrightarrows \mathbb{R}^n$, consider the differential inclusion

$$\dot{x} \in \Phi(x) \qquad x(0) = x_0. \tag{2.7}$$

A Krasovskii solution $x(\cdot)$ on an interval $I = [0, T),\ T > 0$ is an absolutely continuous function $x : I \to \mathbb{R}^n$ such that (2.7) holds almost everywhere on I. It is *maximal* if it has no right extension and it is a *global* solution if $I = \mathbb{R}_{\geq 0}$. For any upper semicontinuous set-valued map Φ such that $\Phi(\xi)$ is compact and convex for every $\xi \in \mathbb{R}^n$, the following properties have been established (see, e.g., [45, Chap. 2, Theorem 3]): (i). the differential inclusion (2.7) has a solution on an interval I; (ii). every solution can be extended to a maximal one; and (iii). if the maximal solution is bounded then it is global.

2.3.2 Convex polytopes

Next, we present two basic representations of convex polytopes and some of their notable examples that are related to our problem. We refer to [46] and [47] for additional material on this topic. Firstly, the vertex representation (*V-representation*) of a convex polytope in $\mathbb{R}^m$ is an m-polytope defined by the convex hull of a finite set of points $\mathscr{U} \subset \mathbb{R}^m$; that is the m-polytope $\mathscr{P}_{\mathrm{V}}(\mathscr{U}) := \mathrm{conv}(\mathscr{U})$. Another way to define an m-polytope is by intersecting finite-number of half-spaces (*H-representation*) that is given by $\mathscr{P}_{\mathrm{H}}(A, b) := \{x \in \mathbb{R}^m | Ax \leq b\}$. Note that both representations of m-polytopes are equivalent, i.e. $\mathscr{P}_{\mathrm{V}}(\mathscr{U}) = \mathscr{P}_{\mathrm{H}}(A, b)$ with appropriate $A \in \mathbb{R}^{n \times m}$ and $b \in \mathbb{R}^n$. When it is clear from the context, we will omit the arguments in $\mathscr{P}_{\mathrm{V}}$ and $\mathscr{P}_{\mathrm{H}}$ in the rest of this thesis.

One simple example of m-polytopes is the m-dimensional simplex, commonly referred to as m-simplex. For particular examples, 1-simplex is a line, 2-simplex is a triangle, and 3-simplex is a tetrahedron.

Definition 2.4 (m-simplex). Let $\mathscr{S} := \{s_0, s_1, \ldots, s_m\}$ with $s_i \in \mathbb{R}^m$, $i = 0, 1, \ldots, m$ be an affinely independent set, i.e. for any $s_i \in \mathscr{S}$, the set $\widetilde{\mathscr{S}_i} := \{\tilde{s} \in \mathbb{R}^m \mid \tilde{s} = s_j - s_i, \forall s_j \in \mathscr{S} \setminus \{s_i\}\}$ is linearly independent. An m-simplex $\mathscr{S}_m$ is defined by,

$$\mathscr{S}_m = \mathrm{conv}(\mathscr{S}) := \left\{ \sum_{i=0}^{m} c_i s_i \;\middle|\; \sum_{i=0}^{m} c_i = 1,\ c_i \geq 0 \right\},$$

and we say that $b_{\mathscr{S}_m} = \frac{1}{m+1} \sum_{i=0}^{m} s_i$ is its barycenter. ◇

Example 2.5. One special case of m-simplices is a *regular* m-simplex $\mathscr{S}_{m,\mathrm{reg}}$ where all vertices have equal distances to its barycenter and, one possibly simple choice for such a simplex is $\mathscr{S}_{m,\mathrm{reg}} := \mathrm{conv}\left(\mathscr{S}_{\mathrm{reg}}\right)$ where

$$\mathscr{S}_{\mathrm{reg}} = \lambda \left\{ e_1, \ldots, e_m, \frac{1 - \sqrt{m+1}}{m} \mathbb{1} \right\} \tag{2.8}$$

for some $\lambda \in \mathbb{R}_{>0}$. ◇

For our purposes, the utility of convex polytopes is seen in partitioning the output space $\mathbb{R}^m$ into a finite number of cells which can then be associated to a control action. In particular, given a finite set $\mathscr{S} \subset \mathbb{R}^m$ with $\mathrm{card}(\mathscr{S}) = q$, the space $\mathbb{R}^m$ can be partitioned into q number of cells where every cell contains all points in $\mathbb{R}^m$ that are closer to an element of $\mathscr{S}$ than any other element. Such cells are commonly referred to as Voronoi cells and are defined as follows.

Definition 2.6. Consider a countable set $\mathscr{S} \subset \mathbb{R}^m$. The Voronoi cell of a point $s \in \mathscr{S}$ is defined by

$$V_{\mathscr{S}}(s) := \{x \in \mathbb{R}^m \mid \|x - s\| \leq \|x - v\|,\ \forall v \in \mathscr{S} \setminus \{s\}\}.$$

◇

Remark 2.7. Note that every Voronoi cell is a closed and convex polyhedron since they can always be represented by the solution of a system of linear inequalities. ◇

2.4 Multi Agent Systems

We consider an undirected graph $\mathscr{G} = (\mathscr{V}, \mathscr{E})$ for describing the network topology of a multi-agent system, where $\mathscr{V}$ is the set of N agents and $\mathscr{E} \subset \mathscr{V} \times \mathscr{V}$ is a set of M edges that define the neighboring pairs. In this thesis, we assume that the graph $\mathscr{G}$ is connected. For every edge k in $\mathscr{G}$, we can associate one node by a positive sign and the pairing node by a negative sign. Correspondingly, the incidence matrix $B \in \mathbb{R}^{N \times M}$ can be defined by

$$b_{i,k} = \begin{cases} +1 & \text{if node } i \text{ has the positive sign in edge } k \\ -1 & \text{if node } i \text{ has the negative sign in edge } k \\ 0 & \text{otherwise} \end{cases}$$

Using B, the Laplacian matrix L is given by $L = BB^\top$ whose kernel, by the connectedness of $\mathscr{G}$, is spanned by $\mathbb{1}_N$.

2.4.1 Multi-Agent Consensus

For every agent i in $\mathscr{G}$, it is described by

$$\dot{x}_i = u_i. \tag{2.9}$$

where $x_i(t) \in \mathbb{R}^m$ and $u_i(t) \in \mathbb{R}^m$ denote the state and input variables, respectively. The distributed consensus control problem is related to the design of distributed control law u_i for each agent based on the information from the neighboring agents so that all agents converge to a consensus point. The well-known control law $u = -(L \otimes I_m)x$ solves this problem, where it can be shown that by using the consensus Lyapunov function $V(x) = \frac{1}{2}\langle x, (L \otimes I_m)\, x\rangle$,

$\lim_{t\to\infty}\|x_i(t)-\bar{x}\|=0$ for all i and $\bar{x}=\frac{1}{N}\sum_i x(0)\in\mathbb{R}^m$. We define the consensus manifold E where all agents agree with each other by $E:=\{\bar{x}\in\mathbb{R}^{mN}|\bar{x}=\bar{x}_1=\bar{x}_2=\ldots=\bar{x}_N\}$.

The stability of the closed-loop system is, in fact, carried out by introducing the relative position variable

$$z_k=\begin{cases}x_i-x_j & \text{if node } i \text{ is the positive end of edge } k,\\ x_j-x_i & \text{if node } i \text{ is the negative end of edge } k,\end{cases} \tag{2.10}$$

and we write its compact form as $z=(B^\top\otimes I_m)x$. The closed-loop system of the consensus problem is then expressed as

$$\dot{z}=-(B^\top B\otimes I_m)z \tag{2.11}$$

and the consensus Lyapunov function becomes $V(z)=\frac{1}{2}\langle z,z\rangle$ so that stability can then be shown by using LaSalle's invariance principle. That is, $z\to 0$ as $t\to\infty$.

The generalization of the result to the case, where binary and ternary quantizers are used, can be found in [3, 4, 21].

2.4.2 Distance-Based Multi-Agent Formation Control

Consider the same set of n agents as described in section 2.4.1. The distributed distance-based formation control problem is, in principal, similar to the control design for consensus problem. The main difference is that in the asymptote, all agents must converge to a prescribed *infinitesimally rigid* formation shape represented by the framework $(\mathcal{G}=(\mathcal{V},\mathcal{E}),x)$ and the given desired distance between connected agents. The framework $(\mathcal{G},x)$ is said to be infinitesimally rigid if $\operatorname{rank}(R(z))=mN-(m+1)\frac{m}{2}$ where $R(z)=D_z^\top(B^\top\otimes I_m)$ is the *rigidity matrix* and D_z takes the form of the block-diagonal matrix $D_z:=\operatorname{diag}(z)\in\mathbb{R}^{Mm\times M}$ with z being the relative position vector as defined in section 2.4.1 [48, 49, 50]. For given desired distance d_k associated to the relative position z_k, $k=1,\ldots,M$, the well-known control law $u=-(B\otimes I_m)D_z e$ where e is the desired error vector defined by

$$e=\begin{bmatrix}\|z_1\|^2-d_1^2, & \cdots, & \|z_M\|^2-d_M^2\end{bmatrix}^\top \tag{2.12}$$

solves the distance-based distributed formation control under the assumption that the given formation graph is infinitesimally rigid.

The stability of above distributed formation control problem can be analyzed by considering the dynamics of the closed-loop autonomous multi-agent system given by

$$\dot{z}=(B^\top\otimes I_m)\dot{x}=-(B^\top B\otimes I_m)D_z e \tag{2.13}$$

$$\dot{e}=D_z^\top\dot{z}=-D_z^\top(B^\top B\otimes I_m)D_z e. \tag{2.14}$$

Using the usual distance-based formation Lyapunov function $J(e) = \frac{1}{4}\langle e, e\rangle$, the local exponential convergence of e to zero can be shown, which means that $\|z_k(t)\| \to d_k$ locally and exponentially as $t \to \infty$.

2

2.5 Positive Real Functions and H^∞ space

Let $G : \mathbb{C} \to \mathbb{C}^{m\times m}$ be a matrix valued complex function. We say that G is positive real if

$$G(s) + G*(s) \succcurlyeq 0, \ \forall s \in \mathbb{C}_+, \ s \text{ not a pole of } G,$$

where $G*$ is the conjugate transpose of G. Moreover, we say that G is strictly positive real if there exists a scalar $\delta > 0$ such that $G - \delta I \succcurlyeq 0$. The space H^∞ is defined by $H^\infty := \{G : \mathbb{C} \to \mathbb{C}^{m\times m} \mid G \text{ is holomorphic and } \|G\|_{H^\infty} := \sup_{s\in\mathbb{C}_+} \|G(s)\| < \infty\}$.

2.6 Absolute stability, ISS & practical stability

Consider the following Lur'e systems

$$\Sigma_{\text{lin}} : \begin{cases} \dot{x}(t) &= Ax(t) + Bu(t) \\ y(t) &= Cx(t) \\ u(t) &\in \Delta(t) - \Psi(y(t)), \end{cases} \tag{2.15}$$

where $x(t) \in \mathbb{R}^n$ is the state, $u(t), y(t) \in \mathbb{R}^m$ are the input and output, respectively, $\Delta : \mathbb{R}_{\geq 0} \to \mathbb{R}^m$ is a locally essentially bounded and a locally integrable function, the matrices A, B, and C are real matrices of suitable dimension, and $\Psi : \mathbb{R}^m \rightrightarrows \mathscr{U}$ with $\mathscr{U} \subseteq \mathbb{R}^m$ is a set-valued nonlinearity. The function $\Delta(t)$ embeds all exogeneous signals, possibly unknown, that can enter the nonsmooth system. When $\Delta \equiv 0$, the system (2.15) can be considered as a closed-loop interconnection of a linear differential inclusion system with system matrices (A, B, C) and a set-valued nonlinearity Ψ. The transfer function of Σ_{lin} is given by $G(s) = C(sI - A)^{-1}B$. The system (2.15) is said to be input-to-state practical stable (ISpS) if there exist $\beta \in \mathscr{KL}$, $\theta > 0$ and $\rho \in \mathscr{K}_\infty$ such that, for all $x(0) \in \mathbb{R}^n$, the solution of (2.15) satisfies

$$\|x(t)\| \leq \beta(\|x(0)\|, t) + \rho(\|\Delta_{[0,t]}\|_\infty) + \theta, \ \forall t \geq 0. \tag{2.16}$$

The system (2.15) is input-to-state stable if it is ISpS with $\theta = 0$.

In [20, 23, 37], the ISpS property of MIMO LTI system (2.15) has been established based on the system matrices (A, B, C) and a strong sector bound condition of Ψ. The sector condition imposed on Ψ is given by $\langle k_1 y - v, k_2 y - v\rangle \leq 0, \ \forall v \in \Psi(y), \ \forall y \in \mathbb{R}^m$ for some scalars $k_1 < k_2$. It will be clear later in Chapter 5 that such sector condition is stronger than the more familiar sector

condition $k_1\|y\|^2 \leq \langle v, y\rangle \leq k_2\|y\|^2,\ \forall v \in \Psi(y),\ \forall y \in \mathbb{R}^m$ for some scalars $k_1 < k_2$.

Remark 2.8 ([23, Remark 3.1]). For some scalars $k_1 < k_2$, the sector condition

$$\langle k_1 y - v, k_2 y - v\rangle \leq 0$$

holds for all $v \in \Psi(y)$ and for all $y \in \mathbb{R}^m$ if and only if

$$\left\| v - \frac{k_1 + k_2}{2} y \right\| \leq \frac{k_2 - k_1}{2}\|y\|,\ \forall v \in \Psi(y),\ \forall y \in \mathbb{R}^m. \tag{2.17}$$

◇

The adaptation of the ISpS property of (2.15) in [23, Theorem 3.4] with stronger controllability and observability condition is stated in the following theorem.

Theorem 2.9. Consider the system Σ_{lin} in (2.15). Suppose that the pair (A, B) is controllable and (A, C) is observable. For the mapping Ψ, assume that there exist scalars $k_1 < k_2$ such that for all $v \in \Psi(y)$ and for all $y \in \mathbb{R}^m$, it holds that $\langle k_1 y - v, k_2 y - v\rangle \leq 0$. In addition, assume that $G(I + k_1 G)^{-1} \in H^\infty$ and that $(I + k_2 G)(I + k_1 G)^{-1}$ is strictly positive real. Then every maximal solution forward complete and there exist positive constants c_1, c_2, and ε such that, for all $x(0) \in \mathbb{R}^n$, every solution x satisfies

$$\|x(t)\| \leq c_1 e^{-\varepsilon t}\|x(0)\| + c_2\|\Delta_{[0,t]}\|_\infty,\ \forall t \in \mathbb{R}_{>0}. \tag{2.18}$$

◇

The proof follows directly from the proof of [23, Theorem 3.4]. It can be seen from above that under the stated assumptions, the solution of (2.15) decays exponentially.

2.7 Uniform and Logarithmic Quantizers

There are two standard types of quantization in literature, namely, the uniform and logarithmic quantizers [22, 51]. The range set of uniform quantizer is a regular grid and can be described by the set $\mathscr{U}_u^\lambda := \{\pm k\lambda \mid k \in \mathbb{Z}_{\geq 0}\}$ with $\lambda > 0$ be the desired uniform step size. One of the standard approach in the uniform quantization is the symmetric uniform quantizer given by

$$Q_u^\lambda(\eta) = \left\lfloor \frac{\eta}{\lambda} + \frac{1}{2} \right\rfloor \lambda. \tag{2.19}$$

Similarly, the range set of logarithmic quantizer is a regular grid and is given by the set $\mathscr{U}_l^\lambda := \{0\} \cup \{\pm\lambda^k \mid k \in \mathbb{Z}\}$ with $\lambda > 1$ be the desired geometric

step size. One example of the logarithmic quantizers is the mapping

$$Q_l^\lambda(\eta) = \begin{cases} 0, & \eta = 0 \\ \text{sign}(\eta)\lambda^{\lfloor \frac{1}{2} + \log_\lambda |\eta| \rfloor}, & \eta \neq 0. \end{cases} \tag{2.20}$$

Note that both the uniform quantizer (2.19) and the logarithmic quantizer (2.20) are scalar functions. Typically, in the vectorized setting, the above quantizers are defined element-wise.

Part I

Nearest Action Control

Contents of this part are based on the following publications:

- B Jayawardhana, **MZ Almuzakki**, and A Tanwani, “Practical Stabilization of Passive Nonlinear Systems with Limited Control," *11th IFAC Symposium on Nonlinear Control Systems (NOLCOS)*, 2019. *(Chapter 3)*
- **MZ Almuzakki**, B Jayawardhana, and A Tanwani, “Nearest neighbor control for practical stabilization of passive nonlinear systems," *Automatica*, vol. 141, p. 110278, 2022. *(Chapter 3)*
- **MZ Almuzakki** and B Jayawardhana, “Cooperative Nearest-Neighbor Control of Multi-Agent Systems: Consensus and Formation Control Problems," *IEEE Control Systems Letters*, vol. 7, pp. 1873-1878, 2023. *(Chapter 4)*
- **MZ Almuzakki**, B Jayawardhana, A Tanwani, and A Vakis, “Exponential Stability of LTI Systems with Infinitely Countable Input Set via Nearest-Action Control," *Submitted*. *(Chapter 5)*

This page intentionally left blank.

Chapter 3 | Nearest Action Control

"Mathematics is a game played according to certain simple rules
with meaningless marks on paper"
-David Hilbert-

Contents

In this chapter, we consider nonlinear systems described by

$$\Sigma : \begin{cases} \dot{x} = f(x) + g(x)u \\ y = h(x) \end{cases} \tag{3.1}$$

where the state $x(t) \in \mathbb{R}^n$ and the input and output signals $u(t), y(t) \in \mathbb{R}^m$. The functions f, g, and h are assumed to be continuously differentiable, $f(0) = 0$, $g(x)$ is full-rank for all x, and $h(0) = 0$. The underlying assumption throughout this chapter is that the input-output system Σ is passive (in appropriate sense). The basic problem we study in this chapter is the stabilization of Σ under limited actuation/information transmission; that is, the control input u can only take values from a finite countable set $\mathscr{U} := \{u_0, u_1, u_2, \ldots, u_p\}$ with $u_i \in \mathbb{R}^m$ for each $i = 0, \ldots, p$.

For the nominal system, it is assumed that we have a stabilizing output feedback law $y \mapsto F(y)$ (when $\mathscr{U}$ is a continuum). As discussed in the introduction, when we impose the constraint that the actuation set $\mathscr{U}$ is finite, two relevant questions for its stabilization are: a) how to map $F(y)$ to an element

in $\mathscr{U}$?; and b) how to determine the minimal cardinality of $\mathscr{U}$? To address these questions for the system class Σ, we design a mapping $\phi : \mathbb{R}^m \to \mathscr{U}$, with $\mathscr{U}$ being finitely countable (and possibly minimal), such that $u = \phi(F(y)) \in \mathscr{U}$ practically stabilizes Σ.

The question of designing the quantization mapping $\phi : \mathbb{R}^m \to \mathscr{U}$ has been addressed in various forms in literature as discussed in Chapter 1. Since the input can only take the available values in the finite countable set $\mathscr{U}$, the quantizer ϕ, in some senses, defines the partition of the input space with respect to $\mathscr{U}$, where each cell of the partition is associated to an element of the set $\mathscr{U}$. In this chapter, we address the question of designing ϕ by fixing the cardinality of the set $\mathscr{U}$ which results in convergence to an *arbitrarily small* ball around the origin. In particular, by exploiting the passivity structure of Σ and using a quantizer based on Voronoi tessellations, we provide conditions relating system dynamics and geometry of the partitions that guarantee practical stability with a finite countable input set $\mathscr{U}$ of fixed cardinality (which will be specified precisely in the discussion that follows).

3.1 Nearest-Action Control for Passive Systems

In this section, we present firstly the practical stabilization result of the origin of general passive systems with unity output feedback and is followed by sector-bounded nonlinearity in the feedback loop. For this purpose, we impose the following assumption on the system Σ.

(A3.0) The system Σ in (3.1) is passive with a proper and positive definite storage function H and, the corresponding autonomous system $\Sigma|_{u=0}$ is large-time initial-state norm-observable for some $\tau > 0$ and $\gamma \in \mathcal{K}_\infty$.

Secondly, we present briefly its extension to practically stabilize constant-incrementally passive systems with corresponding assumption established similar to (A3.0). The motivation behind our design of these elements is to work with minimal number of elements in the set $\mathscr{U}$ which yield the desired performance using the static output feedback only. Toward this end, the only assumption we associate with the set $\mathscr{U}$ is the following:

(A3.1) For a given finite countable set $\mathscr{U} := \{u_0, u_1, u_2, \ldots, u_p\}$, with $u_0 = 0$, there exists an index set $\mathscr{I} \subset \{1, \ldots, p\}$ such that the set $\mathscr{V} := \{u_i\}_{i \in \mathscr{I}} \subset \mathscr{U}$ defines the vertices of a convex polytope satisfying, $0 \in \text{int}\,(\text{conv}\,(\mathscr{V}))$.

An immediate consequence of (A3.1) is the following lemma, which is used in the derivation of our forthcoming main result.

Lemma 3.1. Consider a finite countable set $\mathscr{U} \subset \mathbb{R}^m$ that satisfies (A3.1). Then, there exists $\delta > 0$ such that the Voronoi cell of the origin with respect to $\mathscr{U}$ satisfies

$$V_{\mathscr{U}}(0) \subseteq \mathbb{B}_\delta. \tag{3.2}$$

That is, the following implication holds for each $\eta \in \mathbb{R}^m$

$$\|\eta\| > \delta \Rightarrow \ \exists\, u_i \in \mathscr{U} \text{ s.t. } \|\eta - u_i\| < \|\eta\|. \tag{3.3}$$

$\diamond$

Proof. Based on Assumption (A3.1), consider the sets $\mathscr{I} := \{1, \dots, q\}$, and $\mathscr{V} := \{v_1, \dots, v_q\} \subset \mathscr{U}$ such that $q \leq p$ and $0 \in \operatorname{int}(\operatorname{conv}(\mathscr{V}))$. Let $\mathscr{S} = \mathscr{V} \cup \{0\}$. From the definition of Voronoi cells, it readily follows that $V_{\mathscr{U}}(0) \subseteq V_{\mathscr{S}}(0)$, and therefore, it suffices to show that $V_{\mathscr{S}}(0) \subset \mathbb{B}_\delta$. Toward that end, we first observe that the Voronoi cell $V_{\mathscr{S}}(0)$ can be described as

$$V_{\mathscr{S}}(0) := \mathscr{P}_{\mathrm{H}}\left(\begin{bmatrix} v_1 & \dots & v_q \end{bmatrix}^\top, \ \frac{1}{2}\begin{bmatrix} \|v_1\|^2 & \dots & \|v_q\|^2 \end{bmatrix}^\top\right). \tag{3.4}$$

Thus, from (3.4), we know that $V_{\mathscr{S}}(0)$ is a closed convex polyhedron. It remains to show that $V_{\mathscr{S}}(0)$ is bounded. Indeed, boundedness implies that we can choose $\delta = \max_{\tilde{v} \in V_{\mathscr{S}}(0)} (\|\tilde{v}\|)$, such that $\mathbb{B}_\delta$ is the smallest ball containing the set $V_{\mathscr{S}}(0)$, which by definition of Voronoi cell is equivalent to (3.3).

To show that $V_{\mathscr{S}}(0)$ is bounded, we observe that, under (A3.1), there exists $\mu > 0$ such that $\mathbb{B}_\mu \subset \operatorname{conv}(\mathscr{V})$. Thus, for every $\tilde{v} \in V_{\mathscr{S}}(0)$, $\mu \frac{\tilde{v}}{\|\tilde{v}\|} \in \operatorname{conv}(\mathscr{V})$. Hence, there exist $\lambda_i \geq 0$ such that $\sum_{i=1}^q \lambda_i = 1$ and $\mu \frac{\tilde{v}}{\|\tilde{v}\|} = \sum_{i=1}^q \lambda_i v_i$. Consequently, from (3.4), it follows that

$$\mu \frac{\tilde{v}^\top \tilde{v}}{\|\tilde{v}\|} = \sum_{i=1}^q \lambda_i v_i^\top \tilde{v} \leq \frac{1}{2} \sum_{i=1}^q \lambda_i \|v_i\|^2$$

and hence $\|\tilde{v}\| \leq \frac{1}{2\mu} \sum_{i=1}^q \lambda_i \|v_i\|^2$. $\square$

Example 3.2. A simple example of $\mathscr{U}$ in $\mathbb{R}^2$, satisfying (A3.1) is as follows:

$$\begin{aligned} \mathscr{U}_{\mathrm{ex}} &:= \alpha \left\{0, \begin{bmatrix} \sin(\theta_{\mathrm{ex}}) \\ \cos(\theta_{\mathrm{ex}}) \end{bmatrix}, \begin{bmatrix} \sin\left(\theta_{\mathrm{ex}} + \frac{2\pi}{3}\right) \\ \cos\left(\theta_{\mathrm{ex}} + \frac{2\pi}{3}\right) \end{bmatrix}, \begin{bmatrix} \sin\left(\theta_{\mathrm{ex}} + \frac{4\pi}{3}\right) \\ \cos\left(\theta_{\mathrm{ex}} + \frac{4\pi}{3}\right) \end{bmatrix}\right\} \\ &=: \left\{0, u_{\mathrm{ex},1}, u_{\mathrm{ex},2}, u_{\mathrm{ex},3}\right\} \end{aligned} \tag{3.5}$$

with some $\theta_{\mathrm{ex}} \in \mathbb{R}$ and $\alpha \in (0, \infty)$. For this example, (A3.1) holds by taking $\mathscr{V} := \mathscr{U} \setminus \{0\}$. Following the proof of Lemma 3.1, we have $V_{\mathscr{U}}(0) := \operatorname{conv}\left(\widetilde{\mathscr{V}_0}\right)$ where

$$\widetilde{\mathscr{V}_0} := \alpha \left\{ \begin{bmatrix} \sin\left(\theta_{\mathrm{ex}} + \frac{\pi}{3}\right) \\ \cos\left(\theta_{\mathrm{ex}} + \frac{\pi}{3}\right) \end{bmatrix}, \begin{bmatrix} \sin\left(\theta_{\mathrm{ex}} + \frac{3\pi}{3}\right) \\ \cos\left(\theta_{\mathrm{ex}} + \frac{3\pi}{3}\right) \end{bmatrix}, \begin{bmatrix} \sin\left(\theta_{\mathrm{ex}} + \frac{5\pi}{3}\right) \\ \cos\left(\theta_{\mathrm{ex}} + \frac{5\pi}{3}\right) \end{bmatrix} \right\}.$$

Then, then the smallest δ that satisfies (3.2) in Lemma 3.1 is given by $\delta = \alpha$. $\diamond$

3.1.1 Unity output feedback

Using the result of Lemma 3.1 and the assumptions introduced thus far, we can define a feedback mapping $\phi_{\mathscr{U}}$ which maps the measured outputs to the finite countable set $\mathscr{U}$ to achieve practical stabilization. In this regard, we first consider the so called nearest-action mapping $\phi_{\mathscr{U}} : \mathbb{R}^m \rightrightarrows \mathscr{U}$, defined as

$$\phi_{\mathscr{U}}(\eta) := \underset{v \in \mathscr{U}}{\arg\min} \{\|v - \eta\|\}. \tag{3.6}$$

For the nearest-action mapping above, the following lemma is relevant.

Lemma 3.3. Consider the nearest-action mapping $\phi_{\mathscr{U}}$ given in (3.6) and a finite countable set $\mathscr{U} := \{0, u_1, u_2, \ldots, u_p\}$ satisfying (A3.1). For a fixed $y \in \mathbb{R}^m$, let $\phi_{\mathscr{U}}(-y) = \{u_j\}_{j \in \mathscr{J}}$ for some index set $\mathscr{J} \subset \{1, \ldots, p\}$. Then the inequality

$$-\|u_j\| \cdot \|y\| \leq \langle u_j, y \rangle \leq -\frac{1}{2}\|u_j\|^2 \tag{3.7}$$

holds for all $j \in \mathscr{J}$. ◇

Proof. By the definition of $\phi_{\mathscr{U}}$, the inequality $\|u_j + y\|^2 \leq \|u_k + y\|^2$ holds for $j \in \mathscr{J}$ and $k \in \{0, 1, \ldots, p\}$. By noting that $\|u_j + y\|^2 = \langle u_j + y, u_j + y \rangle = \|u_j\|^2 + 2\langle u_j, y \rangle + \|y\|^2$ and fixing $u_k = 0$, we have that $\langle u_j, y \rangle \leq -\frac{1}{2}\|u_j\|^2$. Moreover $\langle u_j, y \rangle \geq -\|u_j\|\|y\|$. Hence, the inequality (3.7) holds for every $y \in \mathbb{R}^m$. □

For a given output feedback $y \mapsto F(y)$, the quantized feedback control $u = \phi_{\mathscr{U}}(F(y))$, with ϕ given in (3.6), maps $F(y)$ to the nearest element in the set $\mathscr{U}$ with respect to the Euclidean distance. As a straightforward observation, when $\mathscr{U}$ is the continuum space $\mathbb{R}^m$, the solution to the optimization problem (3.6) is $u = \phi_{\mathscr{U}}(F(y)) = F(y)$. Let us first restrict ourselves to the unity output feedback case $F(y) = -y$. By choosing $u = \phi_{\mathscr{U}}(-y)$, the closed system is thus given by

$$\begin{aligned} \dot{x} &= f(x) + g(x)\phi_{\mathscr{U}}(-y) \\ y &= h(x). \end{aligned} \tag{3.8}$$

As $\phi_{\mathscr{U}}(-y)$ is a nonsmooth mapping, we consider instead the following regularized differential inclusion

$$\begin{aligned} \dot{x} &\in \mathscr{K}\big(f(x) + g(x)\phi_{\mathscr{U}}(-y)\big) = f(x) + g(x)\mathscr{K}(\phi_{\mathscr{U}}(-y)) \\ y &= h(x). \end{aligned} \tag{3.9}$$

We note that the solution of (3.8) is basically interpreted in the sense of (3.9). In the following result, we analyze the asymptotic behavior of the solutions of (3.9) and show that they converge to $\mathbb{B}_\epsilon$, for a given $\epsilon > 0$, if the constant δ associated to the set $\mathscr{U}$ in (3.2) is small enough. For a set $\mathscr{U}$ that satisfies

(A3.1), we can reposition its elements without changing the cardinality of $\mathscr{U}$ to get a desired value of $\delta > 0$, and such constructions are addressed in Section 3.2.

Proposition 3.4. Consider a nonlinear system Σ described by (3.1) that satisfies (A3.0), and a finite countable set $\mathscr{U} \subset \mathbb{R}^m$ satisfying (A3.1) so that (3.2) holds for some $\delta > 0$. For a given $\epsilon > 0$, assume that

$$\gamma(\delta) \leq \epsilon. \tag{3.10}$$

Then the control law $u = \phi_{\mathscr{U}}(-y)$, with $\phi_{\mathscr{U}}$ given in (3.6), globally practically stabilizes Σ with respect to $\mathbb{B}_\epsilon$, that is, $\limsup_{t\to\infty} |x(t)| \leq \epsilon$. ⋄

Proof. Based on the property of $\langle \phi_{\mathscr{U}}(-y), y\rangle$ in Lemma 3.3, we can analyze the behavior of the closed-loop system given by (3.9) as follows.

For the storage function H associated with the open-loop system, we evaluate its derivative along the solutions of (3.9) in following two cases:
(i): $0 \notin \phi_{\mathscr{U}}(-y) = \{u_i\}_{i\in J_y}$ so that $J_y \subset \{1,\dots,p\}$. Let $\mathscr{W}_y := \phi_{\mathscr{U}}(-y)$, then

$$\begin{aligned}\dot{H}(x) &= \langle \nabla H(x), \dot{x}\rangle \\ &\in \langle \nabla H(x), f(x) + g(x)\mathscr{K}(\phi_{\mathscr{U}}(-y))\rangle \\ &= \langle \nabla H(x), f(x)\rangle + \langle y, \mathrm{conv}(\mathscr{W}_y)\rangle.\end{aligned}$$

Based on the computation of $\langle \phi_{\mathscr{U}}(-y), y\rangle$, with non-zero $\phi_{\mathscr{U}}(-y)$, it follows that

$$\langle y, \mathrm{conv}(\mathscr{W}_y)\rangle \subset \big[-\|u_{y,\max}\|\,\|y\|\,, -0.5\,\|u_{y,\min}\|^2\big],$$

where we let $\|u_{y,\max}\| := \max_{w\in\mathscr{W}_y}\|w\|$, and $\|u_{y,\min}\| := \min_{w\in\mathscr{W}_y}\|w\|$. Therefore, $\dot{H}(x) \leq -0.5\,\|u_{y,\min}\|^2$; when $0 \notin \phi_{\mathscr{U}}(-y)$, or the other possibility is that,
(ii): $0 = \phi_{\mathscr{U}}(-y) = \{u_0\} = \mathscr{W}_y$ so that $J_y = \{0\}$. In this case, following the same arguments as in case **(i)**

$$\dot{H}(x) \in \langle \nabla H(x), f(x)\rangle + \langle y, \mathrm{conv}(\mathscr{W}_y)\rangle.$$

Since $\{0\}$ is the only element of $\mathscr{W}_y$, $\langle y, \mathrm{conv}(\mathscr{W}_y)\rangle = \{0\}$. This implies that, for the case when $\phi_{\mathscr{U}}(y) = \{0\}$, we have $\dot{H}(x) = 0$.

Combining the two cases, it holds that for $J_y \subset \{0,1,\dots,p\}$, we have $\dot{H}(x) \leq 0$, and $\dot{H}(x) = 0$, if and only if $0 \in \phi_{\mathscr{U}}(-y)$. As $H(x)$ is non-increasing along system trajectories in both the cases **(i)** and **(ii)**, and since H is proper, all system trajectories are bounded and contained in the compact set $\Omega_0 := \{z \in \mathbb{R}^n \,|\, H(z) \leq H(x(0))\}$. Let $\mathscr{Z}_x := \{z \in \mathbb{R}^n \,|\, \phi_{\mathscr{U}}(-h(z)) = \{0\}\}$ and let M be the largest invariant set (with respect to system (3.9)) contained in $\mathscr{Z}_x$. By the LaSalle invariance principle, all trajectories belonging to the compact set Ω_0 converge to the set M, see for example [19, Theorem 6.5].

We next show that, because of the large-time norm observability and Lemma 3.1, it holds that $M \subset \mathbb{B}_\epsilon \subset \mathbb{R}^n$. To see this, take an arbitrary point $z \in M$, and consider a solution of system (3.9) over an interval $[s, s+\tau]$ starting from z; that is, consider $x : [s, s+\tau] \to \mathbb{R}^n$ which solves (3.9) and $x(s) = z \in M$. Due to the forward invariance of set M, the corresponding solution $x(t) \in M$, for each $t \in [s, s+\tau]$. Consequently, $\phi_{\mathscr{U}}(-h(x(t))) = \{0\}$, and because of Lemma 3.1, $|h(x(t))| \leq \delta$ for each $t \in [s, s+\tau]$. Invoking the large-time initial state norm-observability assumption, it holds that $\|x(s)\| = \|z\| \leq \gamma(\delta) \leq \epsilon$, where the last inequality is a consequence of (3.10). Since $z \in M$ is arbitrary, it holds that $M \subset \mathbb{B}_\epsilon$.

In summary, we have shown that

$x(t) \to M \subset \mathbb{B}_\epsilon$ as $t \to \infty$ for all initial conditions $x(0) \in \mathbb{R}^n$, and hence the desired assertion holds. □

As the first application of Proposition 3.4, we are interested in specifying the invariant set when the set of control action is described by a set of equidistant points along each axis of the output space.

Corollary 3.5. Consider the system Σ as in (3.1) satisfying (A3.0), and $\mathscr{U} = \lambda\{-N, -N+1, \ldots, N-1, N\}^m$, with $\lambda > 0$ being the step size and N a positive integer. Then the control law $u = \phi_{\mathscr{U}}(-y)$, where $\phi_{\mathscr{U}}$ is as in (3.6), globally practically stabilizes Σ with respect to $\mathbb{B}_\epsilon$ where $\epsilon > 0$ satisfies $\gamma(\lambda\sqrt{m}) \leq \epsilon$. ⋄

Proof. The proof follows *mutatis mutandis* the proof of Proposition 3.4. The set $\mathscr{U}$ satisfies (A3.1) by taking $\mathscr{V} = \lambda\{-1, 0, 1\}^m \setminus \{0\}$. It is also seen that $\delta = \lambda\sqrt{m}$, and by requiring $\gamma(\lambda\sqrt{m}) \leq \epsilon$, all the hypotheses of Proposition 3.4 hold. □

Remark 3.6. In contrast to the choice of $\mathscr{U}$ in Example 3.2 where we used (3.5) to construct the finite countable set $\mathscr{U}$ in $\mathbb{R}^2$, the constant δ in Corollary 3.5 is less than $\max_{\tilde{v} \in \tilde{\mathscr{V}}} \|\tilde{v}\|$. This is due to the choice of the set $\mathscr{V}$ in the proof of Corollary 3.5 that is dense enough such that $\{z \mid \phi(z) = 0\} \subset \mathrm{conv}(\mathscr{V})$. From this corollary, one can conclude that two-level quantization with $N = 1$ suffices to get a global practical stabilization property for passive nonlinear systems. This binary control law restricts however the convergence rate of the closed-loop system. It converges to the desired compact ball in a linear fashion and may not be desirable when the initial condition is very far from the origin. The use of higher quantization level (e.g., $N \gg 1$) can provide a better convergence rate. ⋄

3.1.2 Sector bounded feedback

We next present a generalization of the result in Proposition 3.4 on how the nearest action rule can be used to quantize more generic nonlinear feedback laws. In Proposition 3.4, when $\mathscr{U}$ is the continuum space of $\mathbb{R}^m$, the resulting control law is simply given by $u = -y$, i.e., it is a unity output feedback law. Using standard result in passive systems theory, the closed-loop system will satisfy $\dot{H} \leq -\|y\|^2$. Furthermore, the application of LaSalle invariance principle with zero-state detectability allows us to conclude that $x(t) \to 0$ asymptotically. As the underlying system is passive, we can in fact stabilize it with any sector-bounded nonlinear feedback of the form $y \mapsto F(y)$, where $F : \mathbb{R}^m \to \mathbb{R}^m$ satisfies

$$k_1\|y\|^2 \leq \langle F(y), -y\rangle \leq k_2\|y\|^2, \quad 0 < k_1 \leq k_2 \tag{3.11a}$$

$$\|F(y)\| \leq k_3\|y\|, \quad k_3 \geq k_1, \tag{3.11b}$$

for all $y \in \mathbb{R}^m$. There are a number of reasons for considering such feedback laws rather than the unity output feedback law. For instance, we can attain a prescribed L_2-gain disturbance attenuation level or we can shape the transient behavior by adjusting the gains on different domain of y. In the following proposition, we consider such sector-bounded output feedback law $F(y)$, and how the nearest action rule can be used to map such feedbacks in the limited control input set $\mathscr{U}$ to guarantee practical stabilization.

Proposition 3.7. Consider a nonlinear system Σ described by (3.1) that satisfies (A3.0), and a finite countable set $\mathscr{U} \subset \mathbb{R}^m$ satisfying (A3.1) so that (3.2) holds for some $\delta > 0$. For the mapping $\phi_{\mathscr{U}}$ given in (3.6), let $\mu_{\min,1} \in (0, 1]$ be such that[1], for all $z \in \mathbb{R}^m$,

$$\phi_{\mathscr{U}}(z) \neq 0 \Rightarrow \langle \phi_{\mathscr{U}}(z), z\rangle \geq \|\phi_{\mathscr{U}}(z)\|\|z\|\mu_{\min,1}. \tag{3.12}$$

Assume that the constants k_1, k_2, k_3 describing the function F, as in (3.11), satisfy

$$\frac{k_1^2}{k_3^2} + \mu_{\min,1}^2 > 1 \tag{3.13a}$$

$$\gamma\big(\delta/k_1\big) \leq \epsilon \tag{3.13b}$$

for a given $\epsilon > 0$. Then the control law $u = \phi_{\mathscr{U}}(F(y))$ globally practically stabilizes Σ with respect to $\mathbb{B}_\epsilon$. ⋄

Proof. We basically show that, for any $y \in \mathbb{R}^m$, we have

$$\langle \phi_{\mathscr{U}}(F(y)), -y\rangle \in \{\kappa_{i,y}\|u_i\|\|y\| \,|\, i \in J_y\} \tag{3.14}$$

[1] The existence of such $\mu_{\min,1}$ is guaranteed by the assumption (A3.1) on $\mathscr{U}$.

for some $J_y \subset \{0,1,\ldots,p\}$ such that $\phi_{\mathscr{U}}(F(y)) = \{u_i\}_{i\in J_y}$ and $\kappa_{i,y} > 0$. The rest of the proof follows a pattern similar to that of Proposition 3.4.

First, with $\phi_{\mathscr{U}}(F(y)) = \{u_i\}_{i\in J_y}$, suppose that $0 \notin \phi_{\mathscr{U}}(F(y))$, so that $J_y \subset \{1,\ldots,p\}$. It follows from (3.6) that $\{u_i\}_{i\in J_y}$ are the closest points to $F(y)$, and we have

$$\langle \phi_{\mathscr{U}}(F(y)), F(y)\rangle \in \{\|u_i\|\|F(y)\|\mu_{i,1} \,|\, i \in J_y\}, \tag{3.15}$$

where $\mu_{i,1} > 0$ is such that $\langle u_i, F(y)\rangle = \|u_i\|\|F(y)\|\mu_{i,1}$. Under the given hypothesis, $\mu_{\min,1} \le \mu_{i,1}$ for each $i \in J_y$, $y \in \mathbb{R}^m$. On the other hand, we have

$$\langle F(y), -y\rangle = \|F(y)\|\|y\|\mu_2. \tag{3.16}$$

Since $k_1\|y\|^2 \le \langle F(y), -y\rangle$ and $\|F(y)\| \le k_3\|y\|$, the minimum value of μ_2 (for all choices of $y \in \mathbb{R}^m$) is given by $\mu_{\min,2} = k_1/k_3$.

Now, note that, in general, $\kappa_{i,y} \in [-1,1]$. It can be shown that if (3.12), (3.13a), and (3.16) hold with $\mu_2 \in [\mu_{\min,2}, 1]$, then there exist $\kappa_{\min} > 0$ such that $\kappa_{i,y} \in [\kappa_{\min}, 1]$. For each $y \in \mathbb{R}^m$ and $i \in J_y$, we introduce the Gram matrix $G_{i,y}$ as

$$G_{i,y} = \begin{bmatrix} \langle -y,-y\rangle & \langle -y,F(y)\rangle & \langle -y,u_i\rangle \\ \langle -y,F(y)\rangle & \langle F(y),F(y)\rangle & \langle F(y),u_i\rangle \\ \langle -y,u_i\rangle & \langle F(y),u_i\rangle & \langle u_i,u_i\rangle \end{bmatrix},$$

having the property that (see also [52]) $G_{i,y} \succcurlyeq 0$ and thus $\det(G_{i,y}) \ge 0$. This implies that

$$\begin{aligned} 0 \le{}& \|y\|^2\|F(y)\|^2\|u_i\|^2 + 2\langle -y,F(y)\rangle\langle F(y),u_i\rangle\langle -y,u_i\rangle \\ &- \|y\|^2\langle F(y),u_i\rangle^2 - \|F(y)\|^2\langle -y,u_i\rangle^2 - \|u_i\|^2\langle -y,F(y)\rangle^2. \end{aligned}$$

By rewriting above inequality in terms of their respective norms in (3.14)–(3.16) with constants $\mu_{i,1}, \mu_2$, and $\kappa_{i,y}$, we have that, for each $y \in \mathbb{R}^m$ and $u_i,\ i \in J_y$

$$\begin{aligned} & \kappa_{i,y}^2 - 2\,\mu_{i,1}\,\mu_2\,\kappa_{i,y} \le 1 - (\mu_{i,1}^2 + \mu_2^2) \\ \Rightarrow\quad & \left(\kappa_{i,y} - \mu_{i,1}\,\mu_2\right)^2 \le 1 - (\mu_{i,1}^2 + \mu_2^2) + \mu_{i,1}^2\,\mu_2^2 \\ \Leftrightarrow\quad & \left|\kappa_{i,y} - \mu_{i,1}\,\mu_2\right| \le \sqrt{1 - (\mu_{i,1}^2 + \mu_2^2) + \mu_{i,1}^2\,\mu_2^2}. \end{aligned}$$

From the last inequality, we can prove whether $\kappa_{i,y} > 0$ whenever condition (3.13a) is satisfied, by only investigating the case where $\kappa_{i,y} \le \mu_{i,1}\,\mu_2$. The

last inequality, paired with condition (3.13a), gives the following result

$$\begin{aligned}\kappa_{i,y} &\geq \mu_{i,1}\ \mu_2 - \sqrt{1-(\mu_{i,1}^2+\mu_2^2)+\mu_{i,1}^2\ \mu_2^2} \\ &= \mu_{i,1}\ \mu_2 - \sqrt{(1-\mu_{i,1}^2)(1-\mu_2^2)} \\ &\geq \mu_{\min,1}(k_1/k_3) - \sqrt{(1-\mu_{\min,1}^2)(1-(k_1/k_3)^2)} \\ &> \mu_{\min,1}(k_1/k_3) - \sqrt{\mu_{\min,1}^2(k_1/k_3)^2} = 0.\end{aligned}$$

Note that the above arguments hold for all $i \in J_y$, and (3.14) holds for some $\kappa_{i,y} > 0$.

Secondly, in case, $J_y = \{0\}$, we have $\phi_{\mathscr{U}}(F(y)) = \{0\}$ and $\langle \phi_{\mathscr{U}}(F(y)), y\rangle = \{0\}$. Thus, (3.14) holds trivially since $u_0 = 0$.

Combining the two cases, we see that (3.14) holds for $J_y \subset \{0, 1, \ldots, p\}$. Following the same line of arguments as in the proof of Proposition 3.4, (3.14) implies that the storage function is nondecreasing along the solutions of the closed-loop system and the solutions converge to a set M, where M is the largest invariant set contained in $\mathscr{Z}_x := \{z \in \mathbb{R}^n \mid \phi_{\mathscr{U}}(F(h(z))) = \{0\}\}$. Hence for any trajectory starting with initial condition $x(s) = z \in M$, it holds that the corresponding output satisfies $\|F(y(t))\| \leq \delta$ for all $t \geq s$. Since $k_1\|v\|^2 \leq \langle F(v), v\rangle \leq \|F(v)\|\|v\|$ holds for all $v \in \mathbb{R}^m$, it follows that $\|y(t)\| \leq \frac{\delta}{k_1}$ for all $t \geq s$. By the property of large-time initial-state norm-observability of $\Sigma|_{u=0}$, it holds that,

$$\|z\| = \|x(s)\| \leq \gamma(\delta/k_1) \leq \epsilon \qquad \forall t \geq s$$

and this holds for each $z \in M$. Hence, $M \subseteq \mathbb{B}_\epsilon$ and in particular, each trajectory converges to $\mathbb{B}_\epsilon$ as $t \to \infty$. □

Remark 3.8. The condition (3.13a) requires that the nonlinearity should lie in a relatively thin sector bound. When $F(y) = ky$, i.e, it is a proportional controller with a scalar gain $k > 0$, then the condition (3.13a) holds trivially, since $\mu_{\min,1} > 0$ and $\frac{k_1}{k_3} = \frac{k}{k} = 1$. Consequently, it follows from this proposition that we can make the practical stabilization ball arbitrary small by assigning a large gain k. ◇

3.1.3 Nonzero equilibrium points

In this section, we consider the stability of Σ as in (3.1) around nonzero equilibrium point collected in the following steady-state relation.

$$\mathscr{E} := \left\{ (x^*, u^*) \in \mathbb{R}^n \times \mathbb{R}^m \,\middle|\, 0 = f(x^*) + g(x^*)u^* \right\}. \tag{3.17}$$

The stabilization of Σ around $x^* \in \mathbb{R}^n$ is then equivalent to stabilizing $\overline{x} = x - x^*$ around the origin, with $\overline{(\cdot)} = (\cdot) - (\cdot)^*$ denoting the incremental

variable. To solve this problem, we consider instead the incremental system given by

$$\overline{\Sigma}: \begin{cases} \dot{\overline{x}} &= \overline{f}(\overline{x}) + g(\overline{x}+x^*)\overline{u}, \\ \overline{y} &= h(\overline{x}+x^*) - h(x^*), \end{cases} \tag{3.18}$$

with $\overline{f}(\overline{x}) = f(\overline{x}+x^*) - f(x^*) + (g(\overline{x}+x^*) - g(x^*))u^*$ where we assume that the system Σ being constant-incrementally passive.

In the case of constant incremental passivity, the corresponding constant input u^* is often known from the knowledge of the nominal system (3.1). Then we can simply design the finite countable input set $\mathscr{U}$ such that it contains u^*. Thus it is natural to adapt the assumption (A3.1) to the current setting that brings us to the following proposition.

Proposition 3.9. Consider the system Σ as in (3.1), and a finite set of control actions $\mathscr{U} = \{u_0, u_1, \ldots, u_p\} \subset \mathbb{R}^m$. Assume that:

(A3.2) Σ is constant-incrementally passive with the proper storage function $H_0(x, x^*)$ for all pair $(x^*, u^*) \in \mathscr{E}$;

(A3.3) $u^* \in \mathscr{U}$, with $u_0 = u^*$, and there exists a subset $\mathscr{V}$ of $\mathscr{U}$ such that $u^* \in \operatorname{int}(\operatorname{conv}(\mathscr{V}))$; and

(A3.4) the autonomous incremental system $\overline{\Sigma}_{u=u^*}$ is large-time initial-state norm-observable, i.e. there exists $\tau > 0$ and $\bar{\gamma} \in \mathcal{K}_\infty$ such that the solution of $\overline{\Sigma}_{u=u^*}$ satisfies $\|\overline{x}(t)\| \leq \bar{\gamma}\left(\|\overline{y}\|_{[t,t+\tau]}\right)$ for all $\overline{x}(0) \in \mathbb{R}^n, t \geq 0$.

Furthermore, for a given $\epsilon > 0$, assume that $\bar{\gamma}(\delta) \leq \epsilon$, where $\delta > 0$ is the smallest number that satisfies

$$V_{\mathscr{U}}(u^*) \subseteq \mathbb{B}_\delta(u^*). \tag{3.19}$$

Then the control law $u = \phi_{\mathscr{U}}(u^* - \overline{y})$, with $\phi_{\mathscr{U}} : \mathbb{R}^m \rightrightarrows \mathscr{U}$ defined in (3.6), globally practically stabilizes Σ with respect to $\mathbb{B}_\epsilon(x^*)$. ⋄

The proof of Proposition 3.9 can be developed similarly to the proof of Proposition 3.4, by noting that

$$\overline{\phi}_{\mathscr{U}}(-\overline{y}) = \phi_{\mathscr{U}}(u^* - \overline{y}) - u^* \tag{3.20}$$

with

$$\overline{\phi}_{\mathscr{U}}(\eta) := \underset{\overline{v} \in \overline{\mathscr{U}}}{\arg\min} \{\|\overline{v} - \eta\|\} \tag{3.21}$$

where the set

$$\overline{\mathscr{U}} := \{\overline{v} \in \mathbb{R}^m \mid \overline{v} = v - u^*; v \in \mathscr{U}\} \tag{3.22}$$

is defined by *shifting* the original input set $\mathscr{U}$ such that u^* is now the origin of the input/output space of the constant incremental system. This means

that we can use the constant-incremental nearest-action map $\overline{\phi}_{\mathscr{U}}$ so that the constant incremental system has the same structure as (3.1). Then the rest of the proof follows from the proof of Proposition 3.4. Finally, since the output and state variables of the constant incremental system converge to $\mathbb{B}_\delta$ and $\mathbb{B}_\epsilon$, respectively, as $t \to \infty$, we can conclude practical stability, i.e. $\overline{y} \to \mathbb{B}_\delta$ and $x \to \mathbb{B}_\epsilon(x^*)$ as $t \to \infty$.

Similar to the previous results, sector bounded nonlinear mapping F that satisfies (3.11) can easily be included in the constant-incrementally passive systems case. This is due to the fact given by (3.20). Then the following proposition is true.

Proposition 3.10. Consider a nonlinear system Σ described by (3.1) that satisfies (A3.2) and (A3.4); and a finite countable set $\mathscr{U} \subset \mathbb{R}^m$ satisfying (A3.3) so that (3.19) holds for some $\delta > 0$. Let $\phi_{\mathscr{U}}$ be as given in (3.6); and let $\mu_{\min,1} \in (0,1]$ be such that (3.12) holds for all $z \in \mathbb{R}^m$. Assume that (3.13a) holds with the mapping F, along with constants k_1, k_2, k_3, satisfying (3.11). For a given $\epsilon > 0$, assume that

$$\bar{\gamma}(\delta/k_1) \leq \epsilon.$$

Then, the control law $u = \phi_{\mathscr{U}}(F(\overline{y}) + u^*)$ globally practically stabilizes Σ with respect to $\mathbb{B}_\epsilon(x^*)$. ◇

3.1.4 An illustrative example

Example 3.11. Consider the following nonlinear system

$$\Sigma_{\text{ex}} : \begin{cases} \dot{x} &= \begin{bmatrix} -x_2 + x_3^3 \\ x_1 \\ -x_1 \end{bmatrix} + \begin{bmatrix} 1 & 0 \\ 0 & 0 \\ 0 & 1 \end{bmatrix} u \\ y &= \begin{bmatrix} x_1 & x_3^3 \end{bmatrix}^\top \end{cases} \tag{3.23}$$

where $x := \begin{bmatrix} x_1 & x_2 & x_3 \end{bmatrix}^\top \in \mathbb{R}^3$ and $y := \begin{bmatrix} y_1 & y_2 \end{bmatrix}^\top, u := \begin{bmatrix} u_1 & u_2 \end{bmatrix}^\top \in \mathbb{R}^2$. It can be checked that by using the proper storage function $H(x) = \frac{1}{2}x_1^2 + \frac{1}{2}x_2^2 + \frac{1}{4}x_3^4$, the system Σ_{ex} is passive, i.e. $\dot{H} = \langle y, u \rangle$. Note that the system Σ_{ex} can be written as a nonlinear port-Hamiltonian system, describing a nonlinear RLC circuit [53]: $\dot{x} = J\nabla H(x) + gu$, $y = g^T \nabla H(x)$ where $J = \left[\begin{smallmatrix} 0 & -1 & 1 \\ 1 & 0 & 0 \\ -1 & 0 & 0 \end{smallmatrix}\right]$ and $g = \left[\begin{smallmatrix} 1 & 0 \\ 0 & 0 \\ 0 & 1 \end{smallmatrix}\right]$.

Furthermore, it can be shown (following the main results in [42]) that Σ_{ex} is also constant-incrementally passive. Indeed, for any $(x^*, u^*) \in \mathscr{E}$, we can define $H_0(x, x^*) = H(x) - H(x^*) - (x - x^*)^T \nabla H(x^*)$ which has a global unique minimum at x^* and is related to the original storage function $H(x)$. It follows immediately that $\dot{H}_0 = \langle \overline{y}, \overline{u} \rangle$.

We will now show that Σ_{ex} satisfies the large-time initial-state norm observability condition. As the bound on x_3 for the large-time norm observability can directly be obtained from the output y, we need to compute the bound on $\left[\begin{smallmatrix} x_1 \\ x_2 \end{smallmatrix}\right]$. If we consider the sub-system of $\left[\begin{smallmatrix} x_1 \\ x_2 \end{smallmatrix}\right]$ with x_1 as its output (and is equal to y_1), it is a linear system with $A = \left[\begin{smallmatrix} 0 & -1 \\ 1 & 0 \end{smallmatrix}\right]$, $B = \left[\begin{smallmatrix} 1 \\ 0 \end{smallmatrix}\right]$, $C = \begin{bmatrix} 1 & 0 \end{bmatrix}$ and its input is $x_3^3 = y_2$. Thus as (A, C) is observable, the observability Gramian is given by

$$W_\pi(t) = \int_t^{t+\pi} e^{A^\top(s-t)} C^\top C e^{A(s-t)} \mathrm{d}s = \frac{\pi}{2} \begin{bmatrix} 1 & 0 \\ 0 & 1 \end{bmatrix},$$

whose inverse is simply given by $W_\pi^{-1} = \frac{2}{\pi} I_2$ and $\|W_\pi^{-1}\| = \frac{2}{\pi}$. Then for any $t > 0$

$$\left[\begin{smallmatrix} x_1(t) \\ x_2(t) \end{smallmatrix}\right] = W_\pi^{-1} \int_t^{t+\pi} e^{A^\top(s-t)} C^\top \left(x_1(s) - \left(H * \left[\begin{smallmatrix} x_3^3 \\ 0 \end{smallmatrix}\right] \right)(s) \right) \mathrm{d}s,$$

where $*$ denotes the convolution operation and H is the convolution matrix kernel given by $H(t) = Ce^{At}$. Since $\|e^{At}\| = 1$ for all t, it follows then that

$$\left\| \begin{bmatrix} x_1(t) \\ x_2(t) \end{bmatrix} \right\| \leq \frac{2}{\pi} \pi \left(\|y_1\|_{[t,t+\pi]} + \|y_2\|_{[t,t+\pi]} \right) \leq 4 \|y\|_{[t,t+\pi]}.$$

Since by the definition of y, $\|x_3\|_{[t,t+\pi]} = \|y_2\|_{[t,t+\pi]}^{\frac{1}{3}} \leq \|y\|_{[t,t+\pi]}^{\frac{1}{3}}$, it follows from the inequality above that

$$\|x(t)\| \leq 4 \|y\|_{[t,t+\pi]} + \|y\|_{[t,t+\pi]}^{\frac{1}{3}}.$$

In other words, the function γ in (2.3) is given by $\gamma(s) = 4s + s^{\frac{1}{3}}$.

Following similar routines, we can check that the autonomous incremental system of Σ_{ex} also satisfies the large-time initial-state norm observability condition with the function $\bar{\gamma}$ as in assumption (A3.4). That is, we first consider the linear incremental subsystem with $\overline{y}_2 = x_3^3 - x_3^{*3}$ as the input and $\overline{y}_1 = x_1 - x_1^*$ as the output which yields similar bounds, i.e.

$$\left\| \begin{bmatrix} \overline{x}_1(t) \\ \overline{x}_2(t) \end{bmatrix} \right\| \leq 2 \left(\|\overline{y}_1\|_{[t,t+\pi]} + \|\overline{y}_2\|_{[t,t+\pi]} \right) \leq 4 \|\overline{y}\|_{[t,t+\pi]}.$$

Accordingly, for $\overline{x}_3$, we have that $\overline{x}_3 = \frac{\overline{y}_2}{x_3^2 + x_3^{*2} + x_3 x_3^*}$. For any $x_3^* \neq 0$, we have that $x_3^2 + x_3^{*2} + x_3 x_3^* \geq \frac{3}{4} x_3^{*2}$, for all x_3. Hence,

$$\begin{aligned} \|\overline{x}(t)\| \leq \left\| \begin{bmatrix} \overline{x}_1(t) \\ \overline{x}_2(t) \end{bmatrix} \right\| + \|\overline{x}_3\| &\leq 4 \|\overline{y}\|_{[t,t+\pi]} + \frac{4}{3x_3^{*2}} \|\overline{y}_2\|_{[t,t+\pi]} \\ &\leq 4 \|\overline{y}\|_{[t,t+\pi]} + \frac{4}{3x_3^{*2}} \|\overline{y}\|_{[t,t+\pi]}. \end{aligned}$$

In other words, the large-time initial-state norm-observability function for the autonomous incremental system of Σ_{ex} is given by $\bar{\gamma}(s) = 4s + \frac{4}{3x_3^{*2}} s^2$.

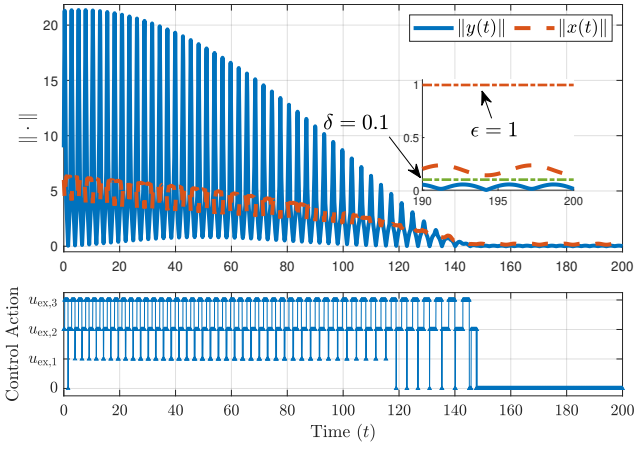

Figure 3.1: Simulation results of Σ_{ex} using the control approach proposed in the Proposition 3.4 with finite countable input set $\mathscr{U}_{ex}$ as in (3.5) and fixed parameters $\theta_{\text{ex}} = 0$ and $\alpha = 0.1$. It can be seen that once both the state x and the output y enters their respective convergence ball, the control input is zero.

We can now use the results in Proposition 3.4 and Proposition 3.9 to practically stabilize Σ_{ex} around any arbitrary steady-state relation $(x^*, u^*) \in \mathscr{E}$. We choose the control set to be $\mathscr{U}_{\text{ex}}$ given in (3.5), and the desired stability margin to be $\epsilon = 1$. Then, based on the function γ computed for the system Σ_{ex}, we get $\gamma(\delta) < 1$ if $\delta \in \left(0, \frac{1}{8}\right]$. Using the same finite countable set as in (3.5) along with the function ϕ as in (3.6), we can fix $\theta_{\text{ex}} = 0$ and $\alpha = 0.1$ such that the system Σ_{ex} is globally practically stable with respect to $\mathbb{B}_\epsilon$, with $\epsilon = 1$, as shown in the simulation results in Figure 3.1.

Furthermore, if we fix $x^* = [\,0\ 0\ -1\,]^\top$, $u^* = [\,1\ 0\,]^\top$, and $\epsilon = 0.5$. Then, by the large-time initial-state norm-observability property of the autonomous incremental system, we can choose $\delta = 0.1$ to generate the finite countable set of control actions. In this case, we can translate the previously used finite countable set such that u^* is among the realizable control actions, i.e. $\overline{\mathscr{U}}_{ex} := \mathscr{U}_{ex} + u^*$ with $\mathscr{U}_{ex}$ being the same the finite countable input as before. The illustration of the resulting control law with the mapping $\phi_{\mathscr{U}}$ is demonstrated in Figure 3.2.

$\diamond$

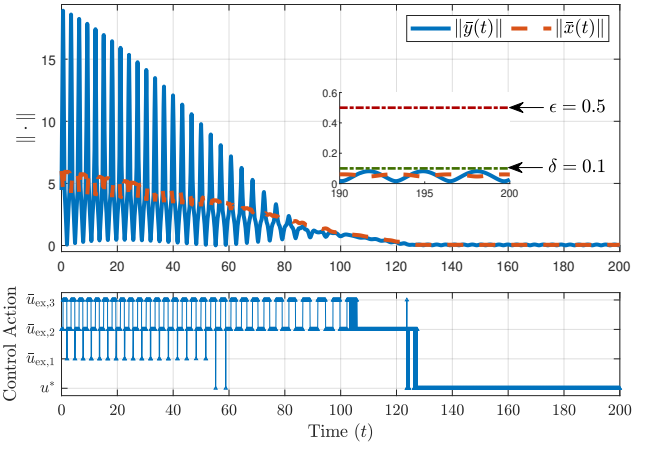

Figure 3.2: Simulation results of Σ_{ex} using the control approach proposed in the Propostion 3.9 with finite countable input set $\overline{\mathscr{U}}_{ex} := \mathscr{U}_{ex} + u^*$ with $\mathscr{U}_{ex}$ given in (3.5). Here, $u^* \in \overline{\mathscr{U}}_{ex}$. Once again, when the state x and the output y enter their respective convergence ball, the control action is switched to u^* for the rest of the simulation.

3.2 Minimal Control Actions: Constructions and Bounds

In the earlier sections, we have shown that a nearest action selection approach is a powerful tool for global practical stabilization of passive nonlinear systems. Indeed, for a given limited choice of static control inputs, assumptions (A3.1) and (A3.3) provide us a way to check the applicability of nearest action selection approach for the practical stabilization problem. If these assumptions hold for a finite countable set $\mathscr{U}$, then it is of interest to compute the smallest number $\delta > 0$ associated with Voronoi cell $V_{\mathscr{U}}(u^*)$, such that $V_{\mathscr{U}}(u^*) \subset \mathbb{B}_\delta(u^*)$. Since our control design achieves convergence up to a ball of radius $\gamma(\delta)$, with $\gamma(\cdot)$ being the output-to-state gain in large-time initial-state norm-observability assumption, the knowledge of δ basically determines how close the trajectories can get to the desired equilibrium with our proposed controller. To obtain such $\mathscr{U}$ of minimal cardinality, the following result, borrowed from [54, Corollary 9.5], is of interest:

Lemma 3.12. For a finite countable set $\mathscr{S} \subset \mathbb{R}^m$, the minimal cardinality of $\mathscr{S}$ such that $\operatorname{int}(\operatorname{conv}(\mathscr{S})) \neq \emptyset$ is equal to $m+1$. ⋄

An immediate consequence is that, for practical stabilization of passive

systems, it suffices to consider a control set $\mathscr{U}$ with $m+2$ elements (including u^*), provided they satisfy a certain geometric configuration.

Corollary 3.13. Let the set $\mathscr{U}$ be such that $u^* \in \operatorname{int}(\operatorname{conv}(\mathscr{U}))$. If $\operatorname{conv}(\mathscr{U} \setminus \{u^*\})$ is an m-simplex, then $\mathscr{U}$ is a minimal set that satisfies (A3.3). ◇

In the remainder of this section, we will work with two particular choices of the set $\mathscr{U}$ with cardinality $m+2$ that satisfy (A3.1) or (A3.3). We give a closed-form expression of δ for these sets in terms of the elements $\mathscr{U}$. For the sake of simplicity, we fix $u^* = 0$ in these computations. The two cases we consider are: the set $\mathscr{U} = \mathscr{S}_{\text{reg}} \cup \{0\}$, where $\mathscr{S}_{\text{reg}}$ is defined as in (2.8) and the set $\mathscr{U} = \mathscr{S}^0_{\text{reg}} \cup \{0\}$, and $\mathscr{S}^0_{\text{reg}} = \mathscr{S}_{\text{reg}} - b_{\mathscr{S}_{\text{reg}}}$ with $b_{\mathscr{S}_{\text{reg}}} = \lambda \frac{\sqrt{m+1}-1}{m\sqrt{m+1}} \mathbb{1}$. Note that the second case is obtained by shifting the barycenter of the first case to the origin.

In the next two lemmas, we basically compute a bound on the sets $V_{\mathscr{S}_{\text{reg}} \cup \{0\}}(0)$ and $V_{\mathscr{S}^0_{\text{reg}} \cup \{0\}}(0)$. It is noted that the results apply to the case when $u^* \neq 0$ since the set $\mathscr{V} = (\mathscr{S}_{\text{reg}} \cup \{0\}) + u^*$ (or $\mathscr{V} = (\mathscr{S}^0_{\text{reg}} \cup \{0\}) + u^*$) is such that $u^* \in \operatorname{int}(\operatorname{conv}(\mathscr{V}))$ and hence it has the same bound.

Lemma 3.14. Consider $\mathscr{S}_{\text{reg}}$ as in (2.8) for some $\lambda > 0$. For the set $V_{\mathscr{S}_{\text{reg}} \cup \{0\}}(0)$, the smallest $\delta > 0$ satisfying $V_{\mathscr{S}_{\text{reg}} \cup \{0\}}(0) \subset \mathbb{B}_\delta$ is given by

$$\delta = \begin{cases} \frac{\lambda}{2}, & \text{if } m = 1, \\ \frac{\lambda}{2}\sqrt{m - 1 + (2 - m - \sqrt{m+1})^2}, & \text{otherwise.} \end{cases}$$

◇

Proof. First, we observe that the vector $x = \begin{bmatrix} x_1 & \dots & x_m \end{bmatrix}^\top \in V_{\mathscr{S}_{\text{reg}} \cup \{0\}}(0)$ if it satisfies

$$x_i \leq \frac{\lambda}{2}, \qquad i = 1, \dots, m, \tag{3.24}$$

$$\frac{1 - \sqrt{m+1}}{m} \mathbb{1}^\top x \leq \lambda \frac{\left(1 - \sqrt{m+1}\right)^2}{2m}. \tag{3.25}$$

Next, we observe that each of the vertices of $V_{\mathscr{S}_{\text{reg}} \cup \{0\}}(0)$ can be obtained by solving m equations taken from (3.24) and/or (3.25). Let $\mathscr{V}$ be the set of all vertices of $V_{\mathscr{S}_{\text{reg}} \cup \{0\}}(0)$. Then $\mathscr{V} = \{\frac{\lambda}{2}\mathbb{1}\} \bigcup_{i=1}^{m} \{\frac{\lambda}{2}\tilde{v}_i\}$ with $\tilde{v}_i$ being a column vector where the i-th element is given by $2 - m - \sqrt{m+1}$ and the other elements are 1. Therefore, the minimum value of δ for which $V_{\mathscr{S}_{\text{reg}} \cup \{0\}}(0) \subset \mathbb{B}_\delta$ is given by

$$\delta_{m=1} = \max_{\tilde{v} \in \mathscr{V}} \{\|\tilde{v}\|\} = \frac{\lambda}{2}\|1\| = \frac{\lambda}{2}$$

and

$$\delta_{m>1} = \max_{\tilde{v}\in\mathscr{V}}\{\|\tilde{v}\|\} = \frac{\lambda}{2}\|\tilde{v}_i\| = \frac{\lambda}{2}\sqrt{m-1+\left(2-m-\sqrt{m+1}\right)^2}.$$

which is the desired expression. □

Next, let us consider the regular m-simplex centered at the origin with vertices $\mathscr{S}^0_{\text{reg}}$.

Lemma 3.15. Consider $\mathscr{S}_{\text{reg}}$ as in (2.8) for some $\lambda > 0$. For the set $V_{\mathscr{S}^0_{\text{reg}}\cup\{0\}}(0)$, the bound $\delta > 0$ such that $V_{\mathscr{S}^0_{\text{reg}}\cup\{0\}}(0) \subset \mathbb{B}_\delta$ is given by $\delta = \lambda\frac{m}{2}\sqrt{\frac{m}{m+1}}$. ⋄

Proof. Similar to the proof of Lemma 3.14, we consider the set $V_{\mathscr{S}^0_{\text{reg}}\cup\{0\}}(0)$ as the solution set of system of inequalities,

$$\left(e_i - \frac{\sqrt{m+1}-1}{m\sqrt{m+1}}\mathbb{1}\right)^\top x \leq \frac{\lambda}{2}\frac{m}{m+1}, \quad i = 1,\ldots,m, \tag{3.26}$$

$$-\frac{1}{\sqrt{m+1}}\mathbb{1}^\top x \leq \frac{\lambda}{2}\frac{m}{m+1}. \tag{3.27}$$

Since all points in $\mathscr{S}^0_{\text{reg}}$ have the same distance from the origin, we can pick all m equations from (3.26) to obtain one of the vertices of $V_{\mathscr{S}^0_{\text{reg}}\cup\{0\}}(0)$, which is $v = \frac{\lambda}{2}\frac{m}{\sqrt{m+1}}\mathbb{1}$.

Therefore, the minimum bound on the set $V_{\mathscr{S}}(0)$ is,

$$\begin{aligned}\delta = \|v\| &= \frac{\lambda}{2}\frac{m}{\sqrt{m+1}}\|\mathbb{1}\| \\ &= \lambda\frac{m}{2}\sqrt{\frac{m}{m+1}}.\end{aligned}$$

which completes the proof. □

From Lemma 3.14 and Lemma 3.15, we can, in fact, construct the minimal set corresponding to the nearest action control approach. In particular, for given admissible reference signal u^*, output-to-state gain $\gamma \in \mathscr{K}$ obtained by choosing $u = u^*$, and a given stability margin $\epsilon > 0$, we first choose $\delta > 0$ satisfying $\gamma(\delta) \leq \epsilon$, a rotation matrix $R \in \mathbb{R}^{m\times m}$, and let $\mathscr{U}$ be defined as follows:

1. $\mathscr{U} := \left(R\mathscr{S}_{\text{reg}} \cup \{0\}\right) + u^*$ with

$$\lambda = \min\left\{2\delta, \frac{2\delta}{\sqrt{m-1+\left(2-m-\sqrt{m+1}\right)^2}}\right\},$$

   or;

2. $\mathscr{U} := \left(R\mathscr{S}^0_{\text{reg}} \cup \{0\}\right) + u^*$ with $\lambda = \frac{2\delta}{m}\sqrt{\frac{m+1}{m}}$.

Example 3.16. The finite countable set $\mathscr{U}_{\text{ex}}$ in Example 3.2 can be constructed by using $\mathscr{U} := \left(R\mathscr{S}_{\text{reg}}(0) \cup \{0\}\right) + u^*$; by fixing $\alpha = \delta$ and

$$R = -\frac{\sqrt{2}}{2}\begin{bmatrix} \sin\theta_{\text{ex}} + \cos\theta_{\text{ex}} & \sin\theta_{\text{ex}} - \cos\theta_{\text{ex}} \\ -\sin\theta_{\text{ex}} + \cos\theta_{\text{ex}} & \sin\theta_{\text{ex}} + \cos\theta_{\text{ex}} \end{bmatrix}.$$

◇

3.3 Summary

We proposed simple ways to select the control actions at each time instance where we have shown that our proposed control laws are able to stabilize the systems up to some desirable distance from the equilibrium. In addition, our results provide an insight on the lower bound on the number of control elements that guarantee practical stability. We have also provided methods to design the finite set of control actions with minimal cardinality.

Chapter 4 | Cooperative Multi Agent Systems

"Nothing is more fairly distributed than common sense: no one thinks he needs more of it than he already has."
-Rene Descartes-

Contents

The consensus (rendezvous/agreement) and formation control problems are two prototypical cooperative control problems in multi-agent systems (MAS). For systems with continuous input space, the problems of designing control laws to achieve consensus or to maintain a formation shape have been well-studied in the literature, for example [55, 56, 57, 58, 59], among many others. However, practical implementation of MAS' control designs may have to deal with physical constraints in the actuators, sensors and mechanisms, or with information constraints in the communication channel. Such constraints may be encountered due to the limitation of digital communication [60, 61] or due to the limitation of the mechanical design of the system such as the use of fixed set of discrete actuation systems in Ocean Grazer wave energy converter [1, 2]. Designs, analysis, and numerical implementation of control laws for such networked systems have also received considerable attention in the literature, see for example [3, 21, 48, 62].

The temporal and spatial discretization of inputs, states and outputs of networked control systems are typically done via quantization operator. There

are three classes of quantizers that are typically used in the literature, namely, uniform, asymmetric, and logarithmic quantizers [51]. The application and analysis of cooperative control with quantizers have been studied, for instance, in [3, 10, 21, 48, 51, 62, 63, 64, 65]. However, when minimality requirement is imposed on the number of control input points or on the number of symbols in the communication channel, the design and analysis tools using aforementioned quantizers can no longer be used to address this problem. An example of such case is mechanical systems with finite discrete actuation points as in [1, 2].

In Chapter 3 [66, 67], these quantization operators are considered as nearest-action operators that map the input value to the available points in a given discrete set $\mathscr{U}$, which can have a finite or infinite number of members. We have shown that for a generic class of m-dimensional passive systems having proper storage function and satisfying the nonlinear large-time initial-state norm observablility condition[1], it can be practically stabilized using only $m+2$ control actions. As a comparison, using the q-ary quantizers[2] [3, 4, 21], where q input values per input dimension are defined, the stabilization of the systems requires $\mathscr{U}$ whose cardinality is q^m (or q^m+1 if the zero element is not in the range of the q-ary quantizers).

In this chapter, we present the application of nearest-action control to the cooperative control of multi-agent systems. We study the combination of the nearest-action selection approach studied in Chapter 3 ([66, 67]) and the standard distributed continuous control laws for multi agent-cooperation as in [3, 48, 59]. Specifically, we study nearest-action distributed control for consensus and distance-based formation control problems.

For this purpose, we consider a MAS represented by an undirected graph $\mathscr{G}=(\mathscr{V},\mathscr{E})$ with N agents and M edges as described in Chapter 2.4. For the graph $\mathscr{G}$, the matrix $B\in\mathbb{R}^{N\times M}$ is the corresponding incident matrix. For every agent i in $\mathscr{G}$, it is described by

$$\dot{x}_i = u_i. \tag{4.1}$$

with $x_i(t)\in\mathbb{R}^m$ being the state and $u_i(t)\in\{0,u_{i,1},u_{i,2},\ldots,u_{i,p_i}\}=:\mathscr{U}_i\subseteq\mathbb{R}^m$ being the input variables. We also define the vector of relative position between communicating agents by $z=(B^\top\otimes I_m)x$..

We show the practical stability property of the closed-loop system where the usual consensus and distance-based formation Lyapunov function are used in the analysis. We present the upper bound of the practical stability of the consensus or formation error that can be computed based on the local bound

[1] We refer interested readers to [41] for a reference to the notion of nonlinear norm observability.

[2] In this case, binary quantizer is given by $q=2$ and ternary quantizer corresponds to $q=3$.

from each individual $\mathscr{U}_i$ at each agent.

4.1 Distributed Nearest Action Control

Prior to presenting the main results on distributed nearest action control for cooperative MAS, we need the following technical lemma, which establishes the relationship between a ball in the range of $(B \otimes I_m)z$ and a ball of the same radius in z. It is used later to get an upperbound on the practical stability of the consensus or formation error.

Lemma 4.1. Consider an undirected and connected graph $\mathscr{G} = (\mathscr{V}, \mathscr{E})$. Let $x_i \in \mathbb{R}^m,\ i = 1, \ldots, N$, be the state variable of the i-th agent as in (4.1) and define $z = (B^\top \otimes I_m)x \in \mathbb{R}^{Mm}$. If both $(B \otimes I_m)z \in \mathbb{B}_\delta^{Nm}$ and $z \in \mathrm{Im}(B^\top \otimes I_m)$ hold then $z \in \mathbb{B}_\delta^{Mm}$. ⋄

Proof. Firstly, by defining the space

$$\Omega := \mathrm{Ker}(B \otimes I_m) \oplus \left(\mathrm{Im}(B^\top \otimes I_m) \cap \mathbb{B}_\delta^{Mm}\right),$$

if $z \in \Omega$ then $(B \otimes I_m)z \in \mathrm{Im}(B \otimes I_m) \cap \mathbb{B}_{m\|B\|\delta}^{Nm}$ (which is a superset ball that contains B_δ^{Nm}). Since $z = (B^\top \otimes I_m)x$, it necessarily holds that $z \in \mathrm{Im}(B^\top \otimes I_m)$. Combining this with $z \in \Omega$, $\|(B \otimes I_m)z\| \leq \delta$ implies that $z \in \Omega \cap \mathrm{Im}(B^\top \otimes I_m)$. Since the non-zero elements of B are either 1 or -1 and since the graph is connected, it follows that for all $z \in \Omega \cap \mathrm{Im}(B^\top \otimes I_m)$, we have

$$\|z\| \leq \|(B \otimes I_m)z\| \leq m\|B\|\delta.$$

Hence, for all $z \in \Omega \cap \mathrm{Im}(B^\top \otimes I_m)$, if $\|(B \otimes I_m)z\| \leq \delta$ then $\|z\| \leq \delta$. Moreover, by definition, $\mathrm{Ker}(B) \cap \mathrm{Im}(B^\top) = \emptyset$, so that

$$\begin{aligned} z &\in \left(\mathrm{Ker}(B \otimes I_m) \cap \mathrm{Im}(B^\top \otimes I_m)\right) \oplus \left(\mathrm{Im}(B^\top \otimes I_m) \cap \mathbb{B}_\delta^{Mm}\right) \\ &= \mathrm{Im}(B^\top \otimes I_m) \cap \mathbb{B}_\delta^{Mm} \end{aligned}$$

We can now conclude that if both $\|(B \otimes I_m)z\| \leq \delta$ and $z \in \mathrm{Im}(B^\top \otimes I_m)$, then $\|z\| \leq \delta$. □

4.1.1 Consensus Protocol With Finite Set of Actions

In this subsection, we propose a nearest-action input-quantization approach for solving the practical consensus problem. In this case, every agent $i \in \{1, \ldots, n\}$ is given by a single-integrator dynamics (4.1) and its control input takes value from a set of finite points $\mathscr{U}_i := \{0, u_{i,1}, u_{i,2}, \ldots, u_{i,p_i}\}$ satisfying (A3.1) along with their respective quantity δ_i satisfying (3.3). For this problem, we propose a nearest-action controller for consensus problem by assigning $u_i = \phi_{\mathscr{U}_i}(-(L \otimes$

$I_m)x)$ with $\phi_{\mathscr{U}_i}$ as in (3.6). The corresponding closed-loop system can be written as

$$\dot{x} = \Phi(-(L \otimes I_m)x) \tag{4.2}$$

where Φ is understood agent-wise, i.e.

$$\Phi(\eta) = \left[\phi_{\mathscr{U}_1}(\eta_1)^\top, \quad \cdots, \quad \phi_{\mathscr{U}_n}(\eta_n)^\top\right]^\top. \tag{4.3}$$

In the relative position coordinate, (4.2) can be rewritten as

$$\dot{z} = (B^\top \otimes I_m)\Phi(-(B \otimes I_m)z). \tag{4.4}$$

The stability of (4.4) is shown in the following proposition.

Proposition 4.2. For given sets of finite control points

$$\mathscr{U}_i := \{0, u_{i,1}, u_{i,2}, \ldots, u_{i,p_i}\},\ i = 1, \ldots, N,$$

satisfying (A3.1) along with their respective Voronoi cell upper bound δ_i satisfying (3.3), consider the closed-loop MAS in (4.4), where Φ is as in (4.3). Then for any initial condition $z(0) = z_0$,

$$z(t) \to \mathbb{B}_\delta \text{ as } t \to \infty$$

where $\delta = \sum_{i=1}^{N} \delta_i$. ◇

Proof. As pursued in Chapter 3, since Φ is a non-smooth mapping, we can embed the differential equation (4.4) into a regularized differential inclusion given by

$$\dot{z} \in (B^\top \otimes I_m)\mathscr{K}(\Phi(-(B \otimes I_m)z)). \tag{4.5}$$

Using the usual consensus Lyapunov function $V(z) = \frac{1}{2}z^\top z$, it follows that

$$\begin{aligned}
\dot{V}(z) &\in \langle (B \otimes I_m)z, \mathscr{K}(\Phi(-(B \otimes I_m)z))\rangle \\
&= \sum_{i=1}^{n} \langle ((b_i \otimes I_m)z, \mathscr{K}(\phi_i(-(b_i \otimes I_m)z))\rangle \\
&= \sum_{i=1}^{n} \langle ((b_i \otimes I_m)z, \operatorname{conv}(\mathscr{W}_i^c)\rangle,
\end{aligned}$$

where b_i is the i-th row vector of the incidence matrix B and $\mathscr{W}_i^c := \phi_i(-(b_i \otimes I_m)z)$. Following Lemma 3.3, it follows that for every $i \in \{1, \ldots, N\}$, we have that

- if $0 \notin \mathscr{W}_i^c$, then

  $$\langle (b_i \otimes I_m)z, \operatorname{conv}(\mathscr{W}_i^c)\rangle \subset [-\|u_i^{\max}\|\|(b_i \otimes I_m)z\|, -0.5\|u_i^{\min}\|^2]$$

  where $\|u_i^{\max}\| = \max_{w_i \in \mathscr{W}_i^c} \|w_i\|$ and $\|u_i^{\min}\| = \min_{w_i \in \mathscr{W}_i^c} \|w_i\|$; or else

- if $0 = \mathscr{W}_i^c$, then

  $$\langle (b_i \otimes I_m)z,\ \operatorname{conv}(\mathscr{W}_i^c)\rangle = \{0\}.$$

Hence, for any given time $t \geq 0$, whenever $-(b_i \otimes I_m)z(t) \notin \text{int}(V_{\mathscr{U}_i}(0))$ for some i, we have $\dot{V}(z(t)) < 0$, i.e., the Lyapunov function $V(z(t))$ is strictly decreasing. Otherwise $\dot{V}(z(t)) = 0$. This implies that all Krasovskii solutions of (4.4) converge to the invariant set $\Psi = \{z | -(b_i \otimes I_m)z \in \text{int}(V_{\mathscr{U}_i}(0)), \forall i\}$. In the set Ψ, for each $i = 1, \ldots, N$, it must be that $\|(b_i \otimes I_m)z\| \leq \delta_i$. Thus

$$\|(B \otimes I_m)z\| \leq \sum_{i=1}^{n} \|(b_i \otimes I_m)z\| \leq \sum_{i=1}^{n} \delta_i = \delta.$$

By using Lemma 4.1 and since $\|(B \otimes I_m)z\| \leq \delta$ and $z = (B^\top \otimes I_m)x$, we can conclude that $\|z\| \leq \delta$.

It has been shown above that the relative position coordinate z converges to a ball with size relative to the finite countable sets of actions of all agents and the network topology. Consequently, all agents represented by position $x_i, i = 1, \ldots, N$ are said to reach consensus in the neighborhood of the consensus manifold E described in Chapter 2.4.1. □

4.1.2 Distance-Based Formation With Finite Sets of Actions

Consider a set of n agents governed by the single integrator dynamics, where each agent can take value only from a given set of finite countable points $\mathscr{U}_i$ as in subsection 4.1.1. Given a desired distance vector $d = \begin{bmatrix} d_1 & \cdots & d_M \end{bmatrix}^\top$ representing desired distance constraints that define the desired formation shape, where for each $k = 1, \ldots, M$, $d_k = d_{ij}$ is the desired distance between the ith and jth agent in the formation. For this problem, we propose the nearest-action distance-based control law $u = \Phi(-(B \otimes I_m)D_z e)$ with Φ be as in (4.3), D_z and e be as described in Chapter 2.4.2. In this case, the closed-loop system represented by (2.13) and (2.14) becomes

$$\dot{z} = (B^\top \otimes I_m)\Phi(-(B \otimes I_m)D_z e) \tag{4.6}$$

$$\dot{e} = D_z^\top (B^\top \otimes I_m)\Phi(-(B \otimes I_m)D_z e). \tag{4.7}$$

The stability of above system is analyzed in the following proposition.

Proposition 4.3. For given sets of finite control points

$$\mathscr{U}_i := \{0, u_{i,1}, u_{i,2}, \ldots, u_{i,p_i}\},\ i = 1, \ldots, N,$$

satisfying (A3.1) along with their respective Voronoi cell upper bound δ_i satisfying (3.3), consider the closed-loop MAS (4.6) and (4.7) where Φ is as in (4.3). Assume that the formation graph is infinitesimally rigid. Then for any initial condition $(z(0), e(0))$ in the neighborhood of the desired formation shape, there exists $\bar{\delta} > 0$ such that $\dot{z}(t) \to 0$, $\dot{e}(t) \to 0$ and $e(t) \to \mathbb{B}_{\bar{\delta}}$. ◇

Proof. Similar to the proof of Proposition 4.2, since Φ is a non-smooth map-

ping, we consider instead the regularized differential inclusion of the closed-loop systems given by

$$\dot{z} \in (B^\top \otimes I_m)\mathscr{K}(\Phi(-(B \otimes I_m)D_z e)) \tag{4.8}$$

$$\dot{e} \in D_z^\top (B^\top \otimes I_m)\mathscr{K}(\Phi(-(B \otimes I_m)D_z e)). \tag{4.9}$$

Using the usual distance-based formation Lyapunov function $J(e) = \frac{1}{4}\langle e, e\rangle$, it follows that

$$\begin{aligned}\dot{J}(e) &= \langle e, D_z^\top (B^\top \otimes I_m)\Phi(-(B \otimes I_m)D_z e)\rangle \\ &= \langle (B \otimes I_m)D_z e, \Phi(-(B \otimes I_m)D_z e)\rangle \\ &\in \left\langle (B \otimes I_m)D_z e, \mathscr{K}(\Phi(-(B \otimes I_m)D_z e))\right\rangle \\ &= \sum_{i=1}^{n}\left\langle (b_i \otimes I_m)D_z e, \operatorname{conv}(\mathscr{W}_i^f)\right\rangle,\end{aligned}$$

where $\mathscr{W}_i^f := \phi_i(-(b_i \otimes I_m)D_z e)$. Following similar computation as before, for every $i \in \{1, \dots, N\}$, we have that

- if $0 \notin \mathscr{W}_i^f$, then

$$\langle (b_i \otimes I_m)D_z e, \operatorname{conv}(\mathscr{W}_i^f)\rangle \subset \left[-\|u_i^{\max}\|\|(b_i \otimes I_m)D_z e\|, -0.5\|u_i^{\min}\|^2\right]$$

  where $\|u_i^{\max}\| = \max_{w_i \in \mathscr{W}_i^f} \|w_i\|$ and $\|u_i^{\min}\| = \min_{w_i \in \mathscr{W}_i^f} \|w_i\|$; else

- if $\{0\} = \mathscr{W}_i^f$, then

$$\langle (b_i \otimes I_m)D_z e,\ \operatorname{conv}(\mathscr{W}_i^f)\rangle = \{0\}.$$

Hence, at any given time $t \geq 0$, whenever $-(b_i \otimes I_m)D_z e \notin \operatorname{int}(V_{\mathscr{U}_i}(0))$ for some i, we can conclude that the Lyapunov function $J(e(t))$ is strictly decreasing. Otherwise $\dot{J}(e(t)) = 0$. By the radially unboundedness of $J(e)$, this means that as $t \to \infty$, the error function e converges to a ball $\mathbb{B}_{c_e}$ for some $c_e > 0$. Moreover, since $\|z\|$ can be written as a continuous function of e, namely $\|z\| = \sqrt{\sum_{k=1}^{M} |e_k + d_k^2|}$, we also have that $z \in \mathbb{B}_{c_z}$ for some $c_z > 0$. The boundedness of e and z implies that all Krasovskii solutions of the system (4.8) and (4.9) converge to the invariant set

$$\Psi = \{(z, e) | -(b_i \otimes I_m)D_z e \in \operatorname{int}(V_{\mathscr{U}_i}(0)),\ \forall i\}$$

where the state (z, e) remains stationary.

For the rest of the proof, we analyze the bound of e in the invariant set Ψ so that we can obtain the ball size around the origin where the formation error state e converges to. By the definition of Ψ above, it follows that

$$\|(b_i \otimes I_m)D_z e\| \leq \delta_i,$$

holds for all $e \in \Psi$ and for all $i = 1, \ldots, n$. Hence we have that

$$\begin{aligned}\|(B \otimes I_m) D_z e\| &\leq \sum_{i=1}^{n} \|(b_i \otimes I_m) D_z e\| \\ &\leq \sum_{i=1}^{n} \delta_i =: \delta.\end{aligned}$$

Using the same argumentation as in the proof of Proposition 4.2, we can conclude using Lemma 4.1 that both $\|(B \otimes I_m) D_z e\| \leq \delta$ and $D_z e \in \mathrm{Im}(B^\top \otimes I_m)$ imply that $\|D_z e\| \leq \delta$. Note that

$$\|D_z e\| = \sqrt{e^\top D_z^\top D_z e} = \sqrt{e^\top D_{\tilde{z}} e}, \tag{4.10}$$

where $\tilde{z} = [\, \|z_1\|^2 \cdots \|z_M\|^2 \,]^\top$. We will now establish the local practical stability of the closed-loop systems for the error state e. Using the radially unbounded function $J(e(t))$ which is non-increasing as a function of t, $\|e(t)\| \leq \|e(0)\|$ for all $t \geq 0$. Let us initialize the agents in the neighborhood of the desired formation shape, so that $\|e(0)\| < \min\{d_i^2\} = c_1$. Thus, in this case,

$$\|z(t)\|^2 = \sum_{k=1}^{M} |e_k(t) + d_k^2| \geq \sum_{k=1}^{M} (d_k^2 - c_1) = c_2^2 > 0,$$

for all $t \geq 0$ and for some $c_2 > 0$. Combining this with (4.10), we get $\|D_z e\| = \sqrt{e^\top D_{\tilde{z}} e} \geq c_2 \|e\|$. Hence we can conclude that in the invariant set Ψ, we have $\|e\| \leq \frac{1}{c_2} \|D_z e\| \leq \frac{\delta}{c_2}$. □

4.2 Numerical Simulations

In this section, we provide numerical analysis to the proposed cooperative nearest-action control of multi-agent systems, for both the consensus problem, as well as, the formation control problem.

For the numerical analysis, we perform Monte-Carlo simulations with 1000 samples of simulation with the following simulation setup:

1. for each simulation, the number of agents are generated randomly between 3 to 7 agents;

2. the agents are initialized in equidistant circular positions with prescribed rigid *communication* networks and then placed on the 2-dimensional Euclidean space with additional random numbers to the initial coordinates;

3. each agent can only realize motion in three distinct directions in the direction of the vertices of an equilateral triangle with fixed length or stay at their current position. The set of actions realizable by each

agent is described by

$$\mathscr{U}_i = \delta_i \begin{bmatrix} \cos(\theta_i) & -\sin(\theta_i) \\ \sin(\theta_i) & \cos(\theta_i) \end{bmatrix} \left\{ \begin{bmatrix} 0 \\ 0 \end{bmatrix}, \begin{bmatrix} \sin(0) \\ \cos(0) \end{bmatrix}, \begin{bmatrix} \sin(\frac{2\pi}{3}) \\ \cos(\frac{2\pi}{3}) \end{bmatrix}, \begin{bmatrix} \sin(\frac{4\pi}{3}) \\ \cos(\frac{4\pi}{3}) \end{bmatrix} \right\}$$

where δ_i is the smallest upper-bound of Voronoi cell satisfying Lemma 3.1 for each agent $i = 1, \ldots, N$ as in Example 3.2 and θ_i is the randomized rotation angle within the interval $[0, 2\pi)$;

4. for each simulation, the corresponding δ_i of each agent is chosen randomly so that $\sum_i \delta_i = 1$, i.e. the maximum error bound is 1; and

5. the results are processed to obtain the 95% confidence interval statistics for the error vectors, which is the vector z for the consensus problem and the vector e for the formation control problem. We also analyze their minimum and maximum trajectories.

Using the above simulation setup, the results are summarized and presented in Figures 4.1–4.4. The motion animation of both cases can be seen in the following video `https://s.id/MAS-NNC`. It can be seen from Figure 4.1 that by using the nearest-action consensus control as proposed in Proposition 4.2, the agents reach practical consensus as expected. Furthermore, Fig. 4.2 shows that in the steady-state, the norm of the error vector z is always below 1 for all samples, which confirms the theoretical result in Proposition 4.2.

Similar to the consensus case, the nearest-action distance-based formation control as proposed in Proposition 4.3 also performs as expected. In the formation control case, the desired distances between communicating agents are set so that the positions of all agents are on a circle with the radius of 1. To show the behaviour of the closed-loop systems using the proposed nearest-action distributed control, a simulation result of a multi-agent system with four agents (taken from the 1000 random simulations) is shown in Fig. 4.3. In this plot, all agents converge close to the desired formation shape. The statistical plot of Monte Carlo simulations as given in Fig. 4.4 shows that the norm of the formation error vector converges to a ball that is smaller than the upper bound as computed in Proposition 4.3. This means that all agents converge close to desired formation shape for all simulations.

Notably, we can observe from the statistical plots in Fig. 4.2 and Fig. 4.4 that there should be much tighter bounds to the practical stability results as the bounds obtained from the Monte Carlo simulations is significantly below of the computed bound from Propositions 4.2 and 4.3.

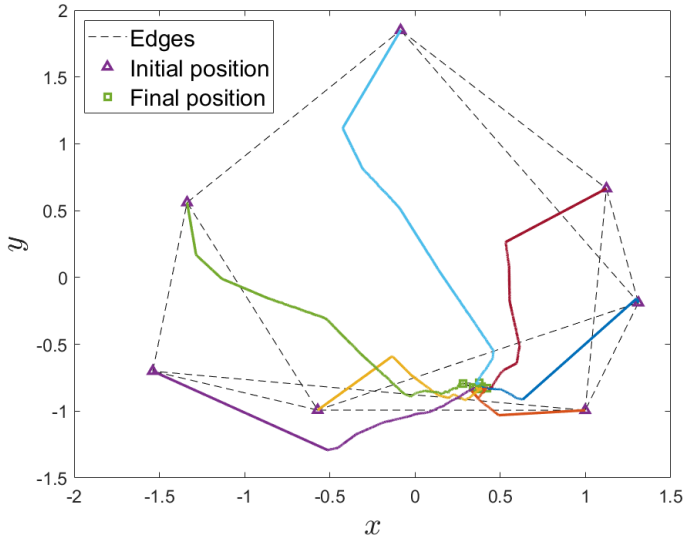

Figure 4.1: An example of consensus mechanism of a system with seven agents communicating over a rigid network where series of actions are chosen by means of nearest-action consensus protocol. This example is taken from one of the 1000 random simulations.

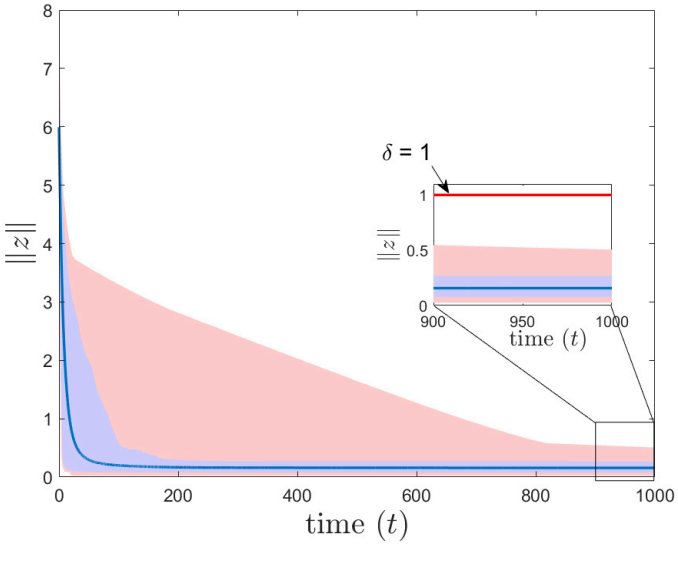

Figure 4.2: Statistics of the norm of consensus error function z with 95% confidence interval (blue area) and 100% data (red area).

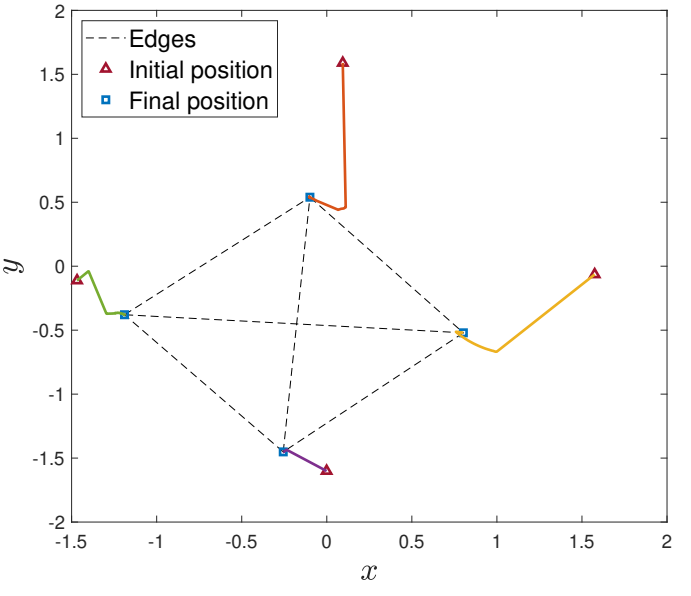

Figure 4.3: An example of agent trajectories for nearest-action formation control taken from the 1000 random simulations.

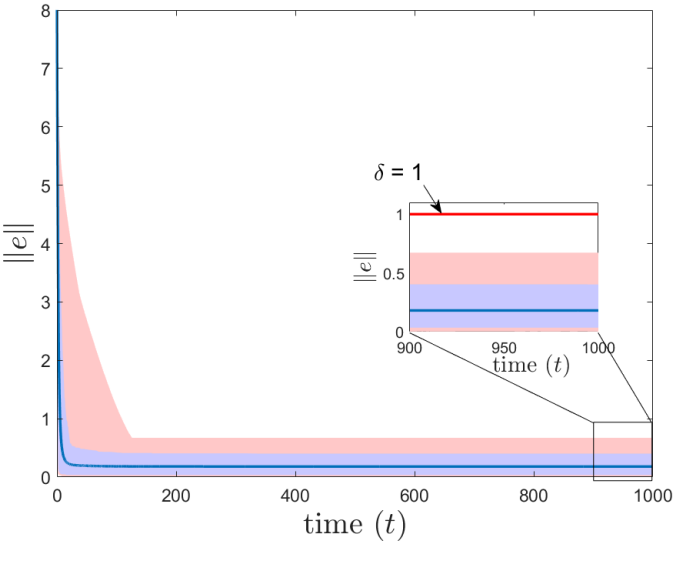

Figure 4.4: Statistics of the norm of formation error function e with 95% confidence interval (blue area) and 100% data (red area).

4.3 Summary

In this chapter, we proposed a nearest-action-based input-quantization procedure for multi agent coordination, namely consensus and distance-based formation control problems where agents can only realize finite countable set of control points. We have provided rigorous analysis for our proposal. Monte Carlo numerical simulations are presented that confirm the practical stability analysis of both consensus and formation control problems.

Chapter 5 | Exponential Stability of LTI Systems with Nearest Action Control

"The knowledge of anything, since all things have causes, is not acquired or complete unless it is known by its causes"

-Ibn Sina-

Contents

In order to practically stabilize a system where only some finite countable actions can be actuated for each time instance, we have proposed a nearest action control (NAC) approach in Chapter 3 for a single agent and in Chapter 4 ([68]) for multi-agent systems. It has been shown that for a given finite countable input set $\mathscr{U}$ satisfying some mild conditions, it is possible to render the closed-loop system practically stable by means of NAC. The ball, to which the state trajectories converge to, depends on the constellation of some elements in $\mathscr{U}$. Particularly, when the cardinality of $\mathscr{U}$ is minimal[1], the closed-loop

[1]By minimality, we mean the smallest number of elements of $\mathscr{U}$ that can be used to

system suffers in terms of control performance, e.g. linear convergence rate as confirmed by numerical results in [66, 68].

In literature, the quantized control systems [22, 69, 70, 71] have been well-studied, which can be considered as the aforementioned NAC problem with an *infinite* countable input set. In these works, the countable input set is obtained via quantization of the input space using either uniform or logarithmic quantizer applied to each input dimension. In this case, the countable input set is given by a grid of (uniform or logarithmic) quantization points and it is assumed that the inputs can be independently actuated. For such quantized control systems, it has been shown that the closed-loop systems can achieve exponential (practical) stability [22, 69, 70, 71]. However, when we consider binary or ternary control systems as studied in [3, 4, 21],which leads to a *finite* countable input set defined on a regular grid, the exponential convergence property is no longer achieved, consistent with the findings in [66, 68].

Motivated by the exponential convergence analysis in the aforementioned works on quantized control systems, we study in this chapter the design and analysis of NAC systems with an infinite countable input set defined on an irregular grid. Specifically, the infinite countable input set is designed based on an admissible minimal $\mathscr{U}$ that is extended to all input space using either uniform or logarithmic distribution. We establish the exponential stability property of the closed-loop systems using the notion of input-to-state practical stability (ISpS).

For analyzing the performance of quantized control systems, the notion of input-to-state stability (ISS) is suitable and has been used in literature [20, 23]. The ISS notion has been developed and used extensively over the past decades to establish the absolute stability and robustness of nonlinear feedback control systems. Some of recent results and applications are [37, 72, 73, 74, 75, 76, 77, 78], among many others. It is also used to establish practical stability of nonlinear systems, as studied in [79, 80, 81, 82]. For the particular case relevant to the this paper, it has been shown in the tutorial paper [23] that under some mild conditions on the linear time invariant (LTI) systems, applying uniform quantizer in the feedback loop renders the system exponentially practically stable. In this chapter we use similar approach as used in [23] to establish the practical exponential stability of the NAC systems with an infinite countable set.

practically stabilized the systems using the nearest action control approach.

5.1 ISS & practical stability with Weak Sector Condition for MIMO LTI Systems

In this chapter, we consider the Lur'e type feedback system Σ_{lin} represented by a differential inclusion (2.15) along with its transfer function and the notion of input-to-state practical stablility (ISpS) defined around (2.16) as described in Chapter 2.6.

Although the ISS property of MIMO linear system (2.15) was established in [23, 37], the stability property requires a strong condition on the sector bound, namely $\langle k_1 y - v, k_2 y - v\rangle \leq 0,\ \forall v \in \Psi(y),\ \forall y \in \mathbb{R}^m$ for some scalars $k_1 < k_2$. In this chapter, we use the more familiar yet weaker version of the sector condition than before, that is $k_1\|y\|^2 \leq \langle v, y\rangle \leq k_2\|y\|^2,\ \forall v \in \Psi(y),\ \forall y \in \mathbb{R}^m$ for some scalars $k_1 < k_2$. One can immediately verify that the former condition implies the latter but not vice versa. Indeed, by multiplying the former sector condition with $\|y\|^2$ and since, by definition, we have $\langle v, y\rangle^2 \leq \|v\|^2\|y\|^2$, it follows that

$$\begin{aligned} 0 &\geq \|y\|^2 \langle k_1 y - v, k_2 y - v\rangle + \langle v, y\rangle^2 - \|v\|^2\|y\|^2 \\ &= k_1 k_2 \|y\|^4 - (k_1 + k_2)\langle v, y\rangle \|y\|^2 \langle v, y\rangle^2 \\ &= \langle k_1 y - v, y\rangle \langle k_2 y - v, y\rangle. \end{aligned}$$

Since $k_1 < k_2$, it must be that $\langle k_1 y - v, y\rangle \leq 0$ and $\langle k_2 y - v, y\rangle \geq 0$ which directly implies $k_1\|y\|^2 \leq \langle v, y\rangle \leq k_2\|y\|^2$. For the converse, we can easily find an example where the latter sector condition does not imply the former. For example, by taking $k_1 = 1,\ k_2 = 2,\ y = \left[\begin{smallmatrix} 0 \\ 2 \end{smallmatrix}\right]$, and $v = \left[\begin{smallmatrix} 1 \\ 2 \end{smallmatrix}\right]$, it can be verified easily that the latter sector condition holds but the former does not.

Remark 5.1. It is useful to note that the sector condition

$$k_1\|y\|^2 \leq \langle v, y\rangle \leq k_2\|y\|^2,\ \forall v \in \Psi(y),\ y \in \mathbb{R}^m,$$

for some scalars $k_1 < k_2$ implies

$$\left\| v - \frac{k_1 + k_2}{2} y \right\| \leq \frac{k_2 - k_1}{2c}\|y\| \tag{5.1}$$

where $c \in (0, 1]$ if $v \neq \frac{k_1+k_2}{2} y$ or $\|v - \frac{k_1+k_2}{2} y\| = 0$, otherwise. ⋄

The adaptation of the ISpS property of (2.15) in Theorem 2.9 with weak sector condition on Ψ is stated in the following theorem.

Theorem 5.2. Consider the system Σ_{lin} in (2.15). Suppose that the pair (A, B) is controllable and (A, C) is observable. For the mapping Ψ, assume that there exist scalars $k_1 < k_2$ such that for all $v \in \Psi(y)$ and for all $y \in \mathbb{R}^m$, it holds that $k_1\|y\|^2 \leq \langle v, y\rangle \leq k_2\|y\|^2$. In addition, assume that $G(I + k_1 G)^{-1} \in H^\infty$ and that $(I + k_2 G)(I + k_1 G)^{-1}$ is strictly positive real. Then every maximal solution

forward complete and there exist positive constants c_1, c_2, and ε such that, for all $x(0) \in \mathbb{R}^n$, every solution x satisfies

$$\|x(t)\| \leq c_1 e^{-\varepsilon t}\|x(0)\| + c_2 \|\Delta_{[0,t]}\|_\infty, \ \forall t \in \mathbb{R}_{>0}. \tag{5.2}$$

$\diamond$

The proof, again, follows directly from the proof of [23, Theorem 3.4]. The only difference is the part where we use Remark 5.1 instead of [23, Remark 3.1] in obtaining the result.

Correspondingly, throughout the rest of this chapter, we assume the following condition.

(A5.0) For the system Σ_{lin} in (2.15), the pair (A, B) is controllable and (A, C) is observable.

(A5.1) For the system Σ_{lin} in (2.15) and the set-valued map Ψ, there exist scalars $k_1 < k_2$ such that

$$k_1\|y\|^2 \leq \langle v, y\rangle \leq k_2\|y\|^2, \ \forall v \in \Psi(y), \ \forall y \in \mathbb{R}^m; \tag{5.3}$$

$G(I + k_1 G)^{-1} \in H^\infty$ and that $(I + k_2 G)(I + k_1 G)^{-1}$ is strictly positive real.

5

Let ω be the minimum upper bound such that $c_2\|\Delta(t)\|_\infty \leq \omega$. For the rest of this chapter, we say that the system (2.15) is globally practically stable with respect to ball $\mathbb{B}_\omega$ (ω-GPS) if (2.15) is ISpS with bias ω, i.e. the global solution of x satisfies

$$\|x(t)\| \leq c_1 e^{-\varepsilon t}\|x(0)\| + \omega, \ \forall t \in \mathbb{R}_{>0}.$$

If, in addition, the solution of (2.15) decays exponentially towards $\mathbb{B}_\omega$, we say that (2.15) is globally exponentially practically stable with respect to ball $\mathbb{B}_\omega$ (ω-GEPS). Correspondingly, the system (2.15) is globally asymptotically stable (GAS) if it is 0-GPS and it is globally exponentially stable (GES) if it is 0-GEPS.

5.2 Nearest Action Control Revisited

In Chapter 3, it has been shown that for a general class of passive nonlinear systems with proper storage function, large-time initial-state norm-observability assumption, and a given limited control actions $\mathscr{U}$, the system can be practically stabilized by using the feedback law $u = \phi_{\mathscr{U}}(-y)$. Note that for linear systems, the large-time norm-observability notion in nonlinear systems is equivalent to the usual observability notion for linear systems [83, Remark 4]. For the linear MIMO system, the unity output-feedback practical stabilization result can be expressed into the following proposition.

Proposition 5.3. Consider the system Σ_{lin} in (2.15) with $\Delta \equiv 0$ satisfying (A5.0) with $G(s)$ being strictly positive real, and a given finite set $\mathscr{U}$ satisfying (A3.1) so that (3.2) holds for some $\delta > 0$. Let $\phi_{\mathscr{U}}$ be as defined in (3.6). Let $\gamma : \mathbb{R}_{\geq 0} \to \mathbb{R}_{\geq 0}$ be defined as,[2]

$$\gamma(\delta) := \delta \, \|(W_\tau(t))^{-1}\| \int_t^{t+\tau} \|e^{A^\top(s-t)} C^\top\| \, \mathrm{d}s, \tag{5.4}$$

where $W_\tau(t) = \int_t^{t+\tau} e^{A^\top(s-t)} C^\top C e^{A(s-t)} \, \mathrm{d}s$, and suppose that for a given $\omega > 0$, it holds that $\gamma(\delta) \leq \omega$. Then, the closed-loop system with $u = \phi(-y)$ is ω-GEPS. ⋄

To prove the above proposition using Theorem 5.2, we need to find suitable constants k_1 and k_2 that satisfy the weak sector condition (5.3) with $\Psi(y)$ be replaced by $-\phi_{\mathscr{U}}(-y)$ for all $y \in \mathbb{R}^m$. By Lemmas 3.1 and 3.3, for all $y \in \mathbb{R}^m \setminus \mathbb{B}_\delta$ and for all $w \in -\phi_{\mathscr{U}}(-y)$, we have $w \neq 0$ and $\frac{1}{2}\|w\|^2 \leq \langle w, y \rangle \leq \|w\| \cdot \|y\|$. The last inequality can be written as $k_1\|y\|^2 \leq \langle w, y \rangle \leq k_2\|y\|^2$ with

$$k_1 = \inf_{\substack{w \in -\phi_{\mathscr{U}}(-y) \\ y \in \mathbb{R}^m \setminus \mathbb{B}_\delta}} \frac{\|w\|^2}{2\|y\|^2} \text{ and } k_2 = \sup_{\substack{w \in -\phi_{\mathscr{U}}(-y) \\ y \in \mathbb{R}^m \setminus \mathbb{B}_\delta}} \frac{\|w\|}{\|y\|}.$$

Then, we can conclude that the weak sector condition (5.3) is satisfied outside the ball $\mathbb{B}_\delta$ with $\Phi(y)$ be replaced by $-\phi_{\mathscr{U}}(-y)$ for all $y \in \mathbb{R}^m \setminus \mathbb{B}_\delta$. We also note that since the transfer function G is already strictly positive real, it follows that the assumption (A5.1) is satisfied outside the ball $\mathbb{B}_\delta$.

In order to apply Theorem 5.2, we write the nearest action map $\phi_{\mathscr{U}}$ as a linear combination of a mapping $\Psi_{\mathscr{U}}(y)$ that satisfies the weak sector condition everywhere and an output-dependent disturbance term $\Delta_{\mathscr{U}}(y)$ given by

$$\Psi_{\mathscr{U}}(y) := \begin{cases} -\phi_{\mathscr{U}}(-y), & y \in \mathbb{R}^m \setminus V_{\mathscr{U}}(0), \\ \frac{k_2+k_1}{2} y, & \text{otherwise.} \end{cases} \tag{5.5}$$

and $\Delta_{\mathscr{U}}(y) := \phi_{\mathscr{U}}(-y) + \Psi_{\mathscr{U}}(y)$, respectively. It follows that the mapping $\Psi_{\mathscr{U}}$ in (5.5) satisfies assumption (A5.1) everywhere. Futhermore, by definition, for all $d \in \Delta_{\mathscr{U}}$, we have that $\|d\| \leq \delta$. Observe that the closed-loop of the linear system in Σ_{lin} with $u = \phi_{\mathscr{U}}(y)$ is equivalent to Σ_{lin} with Δ replaced by $\Delta_{\mathscr{U}}$ and Ψ replaced by $\Psi_{\mathscr{U}}$. Finally, by direct application of Theorem 5.2 and since $\gamma(\delta) \leq \epsilon$, we have that Σ_{lin} with $u = \phi_{\mathscr{U}}(-y) = \Delta_{\mathscr{U}}(y) - \Psi_{\mathscr{U}}(y)$ is ISpS with bias ϵ.

[2] The function γ as described in (5.4) is a natural consequence of the standard observability assumption for LTI systems. Interested readers may consult on [66, Remark 1] for reference.

5.2.1 Nearest Action Control with Uniform and Logarithmic Points Extension

In this chapter, we are interested in the output feedback stabilization of the system Σ_{lin} in (2.15). In Chapter 3, the nearest action control approach is presented where the input u can only take values from a finite countable set $\mathscr{U}$. As remarked above, in the standard multi-valued quantizers, the quantization takes place in each dimension of the input space leading to a regular grid of infinite countable input set $\mathscr{U}$.

Instead of considering the regular grid obtained through element-wise quantization as before, we consider in this chapter the extension of minimal $\mathscr{U}$ studied in Chapter 3 ([66]) to an infinite countable input set defined on the whole input space $\mathbb{R}^m$. It is constructed by enlarging $\mathscr{U}$ using each element $u_i \in \mathscr{U}$ as the vector to which infinitely new elements are generated uniformly or logarithmically. Without loss of generality, for the rest of this chapter, let us consider instead a finite countable set

$$\begin{aligned} \mathscr{U} &:= \{u_1, \dots, u_p \in \mathbb{R}^m : \|u_i\| = 1\} \\ &\text{and } \mathscr{U} \bigcup \{0\} \text{ satisfies (A3.1).} \end{aligned} \tag{5.6}$$

Note that here we explicitly remove the zero (0) element from the set $\mathscr{U}$ used in Section 5.2. More formally, the uniformly-extended infinite countable set $\mathscr{U}_u^{\text{ext}}$ is given by

$$\mathscr{U}_u^{\text{ext},\lambda} := \{k\lambda u \mid k \in \mathbb{Z}_{\geq 0},\ u \in \mathscr{U}\}, \tag{5.7}$$

where $\lambda > 0$ is the desired uniform step size. Similarly, the logarithmically-extended infinite countable set $\mathscr{U}_l^{\text{ext}}$ is given by

$$\mathscr{U}_l^{\text{ext},\lambda} := \{0\} \bigcup \{\lambda^k u \mid k \in \mathbb{Z},\ u \in \mathscr{U}\} \tag{5.8}$$

where $\lambda > 1$ is the desired geometric step size.

Remark 5.4. The use of unit vectors u_i in this extended set is to simplify the presentation of our main results and they are related to the characterization of the convergence ball. In general, we can consider any vectors of any length in the minimal countable set $\mathscr{U}$ to represent directions. Furthermore, if there exists at least one vector $u \in \mathscr{U}$ with $\|u\| \neq 1$, these vectors can be obtained by choosing a suitable step size λ in $\mathscr{U}_u^{\text{ext},\lambda}$ or $\mathscr{U}_l^{\text{ext},\lambda}$. ⋄

By the definition of the nearest action map $\phi_{\mathscr{U}}$ in (3.6), it is easy to see that for the uniformly distributed points, for all $z \in \mathbb{R}^m$, the nearest action mapping can be decomposed into

$$\phi_{\mathscr{U}_u^{\text{ext},\lambda}}(z) = \phi_{\mathscr{U}}(z) Q_u^{\lambda}(\langle z, \phi_{\mathscr{U}}(z)\rangle), \tag{5.9}$$

with Q_u^{λ} be the symmetric uniform quantizer in (2.19). While the standard

uniform quantizer Q_u^λ defined in (2.19) obeys the nearest-action rule, the standard logarithmic quantizer Q_l^λ defined in (2.20) does not. Instead, in the case of (2.20), only the quantized exponent obeys the nearest-action rule, i.e. $-\frac{1}{2} \leq \log_\lambda |\eta| - \left\lfloor \frac{1}{2} + \log_\lambda |\eta| \right\rfloor \leq \frac{1}{2}$. The logarithmic quantizer (2.20) is therefore not suitable for the decomposition of $\phi_{\mathscr{U}_l^{\text{ext},\lambda}}$.

In order for the logarithmic quantizer to satisfy the nearest action rule, for any scalar $\eta \in \mathbb{R}_{>0}$ that is mapped to λ^k, $k \in \mathbb{Z}$, $\lambda \in \mathbb{R}_{>1}$, it must be that

$$\frac{\lambda^{k-1} + \lambda^k}{2} \leq \eta \leq \frac{\lambda^k + \lambda^{k+1}}{2}.$$

By inspecting the upper and lower bound of above inequality, we have that

$$\eta \leq \frac{\lambda^k + \lambda^{k+1}}{2} \Leftrightarrow \lambda^k \geq \frac{2\eta}{\lambda+1} \Leftrightarrow k \geq \log_\lambda \left(\frac{2\eta}{\lambda+1} \right),$$

and

$$\eta \geq \frac{\lambda^{k-1} + \lambda^k}{2} \Leftrightarrow \lambda^k \leq \frac{2\lambda\eta}{\lambda+1} \Leftrightarrow k \leq \log_\lambda \left(\frac{2\lambda\eta}{\lambda+1} \right),$$

respectively. Using the above relationships and considering also the negative part of the input variable, we define the *symmetric* logarithmic quantizer $Q_{sl}^\lambda : \mathbb{R} \to \mathbb{R}$ as

$$Q_{sl}^\lambda(\eta) = \begin{cases} 0, & \eta = 0 \\ \text{sign}(\eta)\lambda^{\left\lfloor \log_\lambda\left(\frac{2\lambda|\eta|}{\lambda+1}\right)\right\rfloor}, & \eta \neq 0. \end{cases} \tag{5.10}$$

By using Q_{sl}^λ, for all $z \in \mathbb{R}^m$, we can decompose $\phi_{\mathscr{U}_l^{\text{ext},\lambda}}$ into

$$\phi_{\mathscr{U}_l^{\text{ext},\lambda}}(z) = \phi_{\mathscr{U}}(z) Q_{sl}^\lambda \left(\langle z, \phi_{\mathscr{U}}(z) \rangle \right). \tag{5.11}$$

Illustrations of the nearest action region obtained using the nearest action map $\phi_{\mathscr{U}_u^{\text{ext},\lambda}}$ in (5.9) or $\phi_{\mathscr{U}_l^{\text{ext},\lambda}}$ in (5.11) is shown in Fig. 5.1. For the logarithmically-extended infinite countable set $\mathscr{U}_l^{\text{ext},\lambda}$, it can be seen from Fig. 5.1(b) that the separating lines perpendicular to the direction of each $u_i \in \mathscr{U}$ (in blue) are equidistant to two black dots. Hence the name *symmetric* for (5.10).

5.3 Absolute Stability Analysis of The Nearest Action Control

In this section, we present our main result on the output-feedback practical stabilization of the system Σ_{lin} described in (2.15) using the *directional* nearest-action feedback control law $u = \phi_{\mathscr{U}}(-y)$ with $\phi_{\mathscr{U}}$ be as in (3.6).

The set of realizable input considered in this section is the extended (possibly infinite) countable sets $\mathscr{U}^{\text{ext}}$ described in Section 5.2.1 along with their

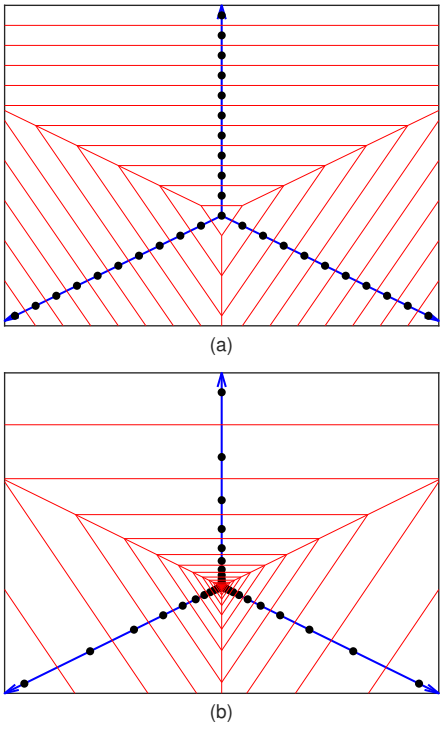

Figure 5.1: Illustration of the nearest action region of the (possibly infinite) realizable actions (represented by the black dots) set distributed (a) uniformly (as in (5.7)) or (b) logarithmically (as in (5.8)) along limited directions (blue arrows) in 2-dimensional input-output space. Here, the central coordinate is 0 (zero action). The region around each action (black dot) enclosed by the red lines represents the Voronoi cell of the respective action, i.e. all points in the enclosed area are mapped to their respective black dots by means of the nearest action map $\phi_{\mathscr{U}^{\text{ext}}}$.

respective decomposable nearest action maps and scalar quantizers. In the general setting, we consider the extended set $\mathscr{U}^{\text{ext}}$ to be

$$\mathscr{U}^{\text{ext}} := \{qu_i \mid u_i \in \mathscr{U}, q \in \mathscr{Q}\} \tag{5.12}$$

where $\mathscr{U}$ is defined in (5.6) and $\{0, q_1, q_2, \dots\} =: \mathscr{Q} \subset \mathbb{R}_{\geq 0}$ with $0 < q_1 < q_2 < \dots$ is a (possibly infinite) countable set containing non-negative scaling factors. Using the set $\mathscr{Q}$, we define a generic non-negative nearest action scalar quantizer $Q : \mathbb{R}_{\geq 0} \to \mathscr{Q}$ as follows

$$Q(\eta) = \phi_{\mathscr{Q}}(\eta) := \underset{q \in \mathscr{Q}}{\arg\min}\{\|q - \eta\|\} \tag{5.13}$$

where $\eta \in \mathbb{R}_{\geq 0}$.

Note that the quantizer Q in (5.13) can be in any form of quantizer obeying the nearest action rule such as the symmetric uniform quantizer Q_u^λ in (2.19). Using (5.13), for all $z \in \mathbb{R}^m$, the nearest action map $\phi_{\mathscr{U}^{\text{ext}}}$ as in (3.6) (with $\mathscr{U}$ be replaced by $\mathscr{U}^{\text{ext}}$) can be decomposed into

$$\phi_{\mathscr{U}^{\text{ext}}}(z) = \phi_{\mathscr{U}}(z) Q(\langle z, \phi_{\mathscr{U}}(z)\rangle). \tag{5.14}$$

Then the following lemma for the setting in (5.12), (5.13), and (5.14) is true.

Lemma 5.5. If for all $\eta \in [\frac{1}{2}q_1, \infty)$, there exists $\kappa_1, \kappa_2 \in \mathbb{R}_{>0}$ with $\kappa_1 < \kappa_2$ so that the scalar quantizer Q satisfies the sector bound

$$\kappa_1 \eta^2 \leq \eta Q(\eta) \leq \kappa_2 \eta^2, \tag{5.15}$$

then for all $z \in \mathbb{R}^n$ and $n \in \mathbb{N}$ satisfying $\langle z, \phi_{\mathscr{U}}(z)\rangle \geq \frac{1}{2}q_1$, the following inequality holds for some $\alpha \in (0, 1]$,

$$\alpha\kappa_1 \|z\|^2 \leq \langle z, \phi_{\mathscr{U}^{\text{ext}}}(z)\rangle \leq \kappa_2 \|z\|^2. \tag{5.16}$$

$\diamond$

Proof. We first note that the nearest action map $\phi_{\mathscr{U}^{\text{ext}}}(z)$ is exactly the direction pointed by the mapping $\phi_{\mathscr{U}}(z)$ multiplied by the positive scalar obtained from quantizing the scalar projection of z in the same direction using the scalar quantizer Q. We also note that since for all $u \in \mathscr{U}$, $\|u\| = 1$, by the definition of $\phi_{\mathscr{U}}$ we have that $\frac{1}{2} \leq \langle z, \phi_{\mathscr{U}}(z)\rangle \leq \|z\|$. This means that there exists a lower bound $\alpha \in (0, 1]$ so that the following holds for all $z \in \mathbb{R}^n$

$$\alpha\|z\| \leq \langle z, \phi_{\mathscr{U}}(z)\rangle \leq \|z\|. \tag{5.17}$$

By taking the upper bound in (5.15), the decomposed nearest action map (5.14), and using the inequality (5.17), it follows that for all $z \in \mathbb{R}^n$ satisfying $\langle z, \phi_{\mathscr{U}}(z)\rangle \geq \frac{1}{2}q_1$ we have

$$\begin{aligned}\langle z, \phi_{\mathscr{U}^{\text{ext}}}(z)\rangle &= \langle z, \phi_{\mathscr{U}}(z) Q(\langle z, \phi_{\mathscr{U}}(z)\rangle)\rangle \\ &= \langle z, \phi_{\mathscr{U}}(z)\rangle Q(\langle z, \phi_{\mathscr{U}}(z)\rangle) \leq \kappa_2 \langle z, \phi_{\mathscr{U}}(z)\rangle^2 \leq \kappa_2 \|z\|^2.\end{aligned}$$

Similarly, for the lower bound in (5.15) we have that

$$\langle z, \phi_{\mathscr{U}^{\text{ext}}}(z)\rangle = \langle z, \phi_{\mathscr{U}}(z)\rangle Q(\langle z, \phi_{\mathscr{U}}(z)\rangle) \geq \kappa_1 \langle z, \phi_{\mathscr{U}}(z)\rangle^2 \geq \alpha\kappa_1 \|z\|^2.$$

Therefore, the inequality (5.16) holds. □

Using the weak sector bound result on $\phi_{\mathscr{U}^{\text{ext}}}$ stated in Lemma 5.5, we can then analyze the stability property of the system Σ_{lin} described by (2.15) using the notion of ISpS as presented in the following proposition.

Proposition 5.6. Consider the system Σ_{lin} in (2.15) satisfying **(A5.0)** and a discrete set $\mathscr{U}^{\text{ext}}$ as in (5.12) constructed from a finite countable set of unit vectors $\mathscr{U}$ that together with $\{0\}$ satisfies **(A3.1)** so that (3.2) holds for some

$\delta > 0$. Let $\phi_{\mathscr{U}^{\text{ext}}}$ be as in (5.14). Suppose that $\phi_{\mathscr{U}^{\text{ext}}}$ satisfies (5.16) for some $\alpha \in (0,1]$ and $0 < \kappa_1 < \kappa_2$. In addition, assume that $G(I+\alpha\kappa_1 G)^{-1} \in H^\infty$ and that $(I+\kappa_2 G)(I+\alpha\kappa_1 G)^{-1}$ is strictly positive real. Then the closed-loop system with $u = \phi_{\mathscr{U}^{\text{ext}}}(-y)$ is ω-GEPS with $\omega = c_2\delta q_1$ for some $c_2 > 0$. ⋄

Proof. We first note that since by the definition of $\phi_{\mathscr{U}^{\text{ext}}}$ in (5.14) and according to Lemma 3.1, for the set $\mathscr{U}^{\text{ext}}$ we have that $V_{\mathscr{U}^{\text{ext}}} \subseteq \mathbb{B}_{\delta q_1}$. In order to successfully apply Theorem 1, and since $\phi_{\mathscr{U}^{\text{ext}}}$ satisfies assumption (A5.1) only outside the ball $\mathbb{B}_{\delta q_1}$, we define $\Psi_{\mathscr{U}^{\text{ext}}}$ as in (5.5) with $\mathscr{U}$ replaced by $\mathscr{U}^{\text{ext}}$, $k_1 = \alpha\kappa_1$, and $k_2 = \kappa_2$, so that the sector condition is satisfied everywhere by means of $\Psi_{\mathscr{U}^{\text{ext}}}$. Following the proof of Proposition 5.3, we can apply the result in Theorem 5.2 to conclude that the system Σ_{lin} is ω-GEPS with $\omega = c_2\delta q_1$ for some $c_2 > 0$. □

5.3.1 Practical Stabilization with Uniformly-Extended Actions

Lemma 5.7. Let $Q_u^\lambda : \mathbb{R} \to \mathbb{R}$ be the uniform quantizer defined in (2.19) along with a given desired stepsize $\lambda > 0$. For all $\sigma > 0$ such that $\frac{\lambda}{2} \le \sigma$, it holds that

$$\left(1 - \frac{\lambda}{2\sigma}\right)\eta^2 \le \eta Q_u^\lambda(\eta) \le \left(1 + \frac{\lambda}{2\sigma}\right)\eta^2, \tag{5.18}$$

for all $\eta \ge \sigma$. ⋄

Proof. By the definition of $Q_u^\lambda(\eta)$ in (2.19), the difference between η and $Q_u^\lambda(\eta)$ satisfies

$$-\frac{\lambda}{2} \le \eta - Q_u^\lambda(\eta) \le \frac{\lambda}{2}.$$

Taking the upper bound of above inequality, it follows that

$$\begin{aligned} \eta - Q_u^\lambda(\eta) \le \frac{\lambda}{2} \qquad \Leftrightarrow \qquad Q_u^\lambda(\eta) &\ge \eta - \frac{\lambda}{2} = \left(1 - \frac{\lambda}{2\eta}\right)\eta \\ &\ge \left(1 - \frac{\lambda}{2\sigma}\right)\eta. \end{aligned}$$

Similarly, using the lower bound $-\frac{\lambda}{2} \le \eta - Q_u^\lambda(\eta)$, it follows that

$$\begin{aligned} \eta - Q_u^\lambda(\eta) \ge -\frac{\lambda}{2} \qquad \Leftrightarrow \qquad Q_u^\lambda(\eta) &\le \eta + \frac{\lambda}{2} = \left(1 + \frac{\lambda}{2\eta}\right)\eta \\ &\le \left(1 + \frac{\lambda}{2\sigma}\right)\eta. \end{aligned}$$

Finally, by combining the upper and lower bounds of $Q_u^\lambda(\eta)$ and multiplying all sides of the combined inequality by η we have the inequality (5.18). □

Proposition 5.8. Consider the system Σ_{lin} described by (2.15) satisfying (A5.0) and a discrete set $\mathscr{U}_u^{\text{ext},\lambda}$ as in (5.7) constructed from a finite countable set of unit vectors $\mathscr{U}$ that together with $\{0\}$ satisfies (A3.1) so that (3.2) holds for some $\delta > 0$. Let $\phi_{\mathscr{U}_u^{\text{ext},\lambda}}$ and Q_u^λ be as in (5.9) and (2.19), respectively, along with a given desired stepsize $\lambda > 0$. Suppose that $\phi_{\mathscr{U}_u^{\text{ext},\lambda}}$ satisfies (5.16) for some $\alpha \in (0,1]$, $\kappa_1 = \left(1 - \frac{1}{2\delta}\right)$, and $\kappa_2 = \left(1 + \frac{1}{2\delta}\right)$. In addition, assume that $G(I + \alpha\kappa_1 G)^{-1} \in H^\infty$ and that $(I + \kappa_2 G)(I + \alpha\kappa_1 G)^{-1}$ is strictly positive real. Then the closed-loop system with $u\phi_{\mathscr{U}_u^{\text{ext},\lambda}}(-y)$ is ω-GEPS with $\omega = c_2\delta\lambda$ for some $c_2 > 0$. ◇

Proof. We first observe that with regards to the nearest action selection approach where $\delta \geq \frac{1}{2}$ is the minimum upper bound satisfying $\mathscr{U} \subseteq \mathbb{B}_\delta$, the condition $\frac{\lambda}{2} \leq \sigma$ in Lemma 5.7 is satisfied with $\sigma = \lambda\delta$. Next, for all $\eta \geq \lambda\delta$, we have that

$$\left(1 - \frac{1}{2\delta}\right)\eta^2 \leq \eta Q_u^\lambda(\eta) \leq \left(1 + \frac{1}{2\delta}\right)\eta^2.$$

Using the result in Lemma 5.5, it follows that for all $z \in \mathscr{R}^n$, $n \in \mathbb{N}$, satisfying $\langle z, \phi_{\mathscr{U}}(z)\rangle \geq \frac{\delta}{2}$, there exists $\alpha \in (0,1]$ so that the mapping $\phi_{\mathscr{U}_u}(z)$ satisfies the sector condition

$$\alpha\left(1 - \frac{1}{2\delta}\right)\|z\|^2 \leq \langle z, \phi_{\mathscr{U}_u^{\text{ext},\lambda}}(z)\rangle \leq \left(1 + \frac{1}{2\delta}\right)\|z\|^2. \tag{5.19}$$

Finally, we use the result in Proposition 5.6 to complete the proof. □

5.3.2 Global Exponential Stabilization with Logarithmically-Extended Actions

We next present the case where the system can only realize actions in the direction contained in $\mathscr{U}$ with logarithmically distributed positive scaling factors. For this purpose, we have that the logarithmic quantizer $Q_{sl}^\lambda(\eta)$ defined (5.10) satisfies the sector condition in (A5.1) as shown in the following lemma.

Lemma 5.9. Let $Q_{sl}^\lambda : \mathbb{R} \to \mathbb{R}$ be the symmetric logarithmic quantizer defined in (5.10) along with a given desired stepsize $\lambda > 1$. Then

$$\left(\frac{2}{\lambda + 1}\right)\eta^2 \leq \eta Q_{sl}^\lambda(\eta) \leq \left(\frac{2\lambda}{\lambda + 1}\right)\eta^2 \tag{5.20}$$

holds for all $\eta \in \mathbb{R}_{\geq 0}$. ◇

Proof. To prove the above lemma, we first observe that from the symmetric property of Q_{sl}^λ we have

$$Q_{sl}^\lambda(\eta)\frac{(\lambda + 1)}{2\lambda} \leq \eta \leq Q_{sl}^\lambda(\eta)\frac{(\lambda + 1)}{2}.$$

By taking the upper and lower bound of above inequality, we have that

$$\eta \leq Q_{sl}^{\lambda}(\eta)\frac{(\lambda+1)}{2} \qquad \Leftrightarrow \qquad Q_{sl}^{\lambda}(\eta) \geq \left(\frac{2}{\lambda+1}\right)\eta,$$

and

$$\eta \geq Q_{sl}^{\lambda}(\eta)\frac{(\lambda+1)}{2\lambda} \qquad \Leftrightarrow \qquad Q_{sl}^{\lambda}(\eta) \leq \left(\frac{2\lambda}{\lambda+1}\right)\eta,$$

respectively. By combining both the upper and lower bound of Q_{sl}^{λ}, we have that

$$\left(\frac{2}{\lambda+1}\right)\eta \leq Q_{sl}^{\lambda}(\eta) \leq \left(\frac{2\lambda}{\lambda+1}\right)\eta.$$

Finally, the inequality (5.20) holds for all $\eta \geq 0$. □

Proposition 5.10. Consider the system Σ_{lin} described by (2.15) satisfying (A5.0) and a discrete set $\mathscr{U}_l^{\text{ext},\lambda}$ as in (5.8) constructed from a finite countable set of unit vectors $\mathscr{U}$ that together with $\{0\}$ satisfies (A3.1) so that (3.2) holds for some $\delta > 0$. Let $\phi_{\mathscr{U}_l^{\text{ext},\lambda}}$ and Q_{sl}^{λ} be as given in (5.11) and (5.10), respectively, along with a given desired step size $\lambda > 1$. Furthermore, assume that (A5.1) holds with $\Psi(y)$ replaced by $-\phi_{\mathscr{U}_l^{\text{ext},\lambda}}(-y)$ for all $y \in \mathbb{R}^m$, $k_1 = \alpha\left(\frac{2\lambda}{\lambda+1}\right)$ for some $\alpha \in (0,1]$, and $k_2 = \left(\frac{2}{\lambda+1}\right)$. Then the closed-loop system with $u = \phi_{\mathscr{U}_l^{\text{ext},\lambda}}(-y)$ is GES. ◇

The last proposition is similar to the result in Proposition 5.8, with the exception that the assumption (A5.1) is already satisfied everywhere. Therefore, applying the result in Proposition 5.6 results in the closed-loop system being 0-GEPS, i.e. the closed-loop system is GES.

5.4 Illustrative Example

In this section, we present a numerical example to validate our main results for both the uniform and logarithmic nearest-action feedback approaches. We consider an interconnected Ocean Battery system where at least one battery is directly connected to the grid. The Ocean Battery is a novel underwater energy storage system based on the concept of pumped hydro storage [84]. It converts electrical energy supplied from renewable sources such as wind and/or floating solar into stored potential energy which is available naturally due to the presence of hydrostatic pressure from the surrounding environment. For practical applications, the Ocean Battery is installed at a certain depth depending on the requirements of the storage system. For offshore application in sufficiently deep waters, for example, the Ocean Battery is installed on the seabed for the optimal operation; alternatively, the effective depth at which

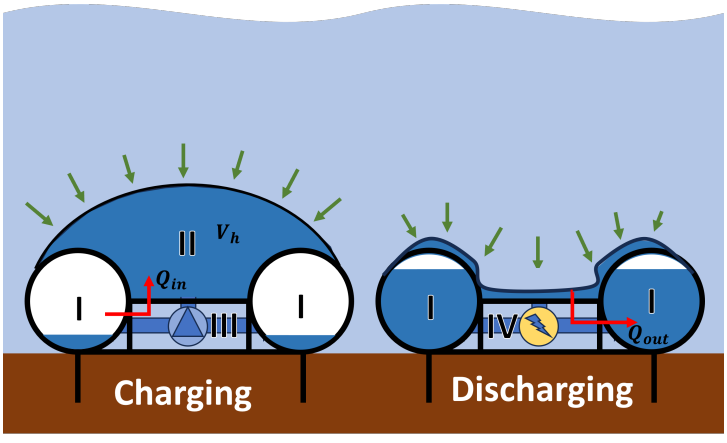

Figure 5.2: Schematic of single ocean battery system sitting on the seabed with I) low-pressure area (rigid reservoir under atmospheric pressure), II) high-pressure area (flexible reservoir under hydrostatic pressure from underwater environment), III) water pump (blue triangle) to pump water from low to high pressure area, and IV) generator to generate electricity by releasing water from high to low pressure area. Left picture shows the battery state when charging while the picture on the right side shows the state when discharging.

the device operates can be increased by burying the rigid reservoir and machine room into the seabed.

In this example, we consider multiple interconnected Ocean Battery systems whose operations follow the schematic presented in Fig. 5.2 where Q^i_{in} and Q^i_{out} are the total in/outflow of water in the i-th battery, and V^i_h is its corresponding water volume in its high-pressure reservoir. We assume that the generator is designed in a way so that the outflow Q^i_{out} remains constant all the time. Furthermore, we consider the use of multi piston-pump power take-off system described in Chapter 7 for the pumps installed in the battery. Specifically, we are looking into a very particular case of only the upstroke motion of the pumps where the incoming wave is increasing linearly over time. A single Ocean Battery system can be described by $\dot{V}^i = Q^i$ where $V^i = V^i_h - V^{i,\text{ref}}_h$ with $V^{i,\text{ref}}_h$ be the target volume of high-pressure fluid in the i-th battery, and Q^i represents the total inflow to the i-th battery, i.e. $Q^i = Q^i_{\text{in}} - Q^i_{\text{out}}$. The aim of our controller is to maintain a target weighted-averaged water volume in the high-pressure reservoirs, i.e. $V_h = V^{\text{ref}}_h$ where $V_h = \text{col}\{V^1_h, \ldots, V^4_h\}$ and $V^{\text{ref}}_h = \text{col}\{V^{1,\text{ref}}_h, \ldots, V^{4,\text{ref}}_h\}$.

For numerical simulation purposes, we consider the system Σ_{lin} in (2.15), representing the dynamics of four interconnected Ocean Batteries as described

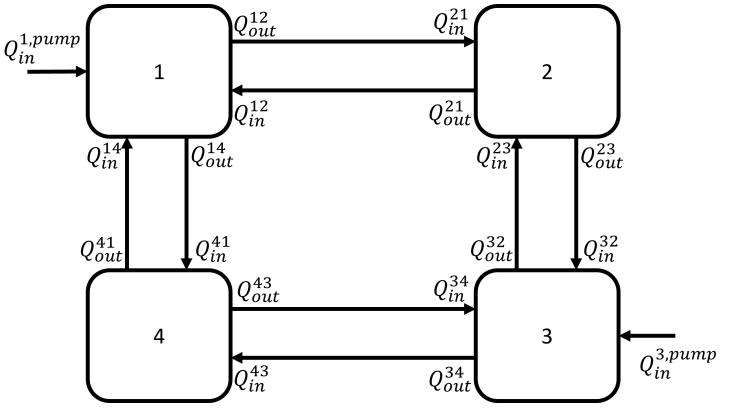

Figure 5.3: A network representing 4 interconnected Ocean Battery systems used in the numerical example of this chapter. Battery systems 1 and 3 have pumping units and high- and low-pressure area while battery systems 2 and 4 only have high-pressure area.

in Figure 5.3, with

$$A = \begin{bmatrix} -0.41 & 0.2 & 0 & 0.2 \\ 0.2 & -0.41 & 0.2 & 0 \\ 0 & 0.2 & -0.41 & 0.2 \\ 0.2 & 0 & 0.2 & -0.41 \end{bmatrix},$$

$$B = \begin{bmatrix} 1 & 0 \\ 0 & 0 \\ 0 & 1 \\ 0 & 0 \end{bmatrix}, \quad C = \begin{bmatrix} \frac{1}{2} & \frac{1}{4} & 0 & \frac{1}{4} \\ 0 & \frac{1}{4} & \frac{1}{2} & \frac{1}{4} \end{bmatrix}.$$

In the context of multiple interconnected Ocean Battery systems, the above system's matrices (A, B, C) can be regarded as an interconnection of distributed storage devices with 4 storage units where only 2 units are connected to the external (renewable) energy sources for charging and they distribute the stored energy between storage systems as described by the off-diagonal elements of A. Each diagonal term in A represents an energy loss and energy transfer to its neighboring storage devices. The matrix B defines which storage devices that are connected to the energy generation for charging, and the matrix C represents the measured weighted-averaged water volume in the high-pressure reservoir of the system. In this example, all pumping units can only be activated proportionally according to the rule set in a countable set of actions $\mathscr{U}$. Let the finite set of unit action vectors $\mathscr{U}$ be given by

$$\mathscr{U} := \left\{ \begin{bmatrix} \sin\frac{2\pi}{9} \\ \cos\frac{2\pi}{9} \end{bmatrix}, \begin{bmatrix} \sin\frac{8\pi}{9} \\ \cos\frac{8\pi}{9} \end{bmatrix}, \begin{bmatrix} \sin\frac{14\pi}{9} \\ \cos\frac{14\pi}{9} \end{bmatrix} \right\}$$

which represents the vertices of an equilateral triangle centered at the origin. The elements in the countable set $\mathscr{U}$ can be seen as the proportion of charge/discharge in the corresponding batteries. For the set $\mathscr{U}$ above, the value of δ satisfying (3.2) is $\delta = 1$. Moreover, the value of α, which is exactly the cosine of the largest possible angle between any points in $\mathbb{R}^2$ to the nearest point in $\mathscr{U}$, is $\alpha = \frac{1}{2}$.

For the simulation, we set $\lambda = 0.5$ for the uniformly extended quantizer and $\lambda = 1.1$ for the logarithmically extended quantizer. It can be checked that with the given tuple (A, B, C), the respective transfer function $(I + k_2 G)(I + k_1 G)^{-1}$ with k_1 and k_2 as stated in Propositions 5.8 and 5.10 is strictly positive real. To be more precise, the values of k_1 and k_2 are $k_1 = \frac{1}{4}$ and $k_2 = \frac{3}{2}$ for the uniformly extended quantizer; and $k_1 = \frac{11}{21}$ and $k_2 = \frac{20}{21}$ for the logarithmically extended quantizer.

The simulation results in Fig. 5.4 and 5.5 confirm that, with additional control actions in each unit vector direction, the practical stabilization and global asymptotic stabilization can be achieved exponentially fast compared to only using $\mathscr{U}$. In addition, logarithmically-extended actions render the system asymptotically stable.

5.5 Summary

In this chapter, we proposed the use of weak sector condition for MIMO systems and briefly shows that the closed-loop system remains ISpS. Moreover, we show that practical stability of the feedback systems with nearest-action input-selection approach can be analyzed using the notion of ISpS. This is achieved by extending the countable action set $\mathscr{U}$ via uniformly-extended actions or via logarithmically-extended actions. The application of nearest-action control using these extended action sets guarantees that the closed-loop system is exponentially practically stable for the uniform one and globally exponentially stable for the logarithmic one.

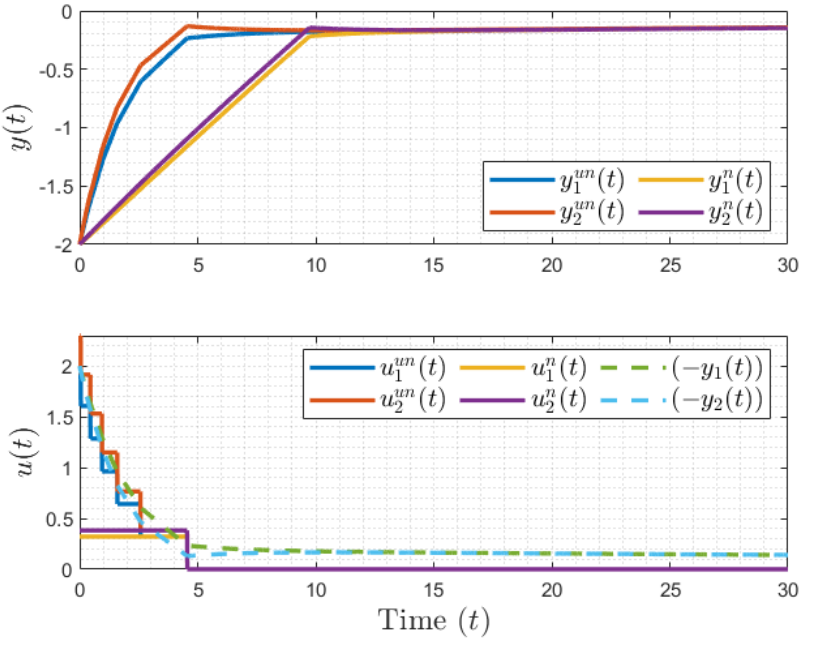

Figure 5.4: Simulation result with and without additional uniformly distributed quantization levels. The top plot shows the output response where the blue and red lines $y_i^{un}(t),\ i=1,2$, are the outputs with additional uniformly distributed quantization levels while the yellow and purple lines $y_i^{n}(t),\ i=1,2$, are the outputs with only single action in each direction. The bottom plot shows the input signals compared to the negative of the output values.

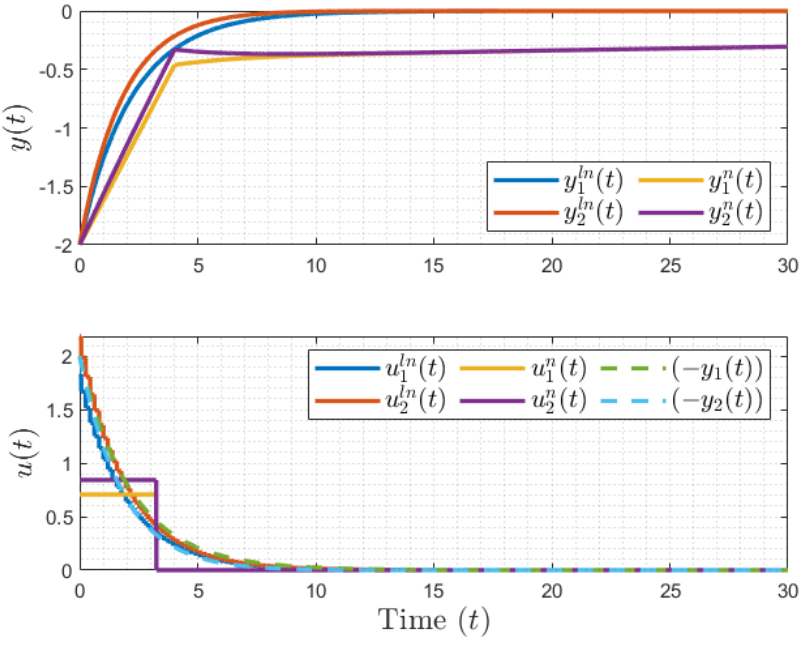

Figure 5.5: Simulation result with and without additional logarithmically distributed quantization levels. The top plot shows the output response where the blue and red lines $y_i^{un}(t),\ i = 1,2$, are the outputs with additional logarithmically distributed quantization levels while the yellow and purple lines $y_i^{n}(t),\ i = 1,2$, are the outputs with only single action in each direction. The bottom plot shows the input signals compared to the negative of the output values.

Part II

Modelling and Simulations of The Ocean Grazer System

Contents of this part are based on the following publication:

- **MZ Almuzakki**, JJ Barradas-Berglind, Y Wei, M Muñoz-Arias, A Vakis, and B Jayawardhana, “A port-Hamiltonian Approach to Cummins’ Equation for Floater Arrays with Linear Power-Take Off Systems," *6th IFAC Workshop on Lagrangian and Hamiltonian Methods for Nonlinear Control (LHMNC)*, 2018.

This page intentionally left blank.

Chapter 6 | A port-Hamiltonian Model for Floaters Array with Linear Power Take-Off

"Science is about knowing, engineering is about doing"

-Henry Petroski-

Contents

A wave energy converter (WEC) is a device that converts (oceanic) wave energy into other consumable forms of energy such as electrical energy, as in most WEC systems, or potential energy, as in the Ocean Grazer WEC. As described in the survey paper of [85], there is a large number of near- and off-shore WECs that have been already proposed. To name a few, we refer to the Wavestar [86], the Pelamis [87] and the Oyster [88] WECs. These WECs typically convert wave energy directly into electrical energy, and are optimized for a narrow spectrum of waves, which makes them susceptible to the

intermittency of the wave energetic content. In this context, their operation is similar to wind-based and solar-based energy conversion systems.

In recent years, a novel WEC has been proposed in the literature, the so-called Ocean Grazer (OG) WEC, which provides adaptability to a wide spectrum of incoming waves and has large storage capacities that can average out the intermittency problem. The OG WEC consists of a series of floating elements, a floater blanket, coupled to individual pumping systems, which pump internal working fluid from a lower reservoir into an upper reservoir [2, 29]. In Figure 6.1a), the concept of the floater blanket is depicted as an array of floating elements, and in Figure 6.1b), the working principle of the OG WEC is sketched. Each floater element B_i is coupled to a pumping system P_i, for $i = 1, \ldots, 4$ that pumps working fluid from a lower to an upper reservoir. Check valves are in place to prevent backflow. Lastly, electrical energy is produced by suitably releasing the stored working fluid through a turbine T.

In the previous work in [33], the OG WEC is modeled using a single floater-piston-pump in the port-Hamiltonian (pH) framework by considering a mechanical system consisting of a water body mass and a floater-piston ensemble, the latter being coupled to a hydraulic system representing the reservoirs. The coupling between these two subsystems was achieved by a switching function that characterized a check valve, coupling the mechanical and hydraulic subsystems, allowing flow in one direction and preventing backflow. Nevertheless, the hydrodynamic couplings were not included, which are important elements when we have to deal with an array of floater-piston-pump systems. In addition, the interpretation of the oscillating water body was worth revisiting. Therefore, in this chapter we cast the well-known Cummins' equation [31] in the pH framework together with a simplified pumping force, i.e., corresponding to a linear power take off (PTO) system. Resultingly, we include the hydrodynamic radiation effects of the multi-floater case in the system model, providing some insights on the passivity and radiation energy of the system.

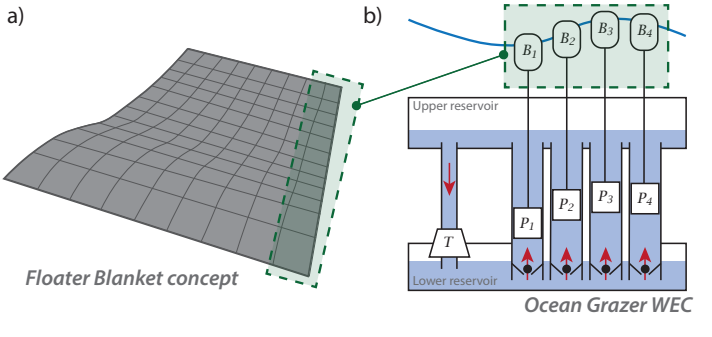

Figure 6.1: a) Floater blanket concept; b) Ocean Grazer WEC.

The main contributions of this chapter can be summarized as follows: i) the formulation of a WEC array in the pH framework for the heaving direction, and ii) the energy interpretation of the body-to-body radiation terms. Accordingly, we use the port-Hamiltonian (PH) framework [89, 90, 91] that has been adopted for complex multi-domain system modeling due to its physical energy interpretation and its generality in dealing with non-linear dynamical systems. Broadly speaking, the WEC control problem cannot be easily formulated as a tracking problem, but it takes the form of an energy maximization problem [92]. Thus, optimal control and model predictive control (MPC) strategies have been widely used for WEC control [93], in which the cost function to be maximized is the absorbed power —often formulated as the product of the pumping force and the pumping system velocity. In our case, for the OG WEC, the function to maximize could be thought of as the potential energy stored at the upper reservoir, thus making it useful to have a model that includes the body-to-body radiation effects that can be later connected to a multi-pump system.

6.1 Cummins' Equation in the pH setting

In this section, we firstly describe the port-Hamiltonian framework. Then, we discuss the Cummins' equation that represents the hydrodynamic effects for the single floater case, followed by the multi-floater case. Whenever it is clear from the context, we omit the time dependency notation in the description of signals/state variables.

6.1.1 The pH Framework

The port-Hamiltonian (pH) framework was introduced in [89], which is based on the description of a system in terms of energy variables, the usage of the port-based modeling through flow and effort variables whose product defines power, and their interconnection structure. The transfer of energy between the physical system and the environment is described through energy elements, dissipation components, and power preserving ports; for further details see [39], [89], and [91]. We consider the input-state-output representation of a pH system, given by

$$\Sigma : \begin{cases} \dot{x} &= [J(x) - R(x)] \frac{\partial H(x)}{\partial x} + G(x)u \\ y &= G(x)^\top \frac{\partial H(x)}{\partial x} \end{cases} \tag{6.1}$$

with states $x \in \mathbb{R}^{\mathcal{N}}$, a skew-symmetric interconnection matrix $J(x) \in \mathbb{R}^{\mathcal{N} \times \mathcal{N}}$, a positive semi-definite dissipation matrix $R(x) \in \mathbb{R}^{\mathcal{N} \times \mathcal{N}}$, and a Hamiltonian

or energy function $H(x) \in \mathbb{R}$. The functions J, R, G and H are assumed to be continuously differentiable, the function H is positive definite and the matrix G is assumed to be full-rank. The control input variable is given by $u \in \mathbb{R}^{\mathscr{M}}$ and the output variable is denoted by $y \in \mathbb{R}^{\mathscr{M}}$. The function H is called the Hamiltonian of the system and it follows that $\dot{H}(x) \leq y^\top u$, i.e., the system is *passive*. If $R = 0$ then $\dot{H}(x) = y^\top u$, i.e., the system is *conservative* or *lossless*.

6.1.2 Cummins' Equation: Single Floater Case

Let us now consider a single floating element with a given geometry. In the seminal work of Cummins [31], potential flow theory is used to describe the radiation hydrodynamic effects in the time domain such that the radiation force $f_r(t)$ in the univariate case for the floating element, with displacement $q(t)$, is given by

$$f_r(t) = \underbrace{-m_\infty \ddot{q}(t)}_{f_{r1}(t)} \underbrace{- \int_0^t \varphi(t-\tau)\dot{q}(\tau)d\tau}_{f_{r2}(t)}, \tag{6.2}$$

where the first term $f_{r1}(t)$ corresponds to the instantaneous effect of the impact to the radiating wave with m_∞ being the constant positive added mass, and the second term $f_{r2}(t)$ describes the dynamical effect of the radiation forces by means of a convolution operation. In describing $f_{r2}(t)$, a convolution kernel φ is used, which depends on the geometry of the floating elements and is typically obtained using hydrodynamics numerical tools, such as NEMOH [94]. Although $f_r(t)$ can be formulated to describe the radiation in all six degrees of freedom (DOF) of the body-fixed frame, i.e., surge, sway, heave, roll, pitch and yaw, in this chapter we are only interested in the heaving motion, i.e., the one DOF case.

In addition to the radiation forces, there are other forces that influence the floating element's dynamics. They are the restoring (or buoyancy) forces and the power take-off (or mechanical) forces from other elements in the WEC system. For a simple geometry (such as a box) and the floater not being completely submerged, the restoring (or buoyancy) force $f_b(t)$ can simply be described by

$$f_b(t) = kq(t) = \rho g A_f q(t), \tag{6.3}$$

where the buoyancy constant $k = \rho g A_f > 0$, with the water density ρ, the gravitational acceleration constant g and the cross-sectional area of the floater A_f. The forces exerted by the power take-off (PTO) system f_{pto} can be described using standard mechanical coupling elements, such as linear springs and dampers. However, in general, f_{pto} is given as a nonlinear function of

the relative displacement and velocity. For example, in [33], f_{pto} is given by a switched system that represents the basic operation of OG hydraulic pumping systems via check valves. In this chapter, for clarity of presentation, we will consider a simplified linear PTO force given by

$$f_{\text{pto}}(t) = k_{\text{pto}} q(t) + b_{\text{pto}} \dot{q}(t), \tag{6.4}$$

where the stiffness constant $k_{\text{pto}} > 0$ and damping constant $b_{\text{pto}} > 0$.

Combining (6.2) with the restoring and PTO forces in (6.3)-(6.4) yields the motion equation of the floating element as

$$\begin{aligned}(m + m_\infty)\ddot{q}(t) + \int_0^t \varphi(t-\tau)\dot{q}(\tau)d\tau \\ + b_{\text{pto}}\dot{q}(t) + kq(t) + k_{\text{pto}} q(t) = f_{\text{ex}}(t),\end{aligned} \tag{6.5}$$

where $m > 0$ is the mass of the floating body and $f_{\text{ex}}(t)$ corresponds to the external excitation force. The dynamical equation in (6.5) corresponds to the well-known Cummins' equation.

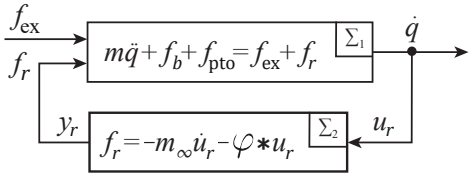

Figure 6.2: Interconnection of the single floater with the radiation force as negative feedback.

The system in (6.5) can be seen as the interconnection of a mechanical system and a radiation system as shown in Fig. 6.2. In order to describe the Cummins' equation in (6.5) as a pH model, we separate the model into two sub-systems, where the first one is the mechanical system Σ_1 and the second one is the radiation system Σ_2. As usual, the Hamiltonian (energy) function of Σ_1 is given by

$$H_1(x_1) = \frac{1}{2}\frac{p^2}{m} + \frac{1}{2}(k + k_{\text{pto}})q^2, \tag{6.6}$$

where $x_1 = \left[\begin{smallmatrix} q \\ p \end{smallmatrix}\right]$ with $p = m\dot{q}$. Using this Hamiltonian function, the pH model of Σ_1 is given by

$$\begin{cases} \dot{x}_1 &= (J_1 - R_1)\frac{\partial H_1(x_1)}{\partial x_1} + \begin{bmatrix} 0 \\ 1 \end{bmatrix} u_1 \\ y_1 &= \begin{bmatrix} 0 & 1 \end{bmatrix} \frac{\partial H_1(x_1)}{\partial x_1} \end{cases} \tag{6.7}$$

where the input u_1 is given by $f_{\text{ex}} + f_r$, the output y_1 is simply the velocity $\dot{q}$ and the matrices $J_1 = \left[\begin{smallmatrix} 0 & 1 \\ -1 & 0 \end{smallmatrix}\right]$ and $R_1 = \left[\begin{smallmatrix} 0 & 0 \\ 0 & b_{\text{pto}} \end{smallmatrix}\right]$. One can immediately check

that $\dot{H}_1 \leq \dot{q}(f_{\text{ex}} + f_r)$. For the radiation system Σ_2, which satisfies (6.2), it is not straightforward to define its pH model. However, if $\dot{q} \mapsto -f_{r2}$ can be described/approximated by a pH model with state variables z, Hamiltonian function $H_{r2}(z)$, interconnection and damping matrices J_{r2} and R_{r2}, respectively and the input matrix G_{r2}, then the pH model of Σ_2 is

$$\begin{cases} \dot{x}_2 &= \left(\begin{bmatrix} J_{r2} & G_{r2} \\ -G_{r2}^\top & 0 \end{bmatrix} - \begin{bmatrix} R_{r2} & 0 \\ 0 & 0 \end{bmatrix} \right) \frac{\partial H_2(x_2)}{\partial x_2} + \begin{bmatrix} 0 \\ 1 \end{bmatrix} u_2 \\ y_2 &= \begin{bmatrix} 0 & 1 \end{bmatrix} \frac{\partial H_2(x_2)}{\partial x_2} \end{cases} \tag{6.8}$$

where $x_2 = \begin{bmatrix} z \\ p_\infty \end{bmatrix}$ with $p_\infty = m_\infty \dot{q}$ and the Hamiltonian

$$H_2(x_2) = \frac{1}{2} \frac{p_\infty^2}{m_\infty} + H_{r2}(z). \tag{6.9}$$

It can be checked that $\dot{H}_2(x_2) \leq \frac{p_\infty}{m_\infty} u_2 = y_2 u_2$, i.e., Σ_2 is passive. Thus, if we consider the interconnection of Σ_1 and Σ_2 with $u_2 = -f_r$ and $y_2 = \frac{p}{m} = \dot{q}$ (where p is the state variable from Σ_1) and the combined Hamiltonian $H(x) = H_1(x_1) + H_2(x_2)$ with $x = \begin{bmatrix} x_1 \\ x_2 \end{bmatrix}$, it follows that $\dot{H}(x) \leq \frac{p}{m} f_{\text{ex}} = \dot{q} f_{\text{ex}}$, namely, the whole wave-structure system for a single floater is *passive* with respect to the supply rate $\dot{q} f_{\text{ex}}$.

6.2 Cummins' Equation: Multi-floater Case

The diagram of the multi-floater system under consideration is shown in Fig. 6.3. Note that the radiation forces considered are only in the heaving direction. Similar to the single floater case, the multi-floater system can be regarded as the interconnection of a mechanical system Σ_1 and a radiation system Σ_2. The accurate description of these systems will be addressed in the sequel.

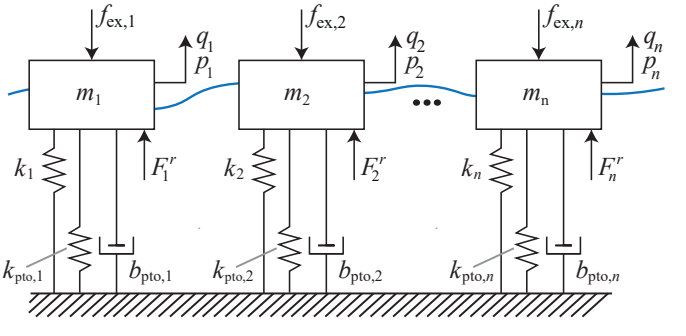

Figure 6.3: Diagram of the multi-floater system.

In order to extend the pH formulation of the single floater to the multi-floater case, we consider $Q = [\, q_1 \; q_2 \; \cdots q_n \,]^\top \in \mathbb{R}^n$ where each entry describes the displacement of the indexed floater, such that the Cummins' equation for the radiation force $F^r(t) = [\, F_1^r \; F_2^r \; \cdots F_n^r \,]^\top \in \mathbb{R}^n$ is given by

$$F^r(t) = -M_\infty \ddot{Q}(t) - \underbrace{\int_0^t \Phi(t-\tau)\dot{Q}(\tau)\mathrm{d}\tau}_{\mathscr{F}^r(t)}, \tag{6.10}$$

where $M_\infty = M_\infty^\top \succ 0$ is the added-mass matrix and $\Phi = \Phi^\top = (\varphi_{ij})_{i,j=1\ldots n} \in \mathscr{L}_2(\mathbb{R}, \mathbb{R}^{n\times n})$ is the $n \times n$ convolution kernel matrix. Note that for identical floaters, $\varphi_{ii} = \varphi_{jj}$ for all $i \neq j$. Here, we denote the second term in the radiation force equation above by $\mathscr{F}^r$.

When we incorporate this Cummins' equation into the equation of motion of the multi-floater, we have

$$(M + M_\infty)\ddot{Q} + \mathscr{F}^r + B_{\text{pto}}\dot{Q} + KQ + K_{\text{pto}}Q = F_{\text{ex}} \tag{6.11}$$

with the mass matrix $M = \text{diag}\{m_1, m_2, \ldots, m_n\} \succ 0$, the buoyancy matrix $K = \text{diag}\{k_1, k_2, \ldots, k_n\} \succ 0$, the PTO stiffness matrix $K_{\text{pto}} \in \mathbb{R}^{n\times n}$, the PTO damping matrix $B_{\text{pto}} \in \mathbb{R}^{n\times n}$ and the external excitation force vector $F_{\text{ex}} \in \mathbb{R}^n$.

If we assume an array of PTO systems which are not mechanically coupled (as in the case of OG WEC), the PTO stiffness and damping matrices can simply be given by $K_{\text{pto}} = \text{diag}\{k_{\text{pto},1}, k_{\text{pto},2}, \ldots, k_{\text{pto},n}\} \succ 0$ and $B_{\text{pto}} = \text{diag}\{b_{\text{pto},1}, b_{\text{pto},2}, \ldots, b_{\text{pto},n}\} \succ 0$, respectively. This is not the case for the radiation terms, where there is interaction among all floating bodies as observed in the structure of M_∞ and Φ. Similar to the single floater case, we can consider the multi-floater system in (6.11) as the interconnection of a series of mechanical systems and the Cummins' equation of radiation forces.

In [95], it is proposed that the modeling/approximation of $\mathscr{F}^r$ is done through individual system identification of each convolution kernel φ_{ij} such that each state-space representation of φ_{ij} (denoted here by Σ_{ij}^r) is passive/positive-real. In the following, we will show that if we follow the approach in [95], we need additional assumptions on Σ_{ij}^r in order to ensure that the interconnected system (6.11) is still passive with respect to the supply rate $\dot{Q}^\top F_{\text{ex}}$. In other words, the passivity of each Σ_{ij}^r does not guarantee passivity of the complete system.

Let us assume now that the convolution map $\varphi_{ij} * \dot{Q}_j$, where $*$ denotes the convolution operator, can be described/approximated by a pH system Σ_{ij}^r given by

$$\Sigma_{ij}^r : \begin{cases} \dot{z}_{ij} & = (J_{ij}^r - R_{ij}^r)\frac{\partial H_{ij}^r(z_{ij})}{\partial z_{ij}} + G_{ij}^r \dot{Q}_j \\ \mathscr{F}_{ij}^r & = (G_{ij}^r)^\top \frac{\partial H_{ij}^r(z_{ij})}{\partial z_{ij}}, \end{cases} \tag{6.12}$$

where z_{ij} corresponds to the state variables, J^r_{ij}, R^r_{ij} are the standard interconnection and damping matrices and H^r_{ij} is a positive definite function. Furthermore, we assume that its time derivative satisfies

$$\dot{H}^r_{ij} \leq -\gamma_{ij}\|\mathscr{F}^r_{ij}\|^2 + \mathscr{F}^r_{ij}\dot{Q}_{ij}, \qquad \gamma_{ij} \geq 0,$$

i.e., Σ^r_{ij} is strictly output passive/L_2-stable with an L_2 gain of γ_{ij}. If $\gamma_{ij} = 0$, we arrive to the same assumption of passivity on Σ_{ij} as in [95]. Using $\mathscr{F}^r_{ij}$, the second term on the RHS of (6.10) satisfies

$$\mathscr{F}^r = \Phi * \dot{Q} = \sum_j \begin{bmatrix} \mathscr{F}^{r\top}_{1j} & \mathscr{F}^{r\top}_{2j} & \cdots & \mathscr{F}^{r\top}_{nj} \end{bmatrix}^\top. \tag{6.13}$$

Following the same steps as in the description of the pH model for the single floater case, we can describe (6.11) as the interconnection of the mechanical system Σ_1 and the radiation system Σ_2 —including the body-to-body radiation systems Σ^r_{ij} together with the added mass terms— that is given by the Cummins equation in (6.10). As it will become clear later, we perform a loop transformation where the damping term in Σ_1 is moved to the radiation system. In this case, the pH model of Σ_1 is given by

$$\Sigma_1 : \begin{cases} \dot{x}_1 &= \begin{bmatrix} 0 & I \\ -I & 0 \end{bmatrix} \frac{\partial H_1(x_1)}{\partial x_1} + \begin{bmatrix} 0 \\ I \end{bmatrix} u_1 \\ y_1 &= \begin{bmatrix} 0 & I \end{bmatrix} \frac{\partial H_1(x_1)}{\partial x_1}, \end{cases} \tag{6.14}$$

where $x_1 = \left[\begin{smallmatrix} Q \\ P \end{smallmatrix}\right]$ corresponds to the state variables,

$$H_1(x_1) = \frac{1}{2}P^\top M^{-1} P + \frac{1}{2}Q^\top (K + K_{\text{pto}})Q$$

is the Hamiltonian function, u_1 is the input port that is given by $(F_{\text{ex}} - F^r - B_{\text{pto}}\dot{Q})$ and y_1 is the output port and represents $\dot{Q}$. The system Σ_2 can be rewritten as

$$F^r = -\dot{P}_\infty(t) - \mathscr{F}^r(t) - B_{\text{pto}} M^{-1}_\infty P_\infty(t) \tag{6.15}$$

where $P_\infty = M_\infty \dot{Q}$ cannot be described by the pH model as before. If we follow the same procedure as in (6.8), then

$$\Sigma_2 : \begin{cases} \dot{x}_2 &= \begin{bmatrix} J^r - R^r & G^r \\ -(G^r)^\top & -B_{\text{pto}} \end{bmatrix} \frac{\partial H_2(x_2)}{\partial x_2} + \begin{bmatrix} 0 \\ I \end{bmatrix} u_2 + \begin{bmatrix} 0 \\ f(Z) \end{bmatrix} \\ y_2 &= \begin{bmatrix} 0 & I \end{bmatrix} \frac{\partial H_2(x_2)}{\partial x_2} \end{cases} \tag{6.16}$$

where $x_2 = \left[\begin{smallmatrix} Z \\ P_\infty \end{smallmatrix}\right]$, $Z = \text{col}\{z_{ij}\}$, $J^r = \text{diag}\{J^r_{ij}\}$, G^r is defined appropriately using G^r_{ij} according to the ordering of z_{ij} in Z and the Hamiltonian function is given by

$$H_2(x_2) = \frac{1}{2}P_\infty M^{-1}_\infty P_\infty + \sum_{ij} H^r_{ij}(z_{ij}). \tag{6.17}$$

In fact, there is an extra term $f(Z)$ in (6.16), such that the second state equation of Σ_2 satisfies (6.15), namely

$$f(Z) = (G^r)^\top \frac{\partial H_2(x_2)}{\partial Z} - \mathscr{F}^r = \left(G^r - \hat{G}^r\right)^\top \frac{\partial H_2(x_2)}{\partial Z}$$

where $\mathscr{F}^r = \sum_j \mathrm{col}_i\{\mathscr{F}^r_{ij}\}$ with $\mathscr{F}^r_{ij}$ as given before in (6.12). Without loss of generality, let us consider $Z = \mathrm{col}\{z_{11}, z_{12}, \ldots, z_{1n}, z_{21}, z_{22}, \ldots, z_{nn}\}$, in which case $G^r = \left[\mathrm{diag}\{G^r_{1j}\}, \mathrm{diag}\{G^r_{2j}\}, \ldots\right]^\top$ and $\hat{G}^r = \mathrm{diag}\{\mathrm{col}\{G^r_{1j}\}, \mathrm{col}\{G^r_{2j}\}, \ldots\}$. Hence, the additional term $f(Z)$ can simply be written as

$$f(Z) = \left[\left(\sum_{i\neq 1} \mathscr{F}^r_{i1} - \sum_{j\neq 1} \mathscr{F}^r_{1j}\right)^\top \quad \left(\sum_{i\neq 2} \mathscr{F}^r_{i2} - \sum_{j\neq 2} \mathscr{F}^r_{2j}\right)^\top \ldots\right]^\top.$$

The time derivative of H_2 satisfies

$$\begin{aligned}\dot{H}_2 \leq & -\lambda_{\min}(B_{\mathrm{pto}})\|\dot{Q}\|^2 - \sum_{ij} \gamma_{ij}\|F^r_{ij}\|^2 \\ & + \dot{Q}^\top u_2 + \frac{1}{2\epsilon}\|\dot{Q}\|^2 + \frac{\epsilon}{2}\sum_{ij}\|F^r_{ij}\|^2,\end{aligned}$$

where we have used Young's inequality for the last inequality. Thus, if the damping matrix B_{pto} (which can also include drag forces on the floaters) and the L_2-gain of the radiation forces γ_{ij} satisfy

$$4\lambda_{\min}(B_{\mathrm{pto}})\min_{ij}\{\gamma_{ij}\} > 1, \tag{6.18}$$

then there is $\epsilon > 0$ such that

$$\lambda_{\min}(B_{\mathrm{pto}}) > \frac{1}{2\epsilon}, \qquad \min_{ij}\{\gamma_{ij}\} > \frac{\epsilon}{2}.$$

Under such an assumption, it follows that $\dot{H}_2 \leq \dot{Q}^\top u_2$, i.e., Σ^r is passive.

Proposition 6.1. Consider the dynamics of multi-floater system as in (6.11) and assume that each body-to-body radiation system Σ^r_{ij} is L_2-stable with an L_2 gain of $\gamma_{ij} > 0$. If (6.18) holds, then the multi-floater systems is passive with respect to the supply rate $\dot{Q}^\top F_{\mathrm{ex}}$. ◇

This proposition shows that if we only assume passivity of each body-to-body radiation system Σ^r_{ij}, then the passivity of the whole multi-floater system cannot be guaranteed. This problem might arise when we want to describe the convolution operation $\Phi * \dot{Q}$ by a state-space representation where we individually identify each body-to-body convolution operation $\varphi_{ij} * \dot{q}_j$ as a decoupled passive system Σ^r_{ij}. We remark also that we do not need to impose strict output passivity for the self-radiation system Σ^r_{ii}. It suffices to assume that Σ^r_{ii} is passive, since the terms that are used in $f(Z)$ do not contain $\mathscr{F}^r_{ii}$. In order to circumvent this problem, we can identify the convolution operation $\Phi * \dot{Q}$ directly as a MIMO passive system. Therefore, if we are able to describe $\Phi * \dot{Q}$ as a MIMO passive system, then the dynamics of multi-floater systems

will be passive as shown in the following proposition.

Proposition 6.2. Consider the dynamics of multi-floater systems as in (6.11) and assume that the convolution operation $\Phi * \dot{Q}$ is a passive mapping and can be described by a pH model with state variables x^r, Hamiltonian function $H^r(x^r)$, interconnection and damping matrices J^r and R^r, respectively and input matrix G^r. Then, the multi-floater system is passive with respect to the supply rate $\dot{Q}^\top F_{\text{ex}}$. ◇

6.3 Radiation Convolution Approximation

6.3.1 Convolution Approximation

Following Proposition 6.2, we need to guarantee that $\Phi * \dot{Q}$ is a MIMO passive mapping in order to ensure the passivity of the interconnection of Σ_1 and Σ_2. Therefore, a linear approximation of $\mathscr{F}^r$ in (6.13) can be found such that the transfer matrix

$$\hat{\mathscr{F}}^r(s) = \begin{bmatrix} \hat{\mathscr{F}}^r_{11}(s) & \dots & \hat{\mathscr{F}}^r_{1n}(s) \\ \vdots & \ddots & \vdots \\ \hat{\mathscr{F}}^r_{n1}(s) & \dots & \hat{\mathscr{F}}^r_{nn}(s) \end{bmatrix} \tag{6.19}$$

is passive/positive-real. Assuming a quadratic energy function of the MIMO radiation convolution term, i.e., $H^r(Z) = Z^\top W Z$, the matrices G^r, J^r, R^r and W can be found such that

$$\hat{\mathscr{F}}^r(s) = (G^r)^\top W \big(sI - (J^r - R^r)W\big)^{-1} G^r \tag{6.20}$$

is positive-real. Alternatively, for the case of individual approximation, one can assume individual quadratic energy functions of the radiation convolution terms, i.e., $H^r_{ij}(z_{ij}) = z_{ij}^\top W_{ij} z_{ij}$, where every entry is approximated by choosing the matrices $G^r_{ij}, J^r_{ij}, R^r_{ij}$ and W_{ij} such that

$$\hat{\mathscr{F}}^r_{ij}(s) = (G^r_{ij})^\top W_{ij} \big(sI - (J^r_{ij} - R^r_{ij})W_{ij}\big)^{-1} G^r_{ij} \tag{6.21}$$

for $i, j = 1, \dots, n$ is positive-real, thus relating $\hat{\mathscr{F}}^r_{ij}$ in (6.21) to the pH system Σ^r_{ij} in (6.12). Note that the procedure in (6.21) is similar to the one in [95]. In the sequel, we describe the identification procedure to find an approximated radiation impulse response function of $\mathscr{F}^r(t)$ for the MIMO case in (6.20). .

6.3.2 Kernel Approximation with Passive Basis Functions

As mentioned in [95], one of the constraints in computing the state space approximation of the radiation impulse response function (IRF) of $\mathscr{F}^r(t)$ is

that at least the diagonal elements of the transfer matrix must be positive-real. However, we can see from Fig. 6.4 that the transfer function of the IRF obtained from WEC-Sim/bemio toolbox [96], referred as the original IRF, is not always positive-real. Thus, a positive-real approximation to (6.19) is necessary.

In here, we impose positive-realness to the radiation IRF by approximating the original IRF with

$$\bar{\varphi}(t) = \sum_{j=1}^{n_j} \bar{\varphi}_j(t) \tag{6.22}$$

where

$$\bar{\varphi}_j(t) = A_j\, e^{-b_j^2 t}\left(\cos(c_j\, t) - \frac{b_j^2}{c_j}\sin(c_j\, t)\right) \text{ and } \left(A_{j,ii}\right) = a_{j,ii}^2,\ \forall i = 1,\ldots,n,$$

i.e. the diagonal elements of A_j are non-negative. Thus, the positive-realness of $\mathscr{F}^r(t)$ is now guaranteed by the transfer function $\hat{\varphi}_j(s) = \frac{A_j\, s}{s^2 + 2\, b_j^2\, s + b_j^4 + c_j^2}$ for any choice of $b_j, c_j \in \mathbb{R}$ and $0 \preccurlyeq A_j \in \mathbb{R}^{n\times n}$. Note that for the case of identical floaters, we have $A_j = A_j^\top$ and $a_{j,ii}^2 = a_{j,11}^2,\ \forall i = 2,\ldots,n$. Furthermore, the positive-realness of the diagonal element of the approximated radiation IRF can also be seen in Fig. 6.4a. In particular, for the identical two-floaters case, the approximated IRF $\bar{\varphi}$ is obtained by applying least squares curve fitting and the optimal approximation is achieved when $n_j = 9$. In addition, Fig. 6.4b shows that the approximated radiation IRF is in good agreement with the original one.

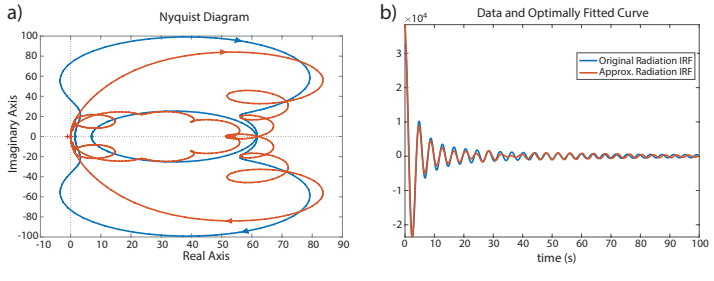

Figure 6.4: a) Nyquist diagram and b) time series plot of the diagonal element of original IRF (blue) and approximated IRF (orange) for two floaters.

6.4 Simulation Results

In this section, simulation results based on the multi-floater system in the pH framework will be shown and compared to the results obtained from WEC-Sim.

Moreover, the time-series plots of the radiation energy are also provided.

The simulation is performed by placing two identical cuboid floaters of $7 \times 7 \times 2$ m in the direction of the incident wave, where the second floater is put behind the first floater. The floater mass is $m = 45000$ kg, the sea water density $\rho = 1025$ kg/m^3, the combined stiffness is $(k + k_{\text{pto}}) = 4.9271 \cdot 10^5$ N/m, and the PTO damping is $b_{\text{pto}} = 1.153 \cdot 10^6$ kg/s. The hydrodynamics data are obtained from NEMOH toolbox [94] and the matrix $W = W^\top \succ 0$ is obtained using semi-definite programming toolbox and solver YALMIP and SeDuMi [97].

6.4.1 Comparison of the Floaters' Displacements

In this simulation, we use regular waves with 4 m wave height and two different wave periods of 5 s and 10 s.

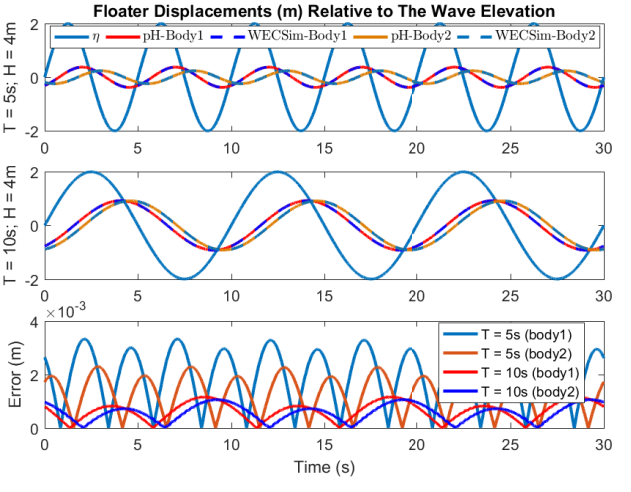

Figure 6.5: Floaters' displacements for a regular wave with periods of 5 s and 10 s, and wave height of 4 m (top and middle), and error between models (bottom).

We can see from Fig. 6.5 that the results from the pH-ode45 simulation are in very good agreement with the WEC-Sim results. However, we can still see some differences in the floaters' displacements' amplitudes and/or phases. One of the possibilities that introduces differences in simulation results is the radiation IRF approximation introduced in Section 6.3.2. Nevertheless, in the case of incident waves with higher wave periods, the differences become smaller.

The above results show that approximating the radiation force's convolution kernel does not give significant changes in the simulation results. Furthermore, the passivity of the radiation effect of the whole system is guaranteed through the (positive-real) approximated IRF.

6.4.2 Radiation Energy

In addition to the floaters' motion, by the nature of the pH-framework, we can directly compute the stored energy within the system during the simulation. In particular, we are interested here in the overall energy of the radiation forces acting on each body. As described in Proposition 6.2, the energy of the radiation system is now given by $H_2(z, P_\infty) = E_k^r(P_\infty) + H^r(z)$, being composed of a kinetic energy component due to the added mass, $E_k^r(P_\infty) = \frac{1}{2} P_\infty^\top M_\infty^{-1} P_\infty$, and the stored energy coming from the convolution terms of the radiation forces, $H^r(z) = \frac{1}{2} z^\top W z$.

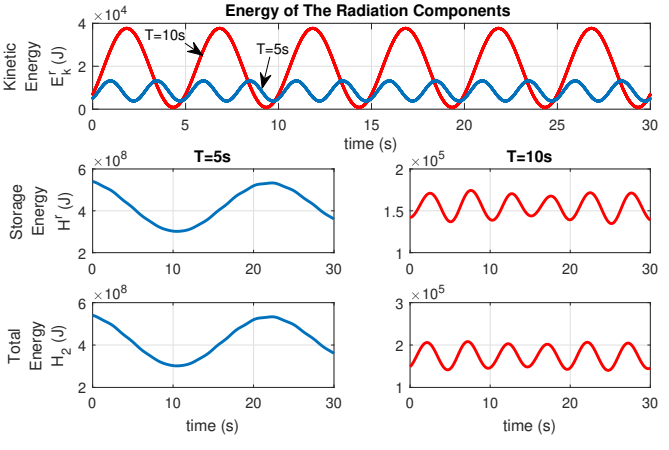

Figure 6.6: The radiation energy of all radiation components in regular wave simulation with wave period of 5 s and 10 s and wave height of 4 m.

The results shown in Fig. 6.6 suggest that, the longer the wave period is, the less radiation energy is stored in the system. This means that, for the lower wave frequencies, the effect of the radiation force components to the total energy of the system will become smaller.

6.5 Summary

In this chapter, we have included the radiation effects described by the Cummins' equation in the pH framework, which enabled us to study the passivity

of the system and the energetic properties of the radiation terms. The convolution terms were included by approximating them with a passive LTI system. A simple example of the multi-floater pH system was simulated and compared against high-fidelity WEC-Sim results, showing good agreement.

Chapter 7 | A Model of the Multi Piston-Pump Power Take-Off Systems

> "No matter what engineering field you're in, you learn the same basic science and mathematics. And then maybe you learn a little bit about how to apply it."
>
> *-Noam Chomsky-*

Contents

This chapter provides briefly the modeling process of the Ocean Grazer multi piston-pump power take-off (MPP-PTO) systems where part of the model motivated the simplified example used in Chapter 5.

7.1 One Column Array Ocean Grazer Wave Energy Converter with Hydraulic Type Pumping System

In this section, we present the modeling of one column array Ocean Grazer wave energy converter (OG-WEC) where each floating element is connected to an MPP-PTO unit as described in Figure 7.1c). For this problem, we will

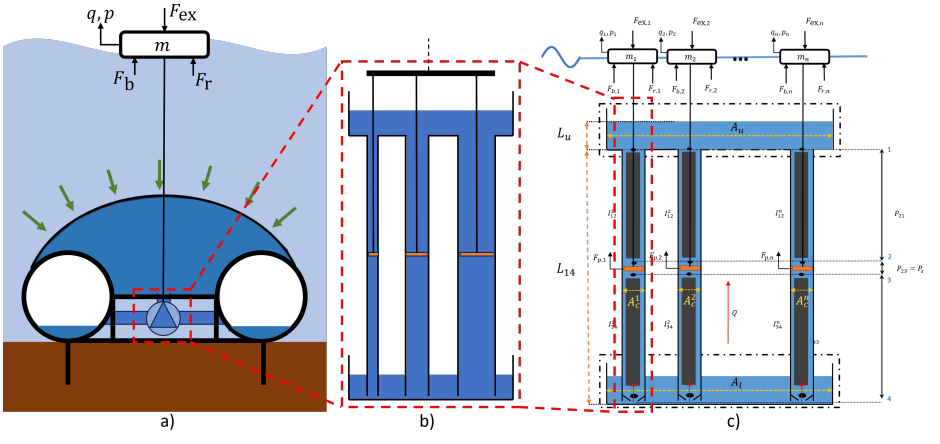

Figure 7.1: Schematic of the Ocean Grazer wave energy converter. a) The Ocean Battery as in Figure 5.2 coupled with hydraulic type adaptive pumping system powered by the heaving motion of the floating elements; b) the MPP-PTO concept where one floating element is connected to three independent pumps with different sizes; c) one column floater arrays where each floater is connected to an MPP-PTO unit. In this figure, the pumping subsystems in red dashed boxes are equivalent.

use the port-Hamiltonian version of Cummins' equation studied in Chapter 6. Furthermore, note that the schematic of the Ocean Battery consisting of one rigid reservoir (low-pressure area) and one flexible reservoir (high-pressure area) as depicted in Figure 7.1a) is equivalent to a pump hydro energy storage system with one lower- and one upper-reservoir as in Figure 7.1c) provided that they have equivalent hydraulic head. Without loss of generality and for the sake of simplicity, the model that is developed in this chapter is based on the schematic in Figure 7.1c).

7

For the schematic in Figure 7.1c), the lower reservoir (low-pressure area) has an area of A_l and the upper reservoir (high-pressure area) has an area of A_u. The behavior of the above multi-floater system is governed by the following system of equations,

$$M_f \ddot{X}_f = -KX_f + F_p + F_{\text{ex}} + F_r \tag{7.1}$$

$$M_p \ddot{X}_p = -F_p + F_h \tag{7.2}$$

where $M_f = \text{diag}\left\{M_f^1, \ldots, M_f^n\right\}$ is the floater mass matrix, $X_f = \text{col}\left\{X_f^1, \ldots, X_f^n\right\}$ is the floater displacement vector, $M_p = \text{diag}\left\{M_p^1, \ldots, M_p^n\right\}$ is the piston mass matrix, $X_p = \text{col}\left\{X_p^1, \ldots, X_p^n\right\}$ is the piston displacement vector, the excita-

tion force from the wave is given by $F_{\text{ex}} = \text{col}\left\{F_{\text{ex}}^1, \ldots, F_{\text{ex}}^n\right\}$, the radiation force due to the motion of the floaters is given by $F_r = \text{col}\left\{F_r^1, \ldots, F_r^n\right\}$, $F_p = -K_r\left(X_f - X_p\right)$ is the force on the connecting cables that acts like springs with spring coefficient matrix $K_r = \text{diag}\left\{K_r^1, \ldots, K_r^n\right\}$, and $F_h = \text{col}\left\{F_h^1, \ldots, F_h^n\right\}$ is the hydraulic forces acting on the pistons. In this model, (7.1) is the Cummins' equation describing the motion of the floaters array as studied in Chapter 6 and (7.2) is the hydraulic type pumping subsystem that is being modeled in the following section.

7.1.1 The Hydraulic Pumping Subsystem

Following the modeling of single hydraulic system Σ_h in [33], the pumping subsystem can be represented by two capacitors (upper and lower reservoirs), two inertors, two resistors, and a pressure source P_s. However, in this work, we assume that there is no resistance and one or more pumps share the same reservoirs in the system.

To model the pumping subsystems, we introduce r_u and r_l as the reference point located at the fluid surface for pressure calculation in upper and lower capacitors, respectively. In order to satisfy the continuity law at the bottom of the lower reservoir, we have that

$$P_{4r_u} + P_{4r_l} = 0 \tag{7.3}$$

where $P_{p_1p_2} = P_{p_1} - P_{p_1}$ is the pressure difference between the pressure P_{p_1} at pressure point p_1 and the pressure P_{p_2} at pressure point p_2. To satisfy the compatibility law along the i-th pipe up to the fluid surface in the upper reservoir, we have

$$P_{4r_u} = P_{43}^i + P_{32}^i + P_{21}^i + P_{1r_u}. \tag{7.4}$$

Substituting (7.4) into (7.3) yields

$$P_s^i = P_{43}^i + P_{21}^i + P_{14} \tag{7.5}$$

where $P_{14} = P_{1r_u} + P_{4r_l}$ and its value is the same for all pumping subsystems, P_s^i is the pressure source that couples the piston in the pumping subsystem i to the i-th floating unit, and $P_{p_1p_2}^i$ is the pressure difference between point p_1 and p_2 as provided in Figure 7.1c).

Pressures in the inertors are given by

$$P_{21}^i = I_{12}^i \dot{Q}_h^i + g\rho_h L_{12} \tag{7.6}$$

and

$$P_{43}^i = I_{34}^i \dot{Q}_h^i + g\rho_h L_{34} \tag{7.7}$$

where ρ_h is the working fluid density, Q_h^i is the upward flow of the fluid along the pipe i proportional to the respective active piston area A_c^i and the piston

displacement. By substituting (7.6) and (7.7) into (7.5) we get

$$P_s^i = I^i \dot{Q}_h^i + g\rho_h L_{14} + P_{14} \tag{7.8}$$

with equivalent inertance $I^i = I_{12}^i + I_{34}^i$.

The flow Q_h^i can be described by

$$Q_h^i = A_c^i \dot{X}_p^i. \tag{7.9}$$

Since all pumps share the same upper and lower reservoirs, the dynamics of pressure in both capacitors can be described by

$$\dot{P}_{1r_u} = \sum_i \frac{Q_h^i}{C_u} \tag{7.10}$$

and

$$\dot{P}_{4r_l} = \sum_i \frac{Q_h^i}{C_l} \tag{7.11}$$

where C_u and C_l are the equivalent capacitance of the upper and lower reservoirs, respectively. Then, the dynamics of the pressure difference between point 1 and 4 becomes

$$\dot{P}_{14} = \sum_i \frac{Q_h^i}{C} \tag{7.12}$$

with the equivalent combined capacitance $C = \frac{C_u C_l}{C_u + C_l}$.

The check valves introduce switching dynamics in the pumping system such that when the piston is moving upward (that is when $\dot{X}_p^i > 0$), the pump is activated. The switching system can be described by $Q_h^i > 0$ and $P_s^i > 0$ when the pump is active, and $Q_h^i = 0$ and $P_s^i = 0$, otherwise. This is due to the fact that during the downward motion of the i-th piston mass, the check valve in the piston is in open-mode that makes the i-th piston area A_c^i becomes zero and followed by the disappearance of the i-th pressure source P_s^i.

For a single floater case that is connected to only one pumping subsystem, we can simply set the value of the fluid flow, the hydraulic force and the dynamics of P_{14} in the system's equation to be zero to indicate that the pump is deactivated. However, in the multi-floater case, the pumps are activated separately depending on the velocity of their respective pistons. Then the generalized hydraulic force F_h is expressed by the following system of equation

$$F_h = -\left(\tilde{N} A_c\right)\left(\tilde{N} P_s\right), \tag{7.13}$$

$$P_s = \tilde{I}\dot{Q}_h + \mathbb{1}(g\rho_h L_{14} + P_{14}), \tag{7.14}$$

$$\dot{P}_{14} = \frac{1}{C}\mathbb{1}^\top Q_h, \tag{7.15}$$

$$Q_h = \left(\tilde{N} A_c\right)\dot{X}_p, \tag{7.16}$$

where $\tilde{I} = \text{diag}\left\{I^1, \ldots, I^n\right\}$, $A_c = \text{diag}\left\{A_c^1, \ldots, A_c^n\right\}$, $\mathbb{1}$ is a column vector with all entries 1, and $\tilde{N}$ is a diagonal matrix containing 1 in the i-th diagonal element when the corresponding pump is active and 0, otherwise. Note that the matrix $\tilde{N}$ is coupled with the piston area and then with the pressure source because when the pump is deactivated, the respected variables will turn to zero.

7.1.2 Model of One Column Array OG-WEC

In order to construct the port-Hamiltonian model of one column array Ocean Grazer WEC, we find it easier to describe and divide the system as given in figure 7.2.

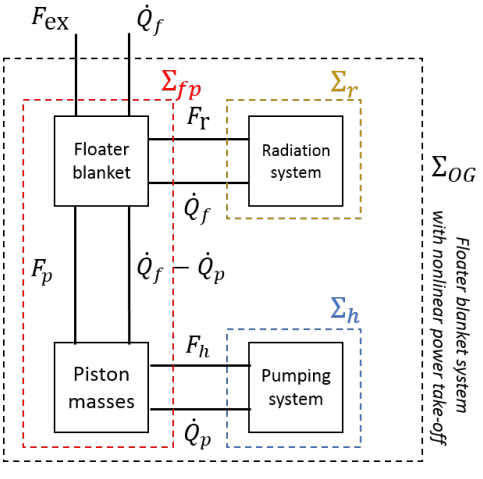

Figure 7.2: Interconnection diagram of a wave energy converter with multiple floating elements (floater blanket) connected to hydraulic-type power take-off units.

7.1.2.1 The floater blanket-pistons ensemble Σ_{fp}

Port-Hamiltonian modeling of the floater blanket-pistons ensemble is as straightforward as the pH model of the floater blanket itself. We first introduce the state variables $x_{fp} = \begin{bmatrix} X_f \\ X_p \\ P_f \\ P_p \end{bmatrix}$ combining the states of the floater blanket with the states of the pistons behavior, where $P_f = M_f \dot{X}_f$ and $P_p = M_p \dot{X}_p$ are the momentum of the floater and piston masses, respectively. Similar to our work

in Chapter 6. The Hamiltonian function is given by

$$H_{fp}\left(x_{fp}\right)=\frac{1}{2}P_f^\top M_f^{-1}P_f+\frac{1}{2}\left(X_f-X_p\right)^\top K_r\left(X_f-X_p\right)+\frac{1}{2}P_p^\top M_p^{-1}P_p+\frac{1}{2}X_f^\top KX_f. \tag{7.17}$$

The pH formulation of Σ_{fp} is then given by

$$\Sigma_{fp}:\begin{cases}\dot{x}_{fp} &= \left[J_{fp}-R_{fp}\right]\frac{\partial H_{fp}\left(x_{fp}\right)}{\partial x_{fp}}+G_{fp}u_{fp},\\ y_{fp} &= G_{fp}^\top\frac{\partial H_{fp}\left(x_{fp}\right)}{\partial x_{fp}},\end{cases} \tag{7.18}$$

where the interconnection matrix is given by $J_{fp}=\left[\begin{smallmatrix}0_{2n\times 2n} & I_{2n\times 2n}\\ -I_{2n\times 2n} & 0_{2n\times 2n}\end{smallmatrix}\right]$, the dissipation matrix is given by $R_{fp}=0_{4n\times 4n}$, the input matrix is given by $G_{fp}=\left[\begin{smallmatrix}0_{2n\times 2n}\\ I_{2n\times 2n}\end{smallmatrix}\right]$, the input is $u_{fp}=\begin{bmatrix}u_{fp1}\\ u_{fp2}\end{bmatrix}=\begin{bmatrix}F_{ex}+F_r\\ F_h\end{bmatrix}$ and the output is $y_{fp}=\begin{bmatrix}y_{fp1}\\ y_{fp2}\end{bmatrix}=\begin{bmatrix}\dot{X}_f\\ \dot{X}_p\end{bmatrix}$.

By computing the time derivative of the Hamiltonian function for the floater blanket-pistons ensemble, we can conclude that Σ_{fp} is a conservative system. Indeed, straightforward computation gives us

$$\begin{aligned}\dot{H}_{fp} &= \left(K_r\left(X_f-X_p\right)+KX_f\right)^\top\dot{X}_f-\left(K_r\left(X_f-X_p\right)\right)^\top\dot{X}_p+\dot{X}_f^\top\dot{P}_f+\dot{X}_p^\top\dot{P}_p\\ &= \dot{X}_f^\top\left(F_e+F_r\right)+\dot{X}_p^\top F_h=y_{fp}^\top u_{fp}.\end{aligned}$$

In this case, we know that all the energy extracted by the floater blanket are delivered to the radiation system Σ_r and the hydraulic system Σ_h.

7.1.2.2 The hydraulic system Σ_h

In this section, we want to first analyze the behavior of the hydraulic system before it is interconnected to the floater blanket-pistons ensemble, then we will analyze the complete interconnection of Σ_{OG} as given in figure 7.2. Based on pump dynamics explained earlier, we let the state of the hydraulic system be $x_h=\left[\begin{smallmatrix}P_{14}\\ Q_h\end{smallmatrix}\right]$ and introduce the generalized Hamiltonian function from [33] as

$$H_h(x_h)=\frac{1}{2}CP_{14}^2+Cg\rho_h L_{14}P_{14}+\frac{1}{2}Q_h^\top\tilde{I}Q_h, \tag{7.19}$$

with equivalent fluid inertance matrix $\tilde{I}\succ 0$ and equivalent capacitance $C>0$. Given the Hamiltonian function (7.19), we can write the hydraulic subsystem Σ_h as

$$\Sigma_h:\begin{cases}\dot{x}_h &= \left[J_h-R_h\right]\frac{\partial H_h}{\partial x_h}+G_hu_h\\ y_h &= G_h^\top\frac{\partial H_h}{\partial x_h}\end{cases} \tag{7.20}$$

where the interconnection matrix is given by $J_h=\left[\begin{smallmatrix}0_{1\times 1} & \frac{1}{C}\mathbb{1}^\top\tilde{I}^{-1}\\ -\frac{1}{C}\tilde{I}^{-1}\mathbb{1} & 0_{n\times n}\end{smallmatrix}\right]$, the dissipation matrix is given by $R_h=0$, the input matrix is given by $G_h=\left[\begin{smallmatrix}0_{1\times n}\\ \tilde{I}^{-1}\end{smallmatrix}\right]$, and

with the external port pair $(u_h, y_h) \in \mathbb{R}^{n+1}$ given by

$$u_h = P_s, \tag{7.21}$$

$$y_h = Q_h. \tag{7.22}$$

Following the usual routine to derive the Hamiltonian function H_h with respect to time, it shows that the hydraulic system without any resistance elements is a conservative system, i.e. $\dot{H}_h = y_h^\top u_h$.

As discussed earlier, there is switching behavior in the pumping system allowing the transfer of energy from the floater blanket-pistons ensemble to the hydraulic subsystem while preventing the reverse processes, thus resulting in the non-decreasing amount of potential energy stored in the upper reservoir. These switching behavior can be formalized through the function

$$\sigma\left(\dot{X}_p\right) = \operatorname{diag}\left\{\frac{1}{2}\left(1 + \operatorname{sign}\left(\dot{X}_p\right)\right)\right\} \tag{7.23}$$

so that the system of equations (7.13), (7.14), (7.15), and (7.16) in pH framework becomes

$$\Sigma_h : \begin{cases} \dot{x}_h &= \begin{bmatrix} 0_{1\times 1} & \frac{1}{C}\left(\sigma\tilde{I}^{-1}\mathbb{1}\right)^\top \\ -\frac{1}{C}\left(\sigma\tilde{I}^{-1}\mathbb{1}\right) & 0_{n\times n} \end{bmatrix} \frac{\partial H_h}{\partial x_h} + \begin{bmatrix} 0_{1\times n} \\ \left(\sigma\tilde{I}^{-1}\right)^\top \end{bmatrix} u_h \\ y_h &= \begin{bmatrix} 0_{1\times n} & \sigma\tilde{I}^{-1} \end{bmatrix} \frac{\partial H_h}{\partial x_h}, \end{cases} \tag{7.24}$$

and the interconnection between the hydraulics and the pistons are given by

$$u_{fp2} = -(\sigma A_c)(\sigma u_h) \tag{7.25}$$

$$y_h = \sigma A_c y_{fp2}. \tag{7.26}$$

Note that we have input-to-input and output-to-output interconnection instead of the usual input-to-output interconnection. For the complete interconnection within Σ_{OG}, for which we need to include the interconnection with the radiation subsystem Σ_r as described by Σ_2 in (6.16), we now have the external port pair to be $(u_{OG}, y_{OG}) = \left(u_{fp1} + u_r, y_{fp1}\right)$ with $u_r = -F_r$. Finally, for the system Σ_{OG}, it is straightforward to see that the whole OG-WEC with MPP-PTO system is a passive system. This is primarily due to the radiation system Σ_r being dissipative as studied in Chapter 6. In addition, we note that the model developed in this section is piecewise linear since for each pumping mode (active/inactive), the corresponding system is still linear. The nonlinearity only comes from the sign function σ described by (7.23) for the switching behavior of the pump.

7.2 Simulations

In this section, we reproduce the simulation results in [1] for one column floaters array with MPP-PTO. The simulation is performed by placing ten identical

cuboid floaters of dimension $7m \times 7m \times 2m$ (length × width × height) close to each other in one column array with the first floater facing the incoming waves. The hydrodynamic coefficients are pre-processed using boundary element method-based code NEMOH [94]. The radiation kernel function obtained from NEMOH is processed further using the method explained in Chapter 6 in order to obtain the matrices A_z, B_z, and C_z, then the positive definite matrix $W_z = W_z^\top$ satisfying $A_z^\top W_z + W_z A_z \preccurlyeq 0$ and $B_z^\top W_z = C_z$ is obtained by using semidefinite programming solver YALMIP and SeDuMi [97]. The general parameters involved in the simulation are provided in the following table.

Table 7.1: General simulation parameters.

Parameter	**Value**
Floater mass (m_f^i)	1650 kg
Sea water density (ρ_{sw})	1025 kg/m^3
Gravitational constant (g)	9.81 m/s^2
Buoyancy force coefficient (K_i)	$4.9271 \cdot 10^5$ N/m
Radiation kernel approximation order (n_o)	9

Furthermore, the floaters are then interconnected to MPP-PTO system with the following specifications on the pistons in each MPP-PTO unit[1].

Table 7.2: Piston specifications for each MPP-PTO unit.

Piston number	**Piston radius (m)**	**Piston mass (kg)**
1	0.2	200
2	0.3	400
3	0.4	700

Using the specifications in table 7.2, we can construct all nonzero possible combinations in the order {piston 1, piston 2, piston 3} where '1' denotes that the respective piston is engaged and '0' otherwise as given in Table 7.3. The rest of the parameters used in the numerical simulations of Σ_{OG} are adapted from [29, 33] and provided in table 7.4.

The simulation is conducted with regular wave input with wave period of $T = 7s$ and wave height of $H = 3.5m$. For the simulations, we use twelve different fixed set of piston combination as given in Table 7.5. Furthermore, we use simple forward Euler discretization method with very small step size to compensate the error due to the switching behavior. In Figure 7.3, we can see the accumulated extracted energy over the time span of 200 seconds. It can be seen that by fixing configuration number 12 to the floaters array, we can

Table 7.3: All possible piston combinations where at least one must be activated at a time.

Comb. nr.	**Piston comb.**	**Combined area A_c (m^2)**	**Combined mass M_p (kg)**
1	$\{1,0,0\}$	0.126	200
2	$\{0,1,0\}$	0.283	400
3	$\{1,1,0\}$	0.408	600
4	$\{0,0,1\}$	0.503	700
5	$\{1,0,1\}$	0.628	900
6	$\{0,1,1\}$	0.785	1100
7	$\{1,1,1\}$	0.911	1300

Table 7.4: Power take-off unit's parameters.

Parameter	**Value**
Cable stiffness (K_r^i)	$6.2093 \cdot 10^6$ N/m
Pipe length (L_{14})	100 m
Working fluid density (ρ_h)	998.2 kg/m^3
Upper reservoir capacitance (C_u)	0.05 m^5/N
Lower reservoir capacitance (C_l)	0.05 m^5/N

Table 7.5: Configurations of the MPP-PTO systems connected to each floater used in the simulation. The first row of the table denotes the floaters number in order where the first floater is the one facing the incoming wave. The numbers in the table for each floater in each combination corresponds to the set of piston combinations in Table 7.3 [1, Table 4].

Floater Nr.	1	2	3	4	5	6	7	8	9	10
Conf. 1	1	1	1	1	1	1	1	1	1	1
Conf. 2	2	2	1	1	1	1	1	1	1	1
Conf. 3	3	3	2	2	1	1	1	1	1	1
Conf. 4	4	4	3	3	2	2	1	1	1	1
Conf. 5	5	5	4	4	3	3	2	2	1	1
Conf. 6	6	6	5	5	4	4	3	3	2	2
Conf. 7	7	7	6	6	5	5	4	4	3	3
Conf. 8	7	7	7	7	6	6	5	5	4	4
Conf. 9	7	7	7	7	7	7	6	6	5	5
Conf. 10	7	7	7	7	7	7	7	7	6	6
Conf. 11	7	7	7	7	7	7	7	7	7	7
Conf. 12	7	6	6	6	5	5	5	5	4	4

absorb the most energy compared to the rest of the configuration. Note that, there might be some other configurations that yield higher energy extraction which need further investigation. In addition, the mean power of all pumping units during the simulation can be seen in Figure 7.4. Our simulation yields comparable results to the one in [1].

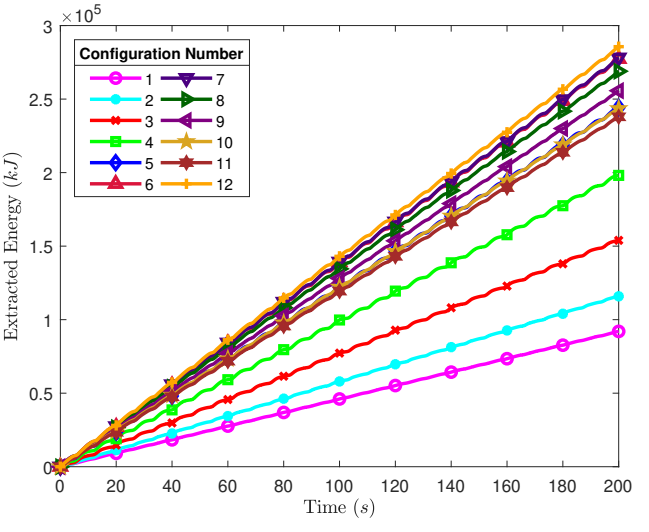

Figure 7.3: Total extracted potential energy with different setups for $200s$ simulation time in regular wave with $T = 7s$ and $H = 3.5m$.

7.3 Summary

In this chapter, we have presented a modeling of one column floaters array with hydraulic type PTO units using the port-Hamiltonian version of the Cummins' equation. The model is validated by some simulations whose configurations are taken from earlier research for the same WEC system in [1]. The simulations show that the model developed in this chapter is in good agreement with the earlier result. In addition, we maintain passivity of the complete OG-WEC system in this model.

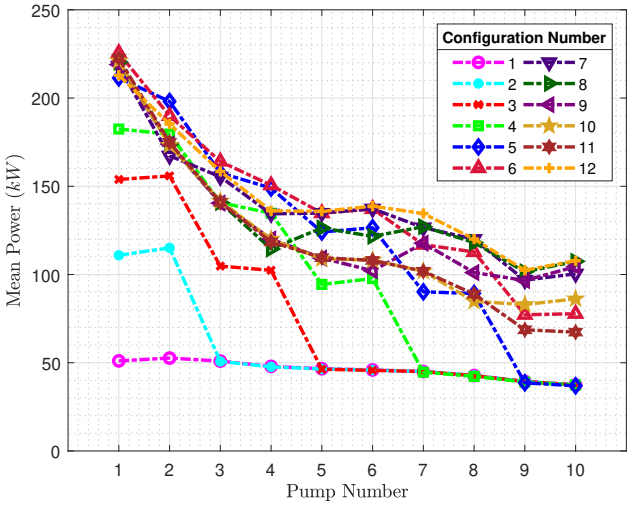

Figure 7.4: Mean power of all hydraulic-type power take-off units with different setups in regular wave with $T = 7s$ and $H = 3.5m$.

Chapter 8 | Conclusions and Outlooks

"Simpler solution does not imply simpler analysis, but when it is proven, it is easier to implement"

-Author-

Contents

In this thesis, we have studied three main problems. The first and second problem concerns control design when a system/an agent in standalone setting or in networked multi-agent setting can only realize actions from a given set of finite countable inputs. The remaining problem deals with improving the convergence rate of the preceeding solutions by considering some geometric extension on the limited actions. In addition to these problems, we also studied the modeling of the Ocean Grazer system, including its multi piston-pump concept, using port-Hamiltonian approach for Cummins' equation. The following sections provide summaries of the main findings of our study as well as some ideas for future works.

8.1 Conclusions Part I

In the first part of this thesis, we have studied the problem of designing control laws and analyzing their closed-loop practical stability when a system or subsystem can only realize actions from a given finite countable set of static actions. Our first main result in Chapter 3 provides the primary theoretical foundations used throughout this thesis where we considered a single agent whose dynamics described by a generic class of passive nonlinear system. Moreover, a notion of

large-time initial-state observability for nonlinear systems was assumed. Using these constructions, we proposed a nearest-action approach to select which input should be implemented by the system at a specific measured output, at a time instance, by employing some standard continuous control laws. We denote our proposed control law by nearest-action control (NAC) and we used La-Salle invariance principle type of approach to analyze the practical stability.

In order for our NAC to successfully practically stabilize the system in study, the given set of finite countable realizable control action $\mathscr{U}$ must satisfy a certain geometric structure, that is $0 \in \text{int}(\text{conv}(\mathscr{U}))$ if the target output corresponds to zero constant input of the system (or $u^* \in \text{int}(\text{conv}(\mathscr{U}))$ when u^* is the corresponding constant input of a constant-incrementally passive nonlinear systems). This condition on $\mathscr{U}$ paired with our NAC yield a natural upper bound for the output practical stability margin. We later found out that such condition on the finite countable input set $\mathscr{U}$ is satisfied if the static actions in $\mathscr{U} \setminus \{0\}$ (or $\mathscr{U} \setminus \{u^*\}$) are the vertices of a simplex structure. These findings allows us to greatly reduce the number of actions necessary to practically stabilize a generic class of passive nonlinear systems. That is, a passive nonlinear system with input/output dimension of m can be practically stabilized by using only $m+2$ number of actions. This is a significant reduction of necessary number of actions when compared to practical stabilization with q-ary quantizers which requires $q^m + 1$ number of necessary actions ($2^m + 1$ number of necessary action for the case of binary quantizer). In addition, for some regular simplices, we computed their explicit upper bound for practical stability with NAC.

It is also worth noting that in Chapter 3 we were able to establish practical stability when a sector bounded continuous feedback law is applied in cascade with our NAC. The practical stability analysis was carried out with the help of a symmetric matrix of inner products, namely Gram matrix. Throughout the analysis, we found out that Gram matrix provides much tighter bound on inequalities involving vectors, matrices, and inner products. Nonetheless, our results showed that when the sector bound on the continuous feedback law is small enough, we can still use NAC to achieve practical stability.

Inspired by out result on NAC for single agent, and also by many results and practicality of multi agent systems (MAS) available in literature, we looked for an application of our NAC to distributed control system in Chapter 4. Specifically, we studied the application of distributed NAC for the problem of cooperative control of MAS, namely consensus and distance-based formation control problems. In Chapter 4, we considered a networked MAS where agents motions are described by single integrator dynamics and, again, can only realize actions from a given set of finite countable inputs. Similar to our results in

Chapter 3, we used the standard continuous control protocols, namely the consensus and distance-based formation control laws, in conjunction with our NAC. We found out that consensus or some desired formations can be achieved up to the total natural upper bound of stability margin of each agent, i.e. the total practical stability margin increases linearly with the number of agents. The results were confirmed by using Monte-Carlo simulations.

Finally, in Chapter 5, we studied about how to improve the performance of our NAC by increasing the number of realizable actions in the directions of the original set of finite countable inputs $\mathscr{U}$. For this problem, we considered multi-input multi-output (MIMO) linear time invariance (LTI) systems, not necessarily passive, instead of the passive nonlinear systems considered in Chapter 3. For LTI systems, the notion of large-time initial-state norm observability in nonlinear systems is equivalent to the usual observability notion which can be observed by using the observability Gramian. As opposed to the LaSalle invariance principle type of analysis used in Chapter 3, in Chapter 5 we used input-to-state practical stability (ISpS) approach in the analysis. Furthermore, we propose the use of weak sector condition for MIMO systems and showed that practical stability with exponential rate can still be achieved when the transfer function of the closed-loop system is strictly positive real. The exponential convergence rate for NAC was enabled by allowing uniform or logarithmic extension in the directions of the original $\mathscr{U}$, confirmed by the simulation results presented in Chapter 5.

8.2 Conclusions Part II

In the second part of this thesis, we have proposed a different way of describing the Cummins' equation that is via port-Hamiltonian approach. In Chapter 6, we were dealing especially with approximation of the radiation components with *enforced* passivity in the Cummins' equation. The main reason for this is that the available toolbox for computing radiation force's hydrodynamics coefficients yields non-passive radiation system while naturally they should be passive. We validated our results in Chapter 6 by comparing simulation results from our approach with the one from existing toolbox. Our results shows a good agreement (with negligible errors) between our approximation with the well-accepted simulator when a simple linear PTO setting is used.

In Chapter 7, we used the port-Hamiltonian approach to Cummins' equation developed in Chapter 6 for the modeling and simulation of one column floaters array with MPP-PTO systems which is a subsystem of the OG-WEC. Our model shows that the full interconnection of OG-WEC is piecewice linear and is passive. Moreover, our simulations yield comparable results to the existing

result of OG-WEC models.

8.3 Future Research Directions

In this section, we present possible future research directions enabled by the proposed NAC in this thesis. Firstly, we have shown in Chapter 3 that for a generic class of passive nonlinear systems, practical stabilization is possible by using only $m+2$ elements in the finite countable control action set $\mathscr{U}$. However, the passivity condition is relatively restrictive as passive systems can, in some sense, be considered as stable systems. One can think of a possibility of reducing the necessary number of elements for practical stabilization of passive systems to a desired static output. An example in this direction is that a simple harmonic oscillator, which is a conservative system, may be practically stabilized to smaller or larger margin/amplitude by using only one nonzero and a zero action in conjunction to our NAC.

In our results for distributed NAC, we have shown that static consensus and distance-based formation can be achieved with total error up to the total natural error for each agent. However, Monte-Carlo simulation in Chapter 4 showed that the upper bound we provided may be too conservative. Thus, it is interesting to investigate the existence of tighter bound compared to ours. On the other hand, in many application of cooperative control for MAS, the agents may have to move from one place to another without interrupting the desired shape. In this case, investigation in the direction of path following, obstacle avoidance, and many other research directions of cooperative MAS are interesting to see.

In Chapter 5, we have shown that for a class of LTI systems, it is possible to improve the convergence rate of our NAC exponentially by placing (possibly infinite) additional control points in the direction of the original finite countable input set. However, when a prescribed performance is desired, the result is still unknown. Research in the direction of finding the optimal placement of some limited amount of additional control actions is particularly interesting. For example, we may only need to add l number of additional control points in some generic ways to improve the performance up to a given desired convergence rate, or to push the convergence ball into a smaller one.

Another interesting topic to investigate is regarding the possibility to use PI control in conjunction with our NAC (PI-NAC) to stabilize constant incrementally passive systems when the corresponding constant input is unknown. With only some minimal set of actions as in Chapter 3, the analysis of PI-NAC is currently not possible since the finite countable input set $\mathscr{U}$ must satisfy $u^* \in \mathrm{int}(\mathrm{conv}(\mathscr{U}))$ and we cannot guarantee that the predicted constant input

provided by PI control to stay within the interior of the convex hull of $\mathscr{U}$, even when we have prior knowledge of the existence of u^* in the set $\mathrm{int}(\mathrm{conv}(\mathscr{U}))$. However, it may be possible now by using the same extended set proposed in Chapter 5 since the input set can now expand countably infinitely.

For the second part of this thesis, the integration of the pH model of the multi-floater system with the non-linear PTO systems of the OG WEC and the corresponding optimal control design to maximize the power generation of the device is of particular interest. Furthermore, the coupling effects of the other 5 DOF of the body-fixed frame in the passivity of the multi-floater system are worth looking at. In addition, validating the pH model for irregular waves is also an interesting endeavour. Finally, the ultimate problem of designing online optimal control for OG WEC with MPP-PTO systems requires further investigation.

Bibliography

[1] Y. Wei, J. J. Barradas-Berglind, M. van Rooij, W. A. Prins, B. Jayawardhana, and A. I. Vakis, "Investigating the adaptability of the multi-pump multi-piston power take-off system for a novel wave energy converter," *Renewable Energy*, vol. 111, pp. 598–610, 2017.

[2] J. J. Barradas Berglind, H. Meijer, M. van Rooij, S. Clemente Pinol, B. Galvan Garcia, W. Prins, A. I. Vakis, and B. Jayawardhana, "Energy capture optimization for an adaptive wave energy converter," in *Proceedings of the 2nd International Conference on Renewable Energies Offshore - RENEW 2016*. CRC Press, Taylor and Francis Group, 2016, pp. 171–178.

[3] C. D. Persis and B. Jayawardhana, "Coordination of passive systems under quantized measurements," *SIAM Journal on Control and Optimization*, vol. 50, no. 6, pp. 3155–3177, 2012.

[4] C. De Persis, "Robust stabilization of nonlinear systems by quantized and ternary control," *Systems & Control Letters*, vol. 58, no. 8, pp. 602–608, 2009.

[5] D. Delchamps, "Stabilizing a linear system with quantized state feedback," *IEEE Trans. Autom. Control*, vol. 35, no. 8, pp. 916–924, 1990.

[6] N. Elia and S. Mitter, "Stabilization of linear systems with limited information," *IEEE Trans. Autom. Control*, vol. 46, no. 9, pp. 1384–1400, 2001.

[7] T. Hayakawa, H. Ishii, and K. Tsumura, "Adaptive quantized control for nonlinear uncertain systems," *Systems & Control Letters*, vol. 58, no. 9, pp. 625–632, 2009.

[8] M. Jafarian and C. De Persis, "Formation control using binary information," *Automatica*, vol. 53, pp. 125 – 135, 2015.

[9] C. Kao and S. Venkatesh, "Stabilization of linear systems with limited information multiple input case," in *Proc. American Control Conference*, vol. 3, 2002, pp. 2406–2411.

[10] J. Cortés, "Finite-time convergent gradient flows with applications to network consensus," *Automatica*, vol. 42, no. 11, pp. 1993–2000, 2006.

[11] F. Ceragioli and C. De Persis, "Discontinuous stabilization of nonlinear systems: Quantized and switching controls," *Systems & Control Letters*, vol. 56, no. 7-8, pp. 461–473, 2007.

[12] D. Liberzon and J. Hespanha, "Stabilization of nonlinear systems with limited information feedback," *IEEE Transactions on Automatic Control*, vol. 50, no. 6, pp. 910–915, 2005.

[13] S. Tatikonda, "Control under communication constraints," Ph.D. dissertation, Massachusetts Institute of Technology, 2000.

[14] M. Fu and C. de Souza, "State estimation for linear discrete-time systems using quantized measurements," *Automatica*, vol. 45, no. 12, pp. 2937–2945, 2009.

[15] F. Bullo and D. Liberzon, "Quantized control via locational optimization," *IEEE Transactions on Automatic Control*, vol. 51, no. 1, pp. 2–13, 2006.

[16] G. Nair, R. Evans, I. Mareels, and W. Mooran, "Topological feedback entropy and nonlinear stabilization," *IEEE Transactions on Automatic Control*, vol. 49, no. 9, pp. 1585–1597, 2004.

[17] F. Colonius, "Minimal bit rates and entropy for exponential stabilization," *SIAM J. Control Optim.*, vol. 50, no. 5, pp. 2988–3010, 2012.

[18] F. Colonius and C. Kawan, "Invariance entropy for control systems," *SIAM J. Control Optim.*, vol. 48, no. 3, pp. 1701–1721, 2009.

[19] B. Brogliato and A. Tanwani, "Dynamical systems coupled with monotone set-valued operators: Formalisms, applications, well-posedness, and stability," *SIAM Review*, vol. 62, pp. 3–129, 2020.

[20] B. Jayawardhana, H. Logemann, and E. P. Ryan, "The circle criterion and input-to-state stability," *IEEE Control Systems Magazine*, vol. 31, no. 4, pp. 32–67, 2011.

[21] M. Jafarian, "Ternary and hybrid controllers for the rendezvous of unicycles," in *2015 54th IEEE Conference on Decision and Control (CDC)*, 2015, pp. 2353–2358.

[22] M. Fu and L. Xie, "The sector bound approach to quantized feedback control," *IEEE Transactions on Automatic Control*, vol. 50, no. 11, pp. 1698–1711, 2005.

[23] B. Jayawardhana, H. Logemann, and E. P. Ryan, "Input-to-state stability of differential inclusions with applications to hysteretic and quantized feedback systems," *SIAM Journal on Control and Optimization*, vol. 48, no. 2, pp. 1031–1054, 2009.

[24] T. Naderi, D. Materassi, G. Innocenti, and R. Genesio, "Revisiting kalman and aizerman conjectures via a graphical interpretation," *IEEE Transactions on Automatic Control*, vol. 64, no. 2, pp. 670–682, 2019.

[25] J. C. C. Henriques, J. C. C. Portillo, L. M. C. Gato, R. P. F. Gomes, D. N. Ferreira, and A. F. O. Falcão, "Design of oscillating-water-column wave energy converters with an application to self-powered sensor buoys," *Energy*, vol. 112, pp. 852–867, oct 2016.

[26] R. Henderson, "Design, simulation, and testing of a novel hydraulic power take-off system for the pelamis wave energy converter," *Renewable Energy*, vol. 31, no. 2, pp. 271–283, feb 2006.

[27] J. Tedd, J. Kofoed, M. Jasinski, A. Morris, E. Friis-Madsen, R. Wisniewski, and J. Bendtsen, "Advanced control techniques for wec wave dragon," in *Proceedings of the 7th European Wave and Tidal Energy Conference*. European Ocean Energy Association, 2007.

[28] A. I. Vakis, H. Meijer, and W. A. Prins, "First steps in the design and construction of the ocean grazer," in *ASME 2014 12th Biennial Conference on Engineering Systems Design and Analysis*. American Society of Mechanical Engineers, 2014, p. V002T09A004.

[29] A. I. Vakis and J. S. Anagnostopoulos, "Mechanical design and modeling of a single-piston pump for the novel power take-off system of a wave energy converter," *Renewable Energy*, vol. 96, pp. 531–547, 2016.

[30] K. M. Nielsen, T. S. Pedersen, P. Andersen, and S. Ambühl, "Optimizing control of wave energy converter with losses and fatigue in power take off," *IFAC-PapersOnLine*, vol. 50, no. 1, pp. 14 680–14 685, jul 2017.

[31] W. Cummins, "The impulse response function and ship motions," David Taylor Model Basin Washington DC, Tech. Rep., 1962.

[32] A. van der Schaft and D. Jeltsema, "Port-hamiltonian systems theory: An introductory overview," *Foundations and Trends® in Systems and Control*, vol. 1, no. 2-3, pp. 173–378, 2014.

[33] J. J. Barradas-Berglind, M. Munoz-Arias, Y. Wei, W. A. Prins, A. I. Vakis, and B. Jayawardhana, "Towards Ocean Grazer's modular power take-off system modeling: a port-Hamiltonian approach," in *Proc. of the IFAC 2017 World Congress*, 2017, pp. 16 233–16 239.

[34] Z. Yu and J. Falnes, "State-space modelling of a vertical cylinder in heave," *Applied Ocean Research*, vol. 17, no. 5, pp. 265–275, 1995.

[35] T. Perez and T. I. Fossen, "A Matlab Toolbox for Parametric Identification of Radiation-Force Models of Ships and Offshore Structures," *Modeling, Identification and Control*, vol. 30, no. 1, pp. 1–15, 2009.

[36] M. Almuzakki, J. Barradas Berglind, Y. Wei, M. Muñoz Arias, A. Vakis, and B. Jayawardhana, "A port-hamiltonian approach to cummins' equation for floater arrays with linear power take-off systems," in *6th IFAC Workshop on Lagrangian and Hamiltonian Methods for Nonlinear Control (LHMNC 2018)*, ser. IFAC-PapersOnLine. IFAC, 2018.

[37] E. Sarkans and H. Logemann, "Input-to-state stability of lur'e systems," *Mathematics of Control, Signals, and Systems*, vol. 27, pp. 439–465, 2015.

[38] J. Willems, "Dissipative dynamical systems. Part I: General theory," *Arch. Rational Mechanics and Analysis*, vol. 45, no. 5, pp. 321–351, 1972.

[39] A. van der Schaft, *L2-Gain and Passivity Techniques in Nonlinear Control*. Springer International Publishing, 2016.

[40] R. Ortega, J. Perez, A. Loria, P. Nicklasson, and H. Sira-Ramirez, *Passivity-based Control of Euler-Lagrange Systems*. Springer London, 2013.

[41] J. Hespanha, D. Liberzon, D. Angeli, and E. Sontag, "Nonlinear norm-observability notions and stability of switched systems," *IEEE Trans. Autom. Control*, vol. 50, no. 2, pp. 154–168, 2005.

[42] B. Jayawardhana, R. Ortega, E. Garcìa-Canseco, and F. Castanos, "Passivity of nonlinear incremental systems: Application to PI stabilization of nonlinear RLC circuits," *Systems & Control Letters*, vol. 56, no. 9, pp. 618 – 622, 2007.

[43] N. Monshizadeh, P. Monshizadeh, R. Ortega, and A. van der Schaft, "Conditions on shifted passivity of port-hamiltonian systems," *Systems & Control Letters*, vol. 123, pp. 55 – 61, 2019.

[44] G. Hines, M. Arcak, and A. Packard, "Equilibrium-independent passivity," *Automatica*, vol. 47, no. 9, pp. 1949–1956, 2011.

[45] J.-P. Aubin and A. Cellina, *Differential Inclusions: Set-Valued Maps and Viability Theory*. Springer-Verlag, 1984.

[46] A. Okabe, B. Boots, K. Sugihara, and S. Chiu, *Spatial Tessellations: Concepts and Applications of Voronoi Diagrams*. John Wiley & Sons, 2009.

[47] C. Toth, J. O'Rourke, and J. Goodman, *Handbook of Discrete and Computational Geometry*, ser. Discrete Mathematics and Its Applications. CRC Press, 2017.

[48] M. Marcantoni, B. Jayawardhana, M. P. Chaher, and K. Bunte, "Secure formation control via edge computing enabled by fully homomorphic encryption and mixed uniform-logarithmic quantization," *IEEE Control Systems Letters*, vol. 7, pp. 395–400, 2023.

[49] B. D. Anderson, C. Yu, B. Fidan, and J. M. Hendrickx, "Rigid graph control architectures for autonomous formations," *IEEE Control Systems Magazine*, vol. 28, no. 6, pp. 48–63, 2008.

[50] L. Asimow and B. Roth, "The rigidity of graphs," *Transactions of the American Mathematical Society*, vol. 245, pp. 279–289, 1978.

[51] J. Wei, X. Yi, H. Sandberg, and K. H. Johansson, "Nonlinear consensus protocols with applications to quantized communication and actuation," *IEEE Transactions on Control of Network Systems*, vol. 6, no. 2, pp. 598–608, 2019.

[52] D. Castano, V. Paksoy, and F. Zhang, "Angles, triangle inequalities, correlation matrices and metric-preserving and subadditive functions," *Linear Algebra and its Applications*, vol. 491, pp. 15–29, 2016.

[53] F. Castanos, B. Jayawardhana, R. Ortega, and E. Garcìa-Canseco, "Proportional plus integral control for set-point regulation of a class of nonlinear RLC circuits," *Circuits systems and signal processing*, vol. 28, no. 4, pp. 609–623, 2009.

[54] A. Brondsted, *An Introduction to Convex Polytopes*. Springer-Verlag New York, 1983.

[55] L. Moreau, "Stability of continuous-time distributed consensus algorithms," in *2004 43rd IEEE Conference on Decision and Control (CDC) (IEEE Cat. No.04CH37601)*, vol. 4, 2004, pp. 3998–4003 Vol.4.

[56] W. Ren, R. Beard, and E. Atkins, "A survey of consensus problems in multi-agent coordination," in *Proceedings of the 2005, American Control Conference, 2005.*, 2005, pp. 1859–1864 vol. 3.

[57] L. Li, M. Fu, H. Zhang, and R. Lu, "Consensus control for a network of high order continuous-time agents with communication delays," *Automatica*, vol. 89, pp. 144–150, 2018.

[58] R. Olfati-Saber, "Flocking for multi-agent dynamic systems: algorithms and theory," *IEEE Transactions on Automatic Control*, vol. 51, no. 3, pp. 401–420, 2006.

[59] K.-K. Oh, M.-C. Park, and H.-S. Ahn, "A survey of multi-agent formation control," *Automatica*, vol. 53, pp. 424–440, 2015.

[60] R. Carli and F. Bullo, "Quantized coordination algorithms for rendezvous and deployment," *SIAM Journal on Control and Optimization*, vol. 48, no. 3, pp. 1251–1274, 2009.

[61] B. S. Park and S. J. Yoo, "Quantized-communication-based neural network control for formation tracking of networked multiple unmanned surface vehicles without velocity information," *Engineering Applications of Artificial Intelligence*, vol. 114, p. 105160, 2022.

[62] Q. Zhang and J.-F. Zhang, "Quantized data–based distributed consensus under directed time-varying communication topology," *SIAM Journal on Control and Optimization*, vol. 51, no. 1, pp. 332–352, 2013.

[63] F. Ceragioli and P. Frasca, "Continuous-time consensus dynamics with quantized all-to-all communication," in *2015 European Control Conference (ECC)*, 2015, pp. 1926–1931.

[64] Z. Sun, H. G. de Marina, B. D. O. Anderson, and M. Cao, "Quantization effects in rigid formation control," in *2016 Australian Control Conference (AuCC)*, 2016, pp. 168–173.

[65] F. Xiao, T. Chen, and H. Gao, "Consensus in time-delayed multi-agent systems with quantized dwell times," *Systems & Control Letters*, vol. 104, pp. 59–65, 2017.

[66] M. Z. Almuzakki, B. Jayawardhana, and A. Tanwani, "Nearest neighbor control for practical stabilization of passive nonlinear systems," *Automatica*, vol. 141, p. 110278, 2022.

[67] B. Jayawardhana, M. Almuzakki, and A. Tanwani, "Practical stabilization of passive nonlinear systems with limited control," *IFAC-PapersOnLine*, vol. 52, no. 16, pp. 460–465, 2019, 11th IFAC Symposium on Nonlinear Control Systems NOLCOS 2019.

[68] M. Z. Almuzakki and B. Jayawardhana, "Cooperative nearest-neighbor control of multi-agent systems: Consensus and formation control problems," *IEEE Control Systems Letters*, vol. 7, pp. 1873–1878, 2023.

[69] L. Xing, C. Wen, Y. Zhu, H. Su, and Z. Liu, "Output feedback control for uncertain nonlinear systems with input quantization," *Automatica*, vol. 65, pp. 191–202, 2016.

[70] L. N. Bikas and G. A. Rovithakis, "Combining prescribed tracking performance and controller simplicity for a class of uncertain mimo nonlinear systems with input quantization," *IEEE Transactions on Automatic Control*, vol. 64, no. 3, pp. 1228–1235, 2019.

[71] H. Liang, Y. Zhang, T. Huang, and H. Ma, "Prescribed performance cooperative control for multiagent systems with input quantization," *IEEE Transactions on Cybernetics*, vol. 50, no. 5, pp. 1810–1819, 2020.

[72] C. Guiver and H. Logemann, "A circle criterion for strong integral input-to-state stability," *Automatica*, vol. 111, p. 108641, 2020.

[73] Y. Xue and P. Zhao, "Input-to-state stability and stabilization of nonlinear impulsive positive systems," *Mathematics*, vol. 9, no. 14, 2021.

[74] Y. Fujii and H. Nakamura, "Design of time-varying input-to-state stability tracking control lyapunov functions for disturbance attenuation," *SICE Journal of Control, Measurement, and System Integration*, vol. 14, no. 1, pp. 157–168, 2021.

[75] Z. Fu and S. Peng, "Input-to-state stability criteria of discrete-time time-varying impulsive switched delayed systems with applications to multi-agent systems," *IEEE Transactions on Circuits and Systems I: Regular Papers*, vol. 69, no. 7, pp. 3016–3025, 2022.

[76] C. Guiver and H. Logemann, "The exponential input-to-state stability property: characterisations and feedback connections," *Mathematics of Control, Signals, and Systems*, pp. 1–24, 2023.

[77] W. Liu, Y. Wang, and Z. Wang, "Robust input-to-state stability of discrete-time singularly perturbed systems with nonlinear perturbation," *Nonlinear Dynamics*, vol. 109, no. 4, pp. 2935–2948, 2022.

[78] M. Tucker and A. D. Ames, "An input-to-state stability perspective on robust locomotion," *IEEE Control Systems Letters*, vol. 7, pp. 2599–2604, 2023.

[79] Z. P. Jiang, A. R. Teel, and L. Praly, "Small-gain theorem for iss systems and applications," *Mathematics of Control, Signals and Systems*, vol. 7, pp. 95–120, 1994.

[80] E. D. Sontag and Y. Wang, "On characterizations of input-to-state stability with respect to compact sets," *IFAC Proceedings Volumes*, vol. 28, no. 14, pp. 203–208, 1995, 3rd IFAC Symposium on Nonlinear Control Systems Design 1995, Tahoe City, CA, USA, 25-28 June 1995.

[81] A. Mironchenko, "Criteria for input-to-state practical stability," *IEEE Transactions on Automatic Control*, vol. 64, no. 1, pp. 298–304, 2019.

[82] H. Damak, M. A. Hammami, and R. Heni, "Input-to-state practical stability for nonautonomous nonlinear infinite-dimensional systems," *International Journal of Robust and Nonlinear Control*, vol. 33, no. 10, pp. 5834–5847, 2023.

[83] J. P. Hespanha, D. Liberzon, D. Angeli, and E. D. Sontag, "Nonlinear norm-observability notions and stability of switched systems," *IEEE Transactions on Automatic Control*, vol. 50, no. 2, pp. 154–168, 2005.

[84] W. A. Prins, M. Van Rooij, A. I. Vakis, and B. Jayawardhana, "Underwater energy storage system," October 5 2021, US Patent 11,136,963.

[85] J. V. Ringwood, G. Bacelli, and F. Fusco, "Energy-maximizing control of wave-energy converters: The development of control system technology to optimize their operation," *IEEE Control Systems*, vol. 34, no. 5, pp. 30–55, 2014.

[86] R. Hansen and M. Kramer, "Modelling and control of the Wavestar prototype," in *Proc. of EWTEC2011*, 2011.

[87] R. Henderson, "Design, simulation, and testing of a novel hydraulic power take-off system for the Pelamis wave energy converter," *Ren. Energy*, vol. 31, no. 2, pp. 271–283, 2006.

[88] M. Lagoun, A. Benalia, and M. H. Benbouzid, "Ocean wave converters: State of the art and current status," in *Proc. of IEEE EnergyCon2010*, 2010, pp. 636–641.

[89] B. Maschke and A. van der Schaft, "Port-controlled Hamiltonian systems: modeling origins and system-theoretic properties," in *Proc. of the IFAC Symposium on Nonlinear Control Systems*, Bordeaux, France, 1992, pp. 282–288.

[90] R. Ortega, A. J. van der Schaft, I. Mareels, and B. Maschke, "Putting energy back in control," *IEEE Control Systems*, vol. 21, no. 2, pp. 18–33, 2001.

[91] V. Duindam, A. Macchelli, S. Stramigioli, and H. Bruyninckx, *Modeling and Control of Complex Physical Systems: The Port-Hamiltonian Approach*. Berlin, Germany: Springer, 2009.

[92] U. A. Korde and J. V. Ringwood, *Hydrodynamic Control of Wave Energy Devices*. Cambridge U.Press, 2016.

[93] N. Faedo, S. Olaya, and J. V. Ringwood, "Optimal control, MPC and MPC-like algorithms for wave energy systems: An overview," *IFAC Journal of Systems and Control*, vol. 1, pp. 37–56, 2017.

[94] A. Babarit and G. Delhommeau, "Theoretical and numerical aspects of the open source BEM solver NEMOH," in *Proc. of the EWTEC2015 Conf.*, 2015.

[95] T. Perez and T. I. Fossen, "A MATLAB toolbox for parametric identification of radiation-force models of ships and offshore structures," *Modeling, Identification and Control*, vol. 30, no. 1, p. 1, 2009.

[96] K. Ruehl, C. Michelen, S. Kanner, M. Lawson, and Y.-H. Yu, "Preliminary verification and validation of WEC-Sim, an open-source wave energy converter design tool," in *Proc. of the OMAE2014 Conf.*, 2014.

[97] J. Löfberg, "YALMIP : A toolbox for modeling and optimization in MATLAB," in *Proc. of the CACSD2004 Conf.*, 2004.

Summary

In various control system applications, implementing an exact control law is often hindered by practical limitations. For instance, Ocean Grazer wave energy converters encounter fixed sets of constant actuator systems in their power take-off systems, while space rockets or shuttles may feature fixed configurations of constant thruster systems. These systems can only execute control actions from a given finite countable set. When the available control actions are *regularly* distributed, following patterns like binary, ternary, uniform, and/or logarithmic distributions, many relevant results in this context are readily accessible. Nevertheless, challenges arise with irregularly distributed control actions, presenting issues not accounted for by these approaches.

In this thesis, we proposed an approach called the nearest-action control (NAC) to address the aforementioned challenge. Initially focusing on a generic class of passive nonlinear multi-input multi-output systems, where inputs are limited to finite countable sets of control actions, we demonstrated the practical stabilization of a nonlinear passive system around an equilibrium point. This was achieved under the assumption of large-time initial-state norm-observability for nonlinear systems and the corresponding constant action lies within the interior of the convex hull of the available control actions.

Moreover, we showed that the minimum number of nonzero actions required for the practical stabilization of a nonlinear passive system is equivalent to the number of vertices in a simplex structure. This insight leads to a significant reduction in the necessary control actions for the practical stabilization of a generic class of passive nonlinear systems. For instance, in comparison to binary or ternary control methods that exhibit exponential growth in the required actions relative to input/output dimensions, our NAC approach results in a linear increase in the required actions. Additionally, we presented constructions for minimal control actions and their corresponding bounds in relation to practical stability.

The NAC framework is extended to cooperative control in multi-agent systems (MAS), specifically addressing consensus and formation control problems. Each agent in the MAS, constrained to finite countable actions, employs NAC

to achieve consensus and formation, with collective maximum error computed as the sum of individual agent errors.

Simulations results for the implementation of our NAC with minimum number of necessary actions in single-/multi-agent systems settings showed that the worst convergence rate is linear, depending on the internal dynamics of the systems. To improve the performance, we combined our NAC with the idea of having uniformly or logarithmically distributed actions in the direction of the given set of finite countable control actions. For linear, not necessarily passive, systems case, we showed using input-to-state practical stability approach that it is possible to make the system converges towards a ball around the equilibrium point exponentially fast.

In addition to the contributions listed above, we provided contributions to the development of mathematical models of the Ocean Grazer wave energy converter (OG-WEC) in the port-Hamiltonian framework. For this part, we first provided a port-Hamiltonian reformulation of the Cummins' equation for the hydrodynamics behavior of the floating elements in OG-WEC by considering simplified linear power take-off. Through port-Hamiltonian reformulation, we showed that the whole system is passive, which means that the whole system is a naturally stable system. Next, we modeled the nonlinear power take-off systems (pump-hydro systems) of the OG-WEC using the port-Hamiltonian framework. We showed that the full interconnection of OG-WEC with nonlinear power take-off system is passive. Finally, our simulation results shows that our model is comparable to the model developed and simulated using existing toolbox.

Samenvatting

In verschillende toepassingen van regelsystemen wordt de implementatie van een exacte regelgeving vaak belemmerd door praktische beperkingen. Zo worden bijvoorbeeld bij de Ocean Grazer golfenergie-omzetters een vaste set van actuatoren gebruikt in hun energie-afvoersystemen, terwijl ruimteraketten of shuttles vaste configuraties van aandrijfsystemen kunnen hebben. Deze systemen kunnen alleen regelacties uitvoeren vanuit een gegeven eindige telbare set. Wanneer de beschikbare regelacties regelmatig verdeeld zijn, volgens verschillende patronen zoals binair, ternair, uniform en/of logaritmisch, zijn veel relevante resultaten in deze context gemakkelijk en toegankelijk. Desalniettemin zijn er uitdagingen wanneer er onregelmatig verdeelde regelacties zijn, die problemen met zich meebrengen die niet worden behandeld door deze benaderingen.

In dit proefschrift hebben we een methode voorgesteld die we 'nearest-action control' (NAC) noemen om de genoemde uitdaging aan te pakken. In eerste instantie gericht op passieve niet-lineaire multi-input multi-output systemen, waarbij invoeren beperkt zijn tot eindige telbare sets regelacties, hebben we de praktische stabilisatie van een niet-lineair passief systeem rond een evenwichtspunt gedemonstreerd. Dit werd bereikt onder de aanname van grote-tijd beginstaat-norm-observeerbaarheid voor niet-lineaire systemen en de overeenkomstige constante actie ligt binnen het convexe omhulsel van de beschikbare regelacties.

Bovendien hebben we aangetoond aan dat het minimumaantal niet-nul acties dat nodig is voor de praktische stabilisatie van een niet-lineair passief systeem equivalent is aan het aantal hoekpunten in een simplexstructuur. Deze inzichten leiden tot een aanzienlijke vermindering van de benodigde regelacties voor de praktische stabilisatie van niet-lineaire passieve systemen. Bijvoorbeeld, in vergelijking met binaire of ternaire regelmethoden die exponentiële groei vertonen in de benodigde acties ten opzichte van de invoer-/uitvoerdimensies, resulteert onze NAC-benadering in een lineaire toename van de benodigde acties. Daarnaast presenteerden we constructies voor minimale regelacties en hun overeenkomstige grenzen met betrekking tot praktische stabiliteit.

De NAC-omkadering wordt uitgebreid naar coöperatieve regeling in multi-agent systemen (MAS), waarbij specifiek consensus- en formatieregelingsproblemen worden aangepakt. Elke agent in de MAS, beperkt tot eindige telbare acties, past NAC toe om consensus en formatie te bereiken, waarbij de totale maximale afwijking wordt berekend als de som van individuele afwijking per agent.

Simulatieresultaten voor de implementatie van onze NAC met het minimumaantal benodigde acties in enkele/multi-agent systeemomgevingen toonden aan dat de slechtste convergentiesnelheid lineair is, afhankelijk van de interne dynamiek van de systemen. Om de prestaties te verbeteren, combineerden we onze NAC met het idee van gelijkmatig of logaritmisch verdeelde acties in de richting van de gegeven set van eindige telbare regelacties. Voor het geval van lineaire, niet noodzakelijk passieve systemen, toonden we met behulp van de input-to-state praktische stabiliteitsbenadering aan dat het mogelijk is om het systeem exponentieel snel naar een bol rond het evenwichtspunt te laten convergeren.

Naast de hierboven genoemde bijdrages leverden we een bijdrage aan de ontwikkeling van wiskundige modellen van de Ocean Grazer golfenergie-omzetter (OG-WEC) in het port-Hamiltoniaanse kader. Voor dit gedeelte hebben we eerst een port-Hamiltoniaanse herformulering gegeven van de Cummins-vergelijking voor het hydrodynamisch gedrag van de drijvende elementen in OG-WEC door het overwegen van vereenvoudigde lineaire energie-afvoer. Via de port-Hamiltoniaanse herformulering toonden we aan dat het hele systeem passief is, wat betekent dat het hele systeem van nature stabiel is. Vervolgens hebben we de niet-lineaire energie-afvoersystemen (pomp-hydro systemen) van de OG-WEC gemodelleerd met behulp van het port-Hamiltoniaanse kader. We toonden aan dat de volledige interconnectie van OG-WEC met het niet-lineaire energie-afvoersysteem passief is. Ten slotte laten onze simulatieresultaten zien dat ons model vergelijkbaar is met het model dat is ontwikkeld en gesimuleerd met behulp van de bestaande toolbox.

Ringkasan

Dalam berbagai aplikasi sistem kendali, penerapan algoritma sistem kendali secara eksak seringkali terhambat oleh keterbatasan yang sifatnya praktikal. Misalnya, desain pembangkit listrik tenaga gelombang permukaan air laut Ocean Grazer (OG-WEC) menggunakan sekumpulan sistem aktuator konstan yang telah ditentukan, sementara roket atau pesawat ulang-alik mungkin hanya memiliki konfigurasi sistem pendorong yang konstan dan terbatas. Sistem-sistem seperti ini hanya dapat menjalankan aksi dari sebuah himpunan terbatas yang dapat dibilang/dicacah, yang telah ditentukan sebelumnya. Ketika aksi-aksi yang ada terdistribusi secara reguler, mengikuti pola-pola seperti pola biner, terner, distribusi seragam, dan/atau logaritmik, banyak hasil yang relevan dalam konteks ini dapat ditemukan dan diakses dengan mudah. Namun demikian, tantangan muncul ketika aksi-aksi yang mungkin dilakukan oleh sistem terdistribusi secara tidak teratur, sehingga hasil-hasil yang sudah ada sebelumnya tidak dapat mengatasi permasalahan ini.

Dalam tesis ini, kami mengusulkan suatu pendekatan yang kami sebut dengan *the nearest-action control* (NAC) atau pengendalian menggunakan tindakan terdekat yang mungkin diterapkan oleh sistem untuk menjawab tantangan di atas. Kami memulai tesis ini dengan berfokus pada sebuah kelas generik yang mencakup sistem nonlinier pasif dengan multi-input multi-output, di mana input kendalinya dibatasi pada himpunan aksi yang terbatas dan dapat dibilang. Kami menunjukkan bahwa stabilisasi praktikal untuk sebuah sistem nonlinier pasif di sekitar titik ekuilibrium yang diharapkan dapat dilakukan menggunakan NAC. Hal ini dapat tercapai dengan asumsi bahwa sistem yang sedang dikaji memenuhi sifat *large-time initial-state norm-observable* dan, di saat yang bersamaan, aksi konstan yang berkaitan dengan target titik ekuilibrium berada tepat di dalam interior dari *convex hull* dari himpunan semua aksi yang tersedia.

Selain itu, kami menunjukkan bahwa banyaknya aksi selain nol yang dibutuhkan untuk stabilisasi praktikal sebuah sistem nonlinear pasif sama dengan banyaknya titik sudut sebuah struktur simpleks. Hasil ini memungkinkan pengurangan yang sangat signifikan dalam hal banyaknya aksi yang dibutuhkan untuk menstabilkan sebuah sistem nonlinier pasif secara praktikal. Misalnya, pada

metode kendali biner atau terner, banyaknya aksi minimum yang diperlukan untuk membuat sebuah sistem nonlinier pasif stabil secara praktikal meningkat secara eksponensial seiring dengan meningkatnya dimensi input/output dari sistem yang ingin dikendalikan. Sedangkan pada metode NAC, banyaknya aksi minimum yang diperlukan tersebut hanya meningkat secara linier terhadap peningkatan dimensi input/output. Dalam tesis ini kami juga menyajikan metode konstruksi untuk membangun aksi-aksi minimal yang diperlukan serta galat maksimum yang mungkin terjadi yang terkait dengan stabilisasi praktikal menggunakan NAC.

Kerangka kerja NAC kemudian kami perluas untuk pengendalian kooperatif dalam sistem multi-agen (*multi-agent system*; MAS), khususnya untuk menjawab masalah konsensus dan pembentukan formasi. Setiap agen dalam MAS yang dikaji, yang dibatasi oleh aksi-aksi yang terbatas dan terbilang, menerapkan NAC untuk mencapai konsensus dan formasi yang diharapkan. Galat maksimum secara kolektif saat tujuan kendali kooperatif tercapai dapat dihitung dengan menjumlahkan galat maksimum dari masing-masing agen yang terlibat dalam proses kendali.

Hasil simulasi dari penerapan NAC yang kami usulkan dengan aksi-aksi yang paling minimum, baik pada kasus *single-agent* maupun pada *multi-agent*, menunjukkan bahwa laju konvergensi terburuk yang mungkin terjadi bersifat linier, bergantung pada dinamika internal dari masing-masing sistem. Untuk meningkatkan performanya, kami menggabungkan NAC dengan kemungkinan adanya ekstensi dari aksi-aksi yang ada yang terdistribusi secara teratur seperti distribusi seragam atau logaritmik. Dengan pendekatan *input-to-state practical stability*, kami menunjukkan bahwa sistem linier, tidak harus pasif, dapat distabilkan secara praktikal ke sekitar titik ekuilibrium dengan laju eksponensial.

Selain beberapa kontribusi yang telah tercantum di atas, kami juga berkontribusi pada pengembangan model matematika untuk OG-WEC dalam kerangka port-Hamiltonian. Bagian ini kami mulai dengan melakukan reformulasi persamaan Cummins' yang menggambarkan perilaku hidrodinamik dari elemen-elemen terapung pada OG-WEC ke dengan kerangka port-Hamiltonian dan membatasi sistem *power take-off*-nya menggunakan sistem linier. Dengan reformulasi ini, kami menunjukkan bahwa keseluruhan sistem yang dikaji merupakan sistem yang pasif yang artinya sistem tersebut stabil secara alami. Selanjutnya, kami memodelkan sistem *power take-off* (PTO) nonlinier milik OG-WEC, yaitu sistem *pump-hydro*, dalam kerangka port-Hamiltonian. Kami menunjukkan bahwa interkoneksi penuh sistem OG-WEC dengan PTO nonlinier juga merupakan sistem yang pasif. Terakhir, hasil simulasi kami menunjukkan bahwa model yang kami kembangkan sebanding dengan model yang dikembangkan dan disimulasikan menggunakan *toolbox* lain yang sudah ada.

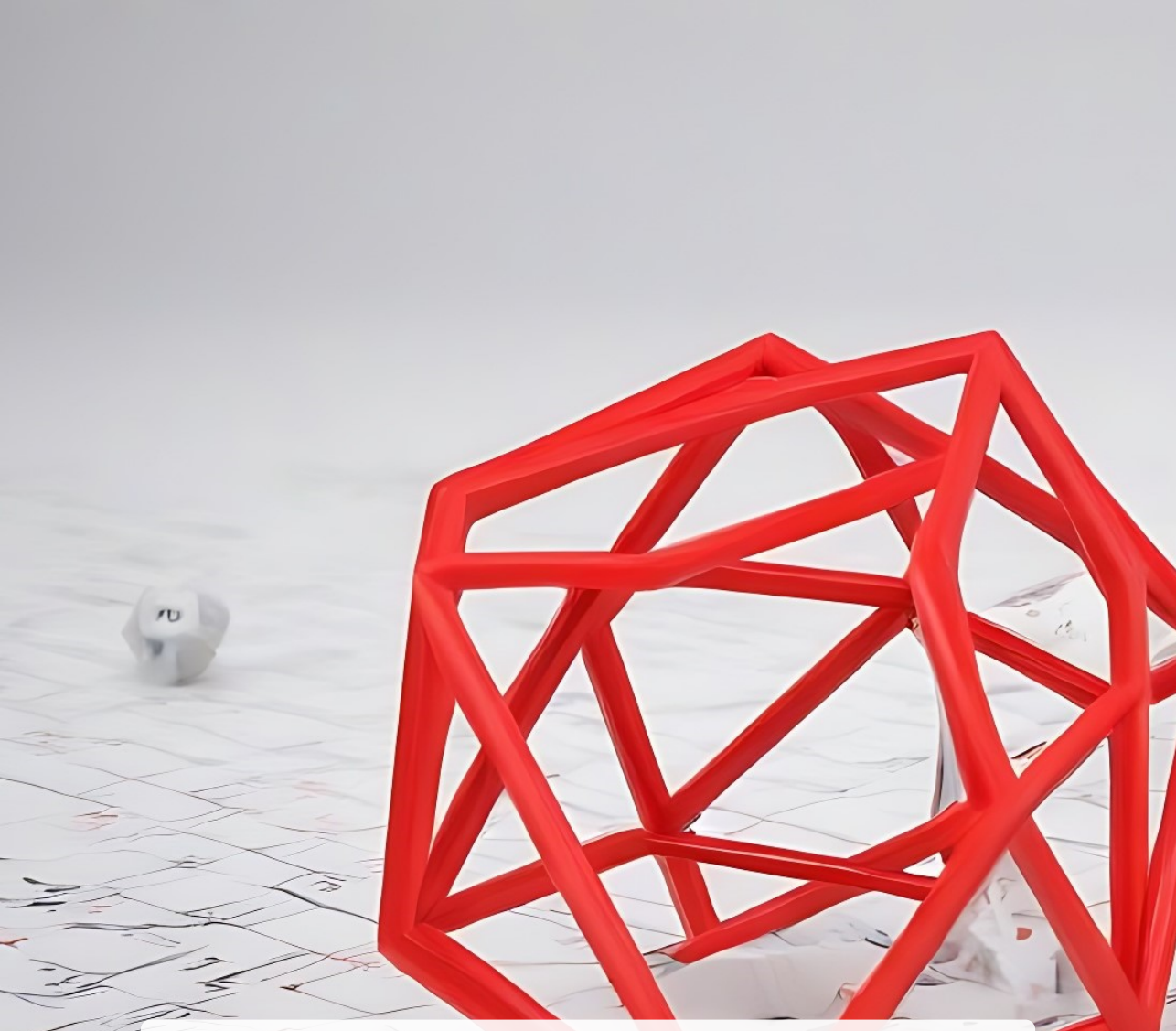

Biography

Muhammad Zaki Almuzakki completed his undergraduate studies in mathematics at Universitas Brawijaya, Indonesia, in 2012, earning a B.Sc. degree. He continued his academic journey by obtaining an M.Sc. degree in applied mathematics from Kanazawa University, Japan, in 2015, followed by another M.Sc. degree in computational science from Institut Teknologi Bandung, Indonesia.

Since 2016, he has been affiliated with the Department of Computer Science at the Faculty of Science and Computer, Universitas Pertamina, Indonesia. In October 2016, he started his Ph.D. in applied mathematics at the University of Groningen, the Netherlands, under the guidance of Prof. Bayu Jayawardhana and Prof. Antonis I. Vakis. His research interests include mathematical modeling and nonlinear control systems.